

**MOLECULAR CHARACTERIZATION OF CATION-
COUPLED TRANSPORTERS: THE H⁺-COUPLED Mg²⁺-
CITRATE TRANSPORTER, CitM, AND THE
Na⁺/SULFATE COTRANSPORTER, hNaSi-1**

APPROVED BY THE SUPERVISORY COMMITTEE

Dr. Ana M. Pajor

Dr. Steven C. King

Dr. Joel P. Gallagher

Dr. Luis Reuss

Dr. Steven A. Weinman

Dean, Graduate School

**MOLECULAR CHARACTERIZATION OF CATION-
COUPLED TRANSPORTERS: THE H⁺-COUPLED Mg²⁺-
CITRATE TRANSPORTER, CitM, AND THE
Na⁺/SULFATE COTRANSPORTER, hNaSi-1**

by

Hongyan Li

DISSERTATION

Presented to the Faculty

of

THE UNIVERSITY OF TEXAS
GRADUATE SCHOOL OF BIOMEDICAL SCIENCES AT GALVESTON

in partial fulfillment

of the requirements

for the degree of

Doctor of Philosophy

THE UNIVERSITY OF TEXAS MEDICAL BRANCH
AT GALVESTON

May 2003

© Hongyan Li, May, 2003, All Rights Reserved

To my dearest parents and everyone else who ever gave me great help and
spirit support during my five-year life in Galveston

ACKNOWLEDGMENTS

I would like to thank the members of my dissertation committee: Ana M. Pajor, Steven C. King, Joel P. Gallagher, Luis Reuss and Steven A. Weinman for their helpful advice and support. Especially, I would like to appreciate my advisor, Ana M. Pajor, for her extreme patience, consideration and encouragement. Also, I would like to thank Steven A. Weinman for his continued encouragement and support.

I would like to thank Leoncio Vergara who helped me to finish the beautiful immunofluorescence image of oocytes.

Finally, I would like to thank our generous frogs who “donate” their thousands of black and yellow oocytes to the experiments performed in this dissertation.

MOLECULAR CHARACTERIZATION OF CATION- COUPLED TRANSPORTERS: THE H⁺-COUPLED Mg²⁺- CITRATE TRANSPORTER, CitM, AND THE Na⁺/SULFATE COTRANSPORTER, hNaSi-1

Publication No. _____

Hongyan Li M.S.

The University of Texas Medical Branch
at Galveston, 2003

Supervising Professor

Ana M. Pajor

In this dissertation, two cation-coupled transporters were characterized at the molecular level. The CitM transporter from *Bacillus subtilis* was functionally expressed and characterized in *E.coli* cells. The human NaSi-1 transporter (hNaSi-1) and mutants were functionally expressed in *Xenopus* oocytes. Antibodies against hNaSi-1 were used to investigate tissue distribution and *N*-glycosylation. The roles of two conserved serine residues in the transport function of hNaSi-1 were investigated using site-directed mutagenesis and radiotracer assay.

CitM belongs to a distinct gene family of secondary active transporters that includes the homologous citrate transporter CitH. In this dissertation, the K_m of CitM for the complex of Mg²⁺-citrate was about 300 μ M in the presence of saturating Mg²⁺ concentrations. CitM has a high substrate specificity for citrate. Other tested di- and tricarboxylic acids did not significantly inhibit citrate uptakes in the presence of Mg²⁺. However, CitM accepts complexes of citrate with metal ions other than Mg²⁺. The transport was inhibited in more alkaline but not in acidic transport buffer and also inhibited by ionophores that affect the transmembrane proton gradient, including FCCP, TCC and nigericin, suggesting a proton-coupled transport. Valinomycin did not affect the uptake

by CitM, supporting an electroneutral transport model in which one proton is coupled to the uptake of one complex of $(\text{Mg}^{2+}\text{-citrate})^{1-}$.

The low affinity Na^+ /sulfate cotransporter, hNaSi-1, belongs to a specific gene family of Na^+ -coupled transporters that includes the high affinity hSUT-1 and the Na^+ -coupled dicarboxylate (NaDC) transporters. Antibodies directed against a peptide of hNaSi-1 recognized the native protein in renal membranes as well as the recombinant protein expressed in *Xenopus* oocytes. There is a single *N*-glycosylation site, Asn-591, located at the extracellular C-terminus in hNaSi-1. Site-directed mutagenesis studies of Ser-260, Ser-288 and the surrounding amino acid residues of hNaSi-1 suggested that these residues are functionally required for hNaSi-1. MTSET inhibition on sulfate uptakes by the four mutants surrounding Ser-260, T257C, T259C, T261C and L263C, was dependent on the cation and substrate used. Since the presence of sodium and sulfate triggers conformational changes during the transport cycle of hNaSi-1, the cation and substrate dependence of MTSET inhibition suggest that these four substituted cysteines move during the transport cycle. Since the four mutated residues are located in TMD-5, this transmembrane domain is also likely to participate in the conformational movement during the transport cycle of hNaSi-1.

TABLE OF CONTENTS

	PAGE
CHAPTER 1: INTRODUCTION	1
CELL MEMBRANE TRANSPORT PROTEINS	1
BACTERIAL PROTON-COUPLED TRANSPORTERS	2
PROTON COUPLED Mg^{2+} -CITRATE TRANSPORTER, CitM	3
<i>Citrate</i>	4
<i>Mg^{2+}-citrate transport system in whole cells and membrane vesicles</i>	5
<i>Mg^{2+}-citrate transporter (CitM)</i>	7
<i>Regulation and physiological role of CitM transporter</i>	9
MAMMALIAN Na^{+} -COUPLED TRANSPORTERS	10
Na^{+} -COUPLED SULFATE TRANSPORTER, NaSi-1	11
<i>The NaDC/NaSi gene family</i>	11
<i>Na^{+}-dependent sulfate transporters</i>	12
AIMS OF STUDIES IN THIS DISSERTATION	22
<i>Aim 1: To characterize the function of CitM expressed in E.coli cells.</i>	22
<i>Aim 2: To make antibodies against hNaSi-1 and to determine its tissue distribution and N-glycosylation site.</i>	23
<i>Aim 3: To test the hypothesis that the region surrounding Ser-260 and Ser-288 in TMDs 5 and 6 are involved in cation and/or substrate binding by hNaSi-1.....</i>	23
CHAPTER 2: FUNCTIONAL CHARACTERIZATION OF CitM, THE Mg^{2+}-CITRATE TRANSPORTER.....	30
INTRODUCTION	30

METHODS	31
<i>Construction of the CitM expression vector</i>	31
<i>Preparation of cells</i>	32
<i>Transport assay</i>	33
<i>Permeabilization of cells</i>	35
<i>Protein assay</i>	35
<i>Data analysis</i>	36
RESULTS	37
<i>Time course of citrate uptake</i>	37
<i>Citrate uptakes as a function of citrate concentrations</i>	38
<i>Substrate specificity of CitM</i>	38
<i>Cation effects on citrate uptakes by CitM</i>	39
<i>Effect of pH on citrate uptakes by CitM</i>	40
<i>Effect of ionophores on citrate uptakes in CitM</i>	41
DISCUSSION	42
 CHAPTER 3: ANTIBODIES AGAINST hNaSi-1 FUSION PROTEIN: TISSUE DISTRIBUTION AND N-GLYCOSYLATION	 55
INTRODUCTION	55
METHODS	58
<i>Isolation of hNaSi-1 cDNA</i>	58
<i>Site-directed mutagenesis of N-glycosylation site</i>	59
<i>Preparation of GST-Si65 fusion protein</i>	60
<i>Preparation and purification of the antibodies</i>	62

<i>Western blotting</i>	62
<i>Preparation of brush border membrane vesicles</i>	63
<i>Transcription of cRNA</i>	64
<i>Preparation and injection of Xenopus oocytes</i>	64
<i>Biotinylation of Xenopus oocytes</i>	65
<i>Preparation and deglycosylation of Xenopus oocyte plasma membranes</i>	66
<i>Immunofluorescence of Xenopus oocytes and human tissue array</i>	67
<i>Radiotracer uptake assay</i>	68
<i>Transport data analysis</i>	69
RESULTS	69
<i>Preparation of the GST-Si65 fusion protein and anti-hNaSi-1 antibodies</i>	69
<i>Western blots of renal brush border membranes</i>	71
<i>Tissue distribution of hNaSi-1</i>	71
<i>N-glycosylation of hNaSi-1 expressed in Xenopus oocytes</i>	73
<i>Immunofluorescence of Xenopus oocytes expressing wild-type hNaSi-1 and mutants N591Y and N591A</i>	75
<i>Kinetics of sulfate uptakes by N591Y and N591A expressed in oocytes.</i>	76
DISCUSSION	77
<i>Specificity of the anti-hNaSi-1 antibodies</i>	78
<i>Tissue distribution</i>	80
<i>N-glycosylation of hNaSi-1</i>	82
CHAPTER 4: THE ROLES OF SERINE 260 AND SERINE 288 IN THE TRANSPORT FUNCTION OF hNaSi-1	94

INTRODUCTION	94
METHODS	98
RESULTS	101
<i>Location of mutated residues in the secondary structure model of hNaSi-1...</i>	101
<i>Functional characterization of S260A and S288A mutants</i>	101
<i>Substituted-cysteine mutagenesis surrounding Ser-260 and Ser-288 in hNaSi-1</i>	
.....	105
<i>Effect of Na⁺ on kinetics of sulfate uptakes</i>	109
DISCUSSION	110
CHAPTER 5: CONCLUSIONS	137
THE BACTERIAL Mg ²⁺ -CITRATE TRANSPORTER, CitM	137
THE HUMAN Na ⁺ -COUPLED SULFATE TRANSPORTER, hNaSi-1	141
<i>Preparation of antibodies against hNaSi-1 and application of antibodies to tissue</i>	
<i>distribution and N-glycosylation</i>	142
<i>Functional roles of Serines 260 and 288 in hNaSi-1</i>	145
APPENDIX: MUTAGENESIS OF CONSERVED TRYPTOPHAN AND	
ASPARTATE RESIDUES IN hNaSi-1	153
INTRODUCTION	153
METHODS	155
RESULTS	157
<i>Transport activity of the mutants expressed in Xenopus oocytes</i>	157
<i>Cell-surface expression of the mutants</i>	157
DISCUSSION AND FUTURE DIRECTION	158

REFERENCES	165
VITA	182

LIST OF FIGURES

Figure	Page
FIGURE 1.1 GENERAL CLASSIFICATIONS OF MEMBRANE TRANSPORT PROTEINS.....	25
FIGURE 1.2 METAL CITRATE COMPLEXES, TAKEN FROM REF. (32).....	26
FIGURE 1.3 DENDROGRAM TREE OF NaDC/NaSi TRANSPORTERS.	27
FIGURE 1.4 SIMPLIFIED TRANSPORT PATHWAY OF SULFATE IN RENAL PROXIMAL TUBULAR EPITHELIAL CELLS.	28
FIGURE 2.1 TIME COURSE OF THE UPTAKE OF 1 mM CITRATE BY CitM EXPRESSED IN <i>E.</i> <i>coli</i>	48
FIGURE 2.2 (A) CITRATE KINETICS OF CitM EXPRESSED IN <i>E. coli</i> DH5 α CELLS. (B) THE SAME UPTAKE DATA (SHOWN IN A) WERE EXPRESSED AS A FUNCTION OF THE Mg-CITRATE CONCENTRATION.	49
FIGURE 2.3 SUBSTRATE SPECIFICITY OF CitM EXPRESSED IN <i>E. coli</i>	50
FIGURE 2.4 EFFECTS OF VARYING Mg ²⁺ CONCENTRATIONS ON CITRATE TRANSPORT IN CitM EXPRESSED IN <i>E. coli</i> DH5 α CELLS.	51
FIGURE 2.5 CATION SPECIFICITY OF CitM EXPRESSED IN <i>E. coli</i>	52
FIGURE 2.6 EFFECT OF EXTERNAL pH ON UPTAKE OF CITRATE BY CitM EXPRESSED IN <i>E.</i> <i>coli</i>	53
FIGURE 2.7 EFFECT OF IONOPHORES ON CITRATE UPTAKE BY CitM EXPRESSED IN <i>E. coli</i>	54
FIGURE 3.1 SECONDARY STRUCTURE MODEL OF hNaSi-1 CONTAINING 11 TRANSMEMBRANE DOMAINS.....	86

FIGURE 3.2 EXPRESSION AND PURIFICATION OF GST AND GST-Si65 FUSION PROTEIN..	87
FIGURE 3.3 WESTERN BLOTS OF RAT AND PIG RENAL BRUSH BORDER MEMBRANE VESICLES..	88
FIGURE 3.4 IMMUNOFLUORESCENCE OF HUMAN TISSUES..	89
FIGURE 3.5 WESTERN BLOT OF DEGLYCOSYLATION OF PLASMA MEMBRANES FROM <i>XENOPUS</i> OOCYTES EXPRESSING WILD-TYPE hNaSi-1 AND THE GLYCOSYLATION SITE MUTANT, N591Y.	90
FIGURE 3.6 WESTERN BLOT OF BIOTINYLATED <i>XENOPUS</i> OOCYTES EXPRESSING WILD- TYPE hNaSi-1 OR THE GLYCOSYLATION SITE MUTANTS, N591Y AND N591A..	91
FIGURE 3.7 IMMUNOFLUORESCENCE OF <i>XENOPUS</i> OOCYTES EXPRESSING WILD-TYPE hNaSi-1 AND THE GLYCOSYLATION SITE MUTANTS, N591Y AND N591A.	92
FIGURE 3.8 KINETICS OF SULFATE UPTAKES BY <i>XENOPUS</i> OOCYTES EXPRESSING WILD- TYPE hNaSi-1 AND THE GLYCOSYLATION SITE MUTANTS, N591Y AND N591A..	93
FIGURE 4.1 THE AMINO ACID RESIDUES OF hNaSi-1 MUTATED IN THIS CHAPTER..	121
FIGURE 4. 2 WESTERN BLOT AND UPTAKES OF <i>XENOPUS</i> OOCYTES EXPRESSING WILD- TYPE hNaSi-1 AND THE MUTANTS, S260A AND S288A..	122
FIGURE 4.3 KINETICS OF SULFATE UPTAKES BY <i>XENOPUS</i> OOCYTES EXPRESSING WILD- TYPE hNaSi-1 AND THE MUTANTS, S260A AND S288A..	123
FIGURE 4.4 Na ⁺ -ACTIVATION OF SULFATE UPTAKES BY <i>XENOPUS</i> OOCYTES EXPRESSING WILD-TYPE hNaSi-1 AND THE MUTANTS, S260A AND S288A.....	124
FIGURE 4.5 CATION SELECTIVITY OF WILD-TYPE hNaSi-1 AND THE MUTANTS, S260A AND S288A, EXPRESSED IN <i>XENOPUS</i> OOCYTES.....	125

FIGURE 4.6 SUBSTRATE SPECIFICITY OF WILD-TYPE hNaSi-1 AND THE MUTANTS, S260A AND S288A, EXPRESSED IN <i>XENOPUS</i> OOCYTES.	126
FIGURE 4.7 SULFATE UPTAKES BY <i>XENOPUS</i> OOCYTES EXPRESSING THE CYSTEINE MUTANTS SURROUNDING Ser-260 AND Ser-288 IN hNaSi-1.....	127
FIGURE 4.8 WESTERN BLOTS OF BIOTINYLATED <i>XENOPUS</i> OOCYTES EXPRESSING WILD-TYPE hNaSi-1 AND THE CYSTEINE MUTANTS..	128
FIGURE 4.9 MTSET SENSITIVITY OF hNaSi-1 CYSTEINE MUTANTS EXPRESSED IN <i>XENOPUS</i> OOCYTES.	129
FIGURE 4.10 CONCENTRATION DEPENDENCE OF MTSET INHIBITION OF SULFATE UPTAKES BY T257C, T259C, T261C, AND L263C.	130
FIGURE 4.11 CATION AND SUBSTRATE DEPENDENCE OF MTSET INHIBITION OF SULFATE UPTAKES BY T257C, T259C, T261C, AND L263C.....	131
FIGURE 4.12 CATION SELECTIVITY OF T257C, T259C, T261C, AND L263C EXPRESSED IN <i>XENOPUS</i> OOCYTES..	132
FIGURE 4.13 EFFECT OF Na ⁺ ON SUBSTRATE KINETICS OF hNaSi-1 EXPRESSED IN <i>XENOPUS</i> OOCYTES.	133
FIGURE 4. 14 Na ⁺ -DEPENDENCE OF K_M AND V_{MAX} OF SULFATE UPTAKES BY WILD-TYPE hNaSi-1 EXPRESSED IN OOCYTES..	134
FIGURE 4.15 SUMMARY OF THE MTSET SENSITIVE RESIDUES SURROUNDING Ser-260 IN TMD 5 OF hNaSi-1.....	135
FIGURE 4.16 A SIMPLIFIED 6-STATE ORDERED BINDING KINETIC MODEL FOR THE hNaSi-1 TRANSPORTER.....	136

FIGURE A.1 THE ASPARTATE AND TRYPTOPHAN RESIDUES MUTATED IN hNaSi-1....	161-
162	
FIGURE A.2 SULFATE UPTAKES OF <i>XENOPUS</i> OOCYTES EXPRESSING MUTANTS OF	
TRYPTOPHAN AND ASPARTATE RESIDUES IN hNaSi-1..	163
FIGURE A.3 WESTERN BLOT OF BIOTINYLATED <i>XENOPUS</i> OOCYTES EXPRESSING WILD-	
TYPE AND TRPTOPHAN TO ALANINE MUTANTS OF hNaSi-1..	164

LIST OF TABLES

Table	Page
TABLE 1.1 MEMBERS OF THE NaDC/NaSi TRANSPORTER FAMILY	29
TABLE 4.1 OLIGONUCLEOTIDE PRIMERS USED FOR PREPARING CYSTEINE MUTANTS OF Ser-260, Ser-288 AND THE 12 SURROUNDING RESIDUES IN TMDs 5 AND 6 OF THE hNaSi-1 TRANSPORTER.	100
TABLE 5.1 COMPARISON OF FUNCTIONS OF WILD-TYPE hNaSi-1 WITH THE TWO ALANINE MUTANTS, S260A AND S288A.	152
TABLE 5.2 SUMMARY OF CATION/SUBSTRATE DEPENDENCE OF MTSET INHIBITION OF SULFATE UPTAKES BY THE FOUR CYSTEINE MUTANTS, T257C, T259C, T261C, AND L263C.	152
TABLE A.1 OLIGONUCLEOTIDE PRIMERS USED FOR PREPARING MUTANTS OF TRYPTOPHAN AND ASPARTATE RESIDUES OF hNaSi-1.....	156

LIST OF ABBREVIATIONS

cDNA	complementary deoxyribonucleic acid
CitH	<i>Bacillus subtilis</i> Ca ²⁺ -citrate transporter
CitM	<i>Bacillus subtilis</i> Mg ²⁺ -Citrate transporter
cRNA	complementary ribonucleic acid
DNA	deoxyribonucleic acid
EGTA	Ethyleneglycol-bis[-aminoethyl]-N, N, N', N'-tetraacetic acid
ELISA	Enzyme-Linked Immunosorbent Assay
FCCP	carbonyl cyanide <i>p</i> -trifluoro-methoxyphenylhydrazone
GCG	Genetics Computer Group
GST	Glutathione S-transferase
GST-Si65	fusion protein of GST with 65 amino acid peptide of Human Na ⁺ /sulfate cotransporter
HEPES	N-2-Hydroxyethylpiperazine-N'-2-ethanesulfonic acid
hNaSi-1	human Na ⁺ /sulfate cotransporter
IgG	Immunoglobulin class G
IPTG	Isopropyl-β-thiogalactopyranoside
kDa	kilodalton
mNaSi-1	mouse Na ⁺ /sulfate cotransporter
mRNA	messenger ribonucleic acid
MS-222	3-aminobenzoic acid ethyl ester
MTSEA	2-aminoethylmethane thiosulfonate
MTSES	2-sulfonatoethylmethane thiosulfonate
MTSET	2-trimethylammonioethylmethane thiosulfonate
NA	Numerical Aperture
NP-40	Nonidet P 40 Substitute

PBS	Phosphate-buffered saline
PCR	Polymerase Chain Reaction
PIPES	Piperazine-N,N'-bis(2-ethanesulfonic acid)
PMSF	Phenylmethanesulfonyl fluoride
PNGase F	Peptide:N-glycosidase F
RNA	Ribonucleic acid
RT-PCR	Reverse Transcription-Polymerase Chain Reaction
TMD	Transmembrane domain
SDS-PAGE	Sodium dodecyl sulfate Polyacrylamide gel electrophoresis
Sulfo-NHS-LC-Biotin	Sulfosuccinimidyl-6-(biotinamido) hexanoate
TCC	Trichlorocarbanilide
UTR	Untranslated region

CHAPTER 1: INTRODUCTION

This dissertation describes the characterization of two cation-coupled transporters at the molecular level. In the first study (Chapter 2), the bacterial proton-coupled Mg^{2+} -citrate transporter, CitM, was characterized in *E.coli* cells. In the second (Chapter 3) and third (Chapter 4) studies, the human Na^{+} -coupled sulfate transporter, hNaSi-1, and its mutants were expressed and investigated in *Xenopus* oocytes. The following background introduction will start from a brief general information of membrane transport proteins and then focus on bacterial proton-coupled transporters and mammalian Na^{+} -coupled transporters.

Cell membrane transport proteins

The cell membrane, with a fluid lipid-bilayer mosaic structure, is essential for all living organisms since it acts like a barrier to protect cells and control the communication between cells and the outside environment. Transmembrane proteins spanning the lipid-bilayer membrane play a key role in cell membrane functions by selectively transporting various substances into and out of cells. Based on recent genome sequencing analysis, about 20 to 40% of the gene products are predicted to be transmembrane proteins (31). Most of these transmembrane proteins are directly or indirectly related to the transport across membranes (118). According to the latest transport commission (TC) system of classification (136; 119; 118), these proteins can be classified as illustrated in [Figure 1.1](#). There are two major types of transport

systems: channels and carriers. Channel proteins form a hydrophilic pore usually with an α -helix or β -strand structure, allowing substances to move down their electrochemical gradients. Based on energy sources, transporter or carrier proteins can be classified into three subtypes: uniporters (facilitated diffusion carriers), primary active transporters and secondary active transporters. The energy for primary active transport process is provided by chemical reactions such as the hydrolysis of adenosine triphosphate (ATP), or by light absorption or mechanical movement. The secondary active transporters accumulate solutes against their electrochemical gradients by using the electrochemical gradient of ions, which is created by the primary active transport process. Among secondary active transporters, there are two major subtypes: symporters (or cotransporters) and antiporters (or exchangers), which transport solute and coupled ions in the same and opposite directions, respectively.

Bacterial proton-coupled transporters

The most distinct feature of bacterial cells is the existence of cell wall (peptidoglycan layer) located outside of cytoplasmic membrane. Gram-negative bacteria such as *Escherichia coli* have another outer membrane (lipopolysaccharide layer) outside of cell wall (4). Although there are some transport proteins such as porins located on the outer membrane, most of the membrane transport proteins exist on the inner cytoplasmic membrane of bacteria cells. The energy source for most of cation-coupled transporters of

bacterial cells comes from the electrochemical gradient of proton or sodium. One of the best studied bacterial membrane transport proteins is the proton-coupled lactose permease from *E.coli* cells (see review (52)). The lactose permease encoded by *lac Y* gene is a secondary active transport protein which transports β -galactosides across the inner cytoplasmic membrane into *E.coli* cells by using the proton electrochemical gradient (or proton motive force). This transporter consists of 417 residues and is predicted to contain 12 transmembrane domains based on hydropathy analysis of the amino acid sequence (18; 53). The right-side-out membrane vesicle studies suggested an ordered transport model in which lactose is released prior to the proton (52). Site-directed mutagenesis studies found that three residues Arg-302, His-322, and Glu-325 are likely to be involved in proton binding (113). Cysteine-scanning mutagenesis studies showed that Glu-126 and Arg-144 may participate in substrate binding and recognition (33). The proton-coupled Mg^{2+} -citrate transporter (CitM) from *Bacillus subtilis* studied in this dissertation is also predicted to have 12 transmembrane domains, and has been functionally expressed in *E.coli*. Previous studies of the lactose permease can provide useful information for the future studies of the structure-function relationships of CitM.

Proton coupled Mg^{2+} -citrate transporter, CitM

The CitM transporter is found in *Bacillus subtilis* and responsible for taking up citrate as a carbon and energy source for the bacteria. In this

section, firstly, chemical features of citrate is briefly introduced, and then the discussion is focused on previous studies of Mg^{2+} -citrate transport systems in whole cells and membrane vesicles as well as on the functional studies of cloned CitM transporter. Finally, the regulation of *citM* gene expression is briefly discussed.

Citrate

Citrate (citric acid), a six-carbon acid, has three negatively charged carboxylic groups at neutral pH ([Figure 1.2](#)). As an intermediate in the Krebs cycle (or citric acid cycle), citrate is an important carbon and energy source for bacteria. Citrate can also bind many divalent metal ions, such as Mg^{2+} , Mn^{2+} and Ca^{2+} (37). There are three different forms of metal-citrate complexes: bidentate, tridentate and binuclear complex (32). Figure 1.2 only shows the two former complexes. The binuclear complex is less common and more complicated, involving two citrate molecules and two metal ions thus will not be mentioned here. Both bidentate and tridentate complexes contain one metal ion and one citrate. In the bidentate complex, the central and one terminal carboxylic acid groups of citrate bind a metal ion and another terminal carboxylic acid group and the hydroxyl group are free. In the tridentate complex, the hydroxyl group of citrate is also involved in binding a metal ion besides the two carboxylic acid groups. Divalent metal ions including Mg^{2+} , Ca^{2+} and Ni^{2+} can form bidentate complexes with citrate, whereas Cu^{2+} and Cd^{2+} usually bind citrate in tridentate form (32).

Mg²⁺-citrate transport system in whole cells and membrane vesicles

Some bacteria only transport free citrate while other bacteria including *Pseudomonas fluorescens* (73), *Bacillus subtilis* (11; 141) and a *Klebsiella* species (17) are found to be able to transport metal-citrate complexes across inner cytoplasmic membrane into cell. The Mg²⁺-citrate transport system of *B. subtilis* is the best studied one.

Studies of Mg²⁺-citrate transport system in whole cells

In 1971, Willecke's group found that the active citrate transport in whole cell *B. subtilis* was a citrate-inducible system with an apparent K_m of 2.3 mM for citrate (142). Two years later, Willecke's group further found that citrate transport in *B. subtilis* was dependent on the presence of Mg²⁺, or other divalent metal ions such as Mn²⁺, Co²⁺, and Ni²⁺ (141). Willecke proposed three possibilities for the simultaneous transport of citrate and Mg²⁺: two separate carrier systems transport citrate and Mg²⁺ at the same time; only one carrier system transports citrate and Mg²⁺ but they bind the transport protein at two different sites; citrate and Mg²⁺ are transported as a complex by one transport system (141). According to Willecke's experiments, citrate-dependent Mg²⁺ uptake was only observed in citrate induced cells, and the mutant which lacked the high-affinity Mg²⁺ transport system also had similar citrate-Mg²⁺ transport as the parent cell, suggesting that the citrate-dependent Mg²⁺ uptake was not due to the high affinity Mg²⁺ transport system but most likely due to another Mg²⁺ transport system which can be induced by citrate (141). Furthermore, the citrate-dependent Mg²⁺ transport ($K_m = 0.45$ mM and $V_{max} =$

145 $\mu\text{moles/min/g}$ of dry weight) and the Mg^{2+} -dependent citrate transport ($K_m = 0.55 \text{ mM}$ and $V_{max} = 123 \text{ } \mu\text{moles/min/g}$ of dry weight) had similar kinetic properties, indicating that the two substrates are more likely to be taken up as a complex than at two different binding sites of the protein. Willecke's studies also suggested that the complex was likely to be formed by one citrate and one Mg^{2+} ion thus having one net negative charge. Willecke's group also observed that the Mg^{2+} -citrate transport could be inhibited by a potassium ionophore, valinomycin, but restored by the addition of extracellular K^+ , and suggested that high intracellular K^+ concentration was probably required for the transport. However, my studies in Chapter 2 did not show inhibition effect of valinomycin on Mg^{2+} -citrate transport. In 1974, another study was performed also by Willecke's group using a citrate analogue (2-Fluoro-L-erythro-[3,4,5,6- $^{14}\text{C}_4$] citrate), which could be transported by the same Mg^{2+} -citrate transport system but not metabolized in the cell, and similar kinetic properties for Mg^{2+} ($K_m = 0.4 \text{ mM}$) and for citrate analogue ($K_m = 0.3 \text{ mM}$) were obtained (86). However, the unresolved question in these studies was: if the Mg^{2+} -citrate transport was electrogenic, how the bacteria compensated for the inward negative flow of the complex. In my studies, the results support an electroneutral transport model.

Studies of Mg^{2+} -citrate transport system in membrane vesicles

In 1983, Bergsma and Konings' studies of citrate transport in membrane vesicles from *B. subtilis* found that the metal citrate complex is the transported substrate and the transport is driven by the proton-motive force (11). According to Bergsma and Konings' studies, citrate uptakes were dependent on Mn^{2+} ,

Zn^{2+} , Mg^{2+} , Ba^{2+} , Be^{2+} , Ca^{2+} , Cu^{2+} , Co^{2+} , or Ni^{2+} and no measurable uptakes were seen in the absence of divalent metal ions. The apparent K_m for citrate transport in membrane vesicles was 40 μM in the presence of 10 mM Mg^{2+} and the K_m for Mg^{2+} was 250 μM at a citrate concentration of 125 μM . Bergsma and Konings' studies also showed that accumulation of Ca^{2+} in cell only occurred in the presence of citrate, and that citrate and Ca^{2+} were taken up in the same quantities, which was consistent with Willecke's suggestion that citrate is likely to be transported as a complex with a divalent metal ion (141). Moreover, the citrate uptake was affected by two ionophores, valinomycin (a K^+ ionophore) and nigericin (K^+/H^+ exchanger) and inhibited by an uncoupler molecule, carbonylcyanide *p*-trifluoromethoxy-phenylhydrazone, indicating that the metal-citrate transport is likely to be driven by proton motive force. Bergsma and Konings' studies also suggested that the transport was coupled with one proton at pH 4.7 and two protons at pH 8.0 (11). However, the responsible transport proteins for the transport of Mg^{2+} -citrate complex was not yet known at that time.

Mg^{2+} -citrate transporter (CitM)

In 1996, the gene coding for a Mg^{2+} -citrate transporter was isolated from *B. subtilis* and named CitM by Lolkema's group (14). At the same time another gene coding for an unknown protein, which has 60% amino acid sequence identity with CitM was also isolated from *B. subtilis* and called CitH (14). The length of the open reading frames for CitM and CitH are 1,302 bp and 1,278 bp, respectively, and the amino acid sequence analysis of CitM and CitH

predicted 12 transmembrane domains. Functional studies in *E.coli* cells transformed with *citM* gene showed that the citrate uptake was strictly dependent on Mg^{2+} , which agrees with the previous studies in whole cells and membrane vesicles. On the contrary, the citrate uptake in *E.coli* cells expressing CitH was independent of Mg^{2+} . Na^+ ions were also tested but did not show effect on the citrate transport for either of the two transporters. Valinomycin resulted in a slight decrease in citrate uptakes while nigericin resulted in a significant reduction of citrate uptakes for both of the two transporters. Based on these results, it seemed that CitM transports the monovalent Mg^{2+} -citrate complex whereas CitH transports citrate alone and both of these transporters were electrogenic. However, four years later, Lolkema's group reported a contradictory result that CitH transported a metal citrate complex but not free citrate (61). The metal ion dependence of CitH was restudied and it was found that CitM and CitH had complementary metal ion specificity (61). CitM transports citrate only with Mg^{2+} , Ni^{2+} , Mn^{2+} , Co^{2+} , and Zn^{2+} but not Ca^{2+} , Ba^{2+} , and Sr^{2+} whereas CitH transports citrate with Ca^{2+} , Ba^{2+} , and Sr^{2+} but not Mg^{2+} , Ni^{2+} , Mn^{2+} , Co^{2+} , and Zn^{2+} (61). Citrate uptakes by CitH in the absence of divalent metal ions, which was reported previously, was probably due to residual metal ions such as Ca^{2+} in the cell resuspension. The citrate dependence of Ni^{2+} and Ca^{2+} uptakes in *E.coli* expressing CitM and CitH agreed with Willecke's suggestion that the transported substrate is likely to be the metal ion-citrate complex (141). The kinetic constants of both transporters for citrate in the presence of different metal ions were similar, from 33 to 63 μM , however, the maximum uptake rates for citrate were different (61). Co^{2+}

and Mn^{2+} produced the highest and lowest maximum uptake rates for CitM, respectively, whereas CitH showed the highest maximum uptake rate with Ca^{2+} (61). Although CitM had been cloned and compared to CitH, the functional characterization of CitM was not yet completed and also the transport mechanism (or structure of substrate and cation binding sites) of CitM is almost unknown.

Regulation and physiological role of CitM transporter

More than 30 years ago, Willecke and Pardee observed that citrate uptake in *B. subtilis* could be induced by citrate but inhibited by glucose (142). It was not until recently that the regulation of Mg^{2+} -citrate transporters was studied at the transcriptional level (140; 145). Expression of the *citM* gene is positively regulated by two-component regulatory proteins CitS and CitT, which are sensitive to the presence of citrate in the medium (145). Therefore, Mg^{2+} -citrate transport is inducible in citrate containing medium. On the other hand, Mg^{2+} -citrate transport can be inhibited in medium containing glucose, glycerol, inositol, or succinate-glutamate, indicating that the repression of *citM* gene expression is probably related to the carbon catabolite repression system (140; 145). Therefore, it seemed that expression of CitM is strictly dependent on the medium components. The cotransported metal ions may have some physiological roles in biological activities of bacterial cells. For example, Ni^{2+} serves as a cofactor for some enzymatic reactions (61). Since CitM can transport complex of citrate with not only Mg^{2+} but also some other divalent heavy metal ions such as Zn^{2+} , Co^{2+} , and Ni^{2+} , bacterial cells expressing CitM

have been applied to remove toxic heavy metal ions from radioactive or industry wastes (32; 51; 113). However, recent studies found that under high concentrations of metal ions, CitM could also increase the toxicity of heavy metal ions in bacterial cells in the presence of citrate thus inducing the resistance and/or tolerance of bacteria to toxic metal ions (60). One way to solve the problem is to express CitM in a heterologous system which is more resistant to metal ions (60).

Mammalian Na⁺-coupled transporters

Most secondary active transporters in mammalian cells transport substrates by coupling with Na⁺ or H⁺, whereas some transport processes are also coupled with Cl⁻ or K⁺. In this section, the Na⁺-coupled transporters in epithelial cells are discussed. Mammalian epithelial cells form an epithelial sheet that lines gastrointestinal tracts or tubules in some internal organs such as kidney. Epithelial cell membranes are divided into two separate domains: the apical membrane (facing the lumen side) and the basolateral membrane (facing the blood side). Membrane transport proteins distributed on the two domains are usually different to allow vectorial transport from the lumen to blood side. There are various Na⁺-coupled transporters distributed on the apical membrane of epithelial cells of kidney or small intestine. These transporters play an important role in absorption or reabsorption of nutrients from the lumen to blood side via secondary active transport process. Some of these transporters have been intensively studied, including the Na⁺/glucose

cotransporter (SGLT1), Na^+ /phosphate cotransporter (NaPi-2), and Na^+ /dicarboxylate cotransporter (NaDC-1). The Na^+ /sulfate cotransporter (NaSi-1) studied in this dissertation belongs to the same transporter gene family as the Na^+ /dicarboxylate cotransporter.

Na^+ -coupled sulfate transporter, NaSi-1

The NaDC/NaSi gene family

As shown in [Figure 1.3](#), the low affinity Na^+ -dependent sulfate transporter or Na^+ /sulfate cotransporter, NaSi-1, belongs to a specific gene family (called NaDC/NaSi gene family in this dissertation), which also includes the high affinity Na^+ -dependent sulfate transporter, hSUT-1, and the Na^+ /dicarboxylate cotransporters, NaDC-1, NaDC-2 and NaDC-3. Two recently isolated transporters, a Na^+ /citrate cotransporter (NaCT) (49) and a Na^+ -independent dicarboxylate and citrate transporter (Indy), which is encoded by a longevity gene *Indy* (“I’m not dead yet”), were also included in this family (48).

In past years, many members of the NaDC/NaSi gene family have been isolated and functionally characterized. The human NaDC/NaSi gene family is also called SLC13 (solute carrier family 13). [Table 1.1](#) summarizes transporter members in the NaDC/NaSi gene family. NaDC-1 is the best studied among Na^+ /dicarboxylate cotransporters (see review (89)). The gene coding for NaDC-1 was originally isolated from a rabbit kidney cDNA library by functional expression in *Xenopus* oocytes (87). Pajor’s group proposed a secondary

structure model for NaDC-1, which contains 11 putative transmembrane domains (TMDs) with the amino and carboxy terminals exposed to inside and outside of cell, respectively. There is direct experimental evidence for this model. Experiments performed with antifusion protein antibodies against NaDC-1 showed that the C-terminal residue, Asn-578, was used for glycosylation, indicating that the C-terminus of NaDC-1 is exposed to the extracellular side of cell (95). Also, results from immunofluorescence experiments of NaDC-1 showed that the N-terminus and hydrophilic loop between transmembrane 4 and 5 are located intracellularly (148). Therefore, the secondary structure model containing 11 TMDs is used for the transporter members in the NaDC/NaSi gene family. However, more experiments are needed to give a more detailed profile of the secondary structure model for the gene family. The following discussion will focus on the Na^+ -dependent sulfate transporter.

Na^+ -dependent sulfate transporters

Sulfate anions and homeostasis

Sulfate (SO_4^{2-}) is a divalent anion formed by one sulfur (S^{6+}) and four tetrahedrally bound oxygen molecules (O^{2-}). This inorganic anion is a very important element in humans because of its involvement in many physiological and pathophysiological processes (9; 76; 82; 83). Sulfate plays a key role in sulfate conjugation reactions (termed sulfations or sulfonations), which are involved in the biotransformation and detoxification of many exogenous compounds (such as analgesics, anti-inflammatory agents, adrenergic

stimulants and blockers, and steroids) and endogenous compounds (such as bile acids). Sulfation is also essential for the biological activities of many endogenous compounds such as cholecystokinin, gastrin, heparin, and heparin sulfate. Also, sulfate is involved in the biosynthesis of structural components of membranes and tissues, such as sulfated glycosaminoglycans (major components of cartilage and other tissues). Therefore, sulfate anions are essential for maintaining normal physiological functions in humans. For example, previous studies found that gene mutations in *Dystrophic Dysplasia Sulfate Transporter* (DTDST), a sulfate/chloride anion exchanger, which is located in many tissues especially small intestine and cartilage, can cause severe osteochondrodysplasia because of undersulfation of cartilage proteoglycans (a core protein plus glycosaminoglycans) (9).

Normally, the plasma concentration of sulfate in the human body is from 0.47 mM at birth to 0.33 mM in adulthood (9). Sulfate homeostasis is partially controlled by sulfate reabsorption via renal proximal tubules. Previous studies identified two renal sulfate transport systems: Na^+ -dependent sulfate transporter (NaSi-1) and Na^+ -independent sulfate/anion exchanger (Sat-1), which are located on the apical and basolateral membranes of renal proximal tubular epithelial cells, respectively (9). Sat-1 belongs to a different gene family than NaSi-1. [Figure 1.4](#) illustrates a simplified pathway of sulfate reabsorption across renal proximal tubular epithelial cells. Sulfate is absorbed by NaSi-1 across the apical membrane into cell and then exited via Sat-1 across the basolateral membrane into blood circulation. Therefore, NaSi-1 and Sat-1 play

very important roles in maintaining the sulfate homeostasis in the human body. Another way for the absorption of sulfate by the human body is small and large intestines (82), however, no experimental evidence has been reported for the location of human NaSi-1 proteins in intestine.

Na⁺/sulfate cotransport in isolated tubules, membrane vesicles and cell lines

In past years, many studies have been performed on Na⁺-dependent sulfate transport process in membrane vesicles and cultured cells. In 1960, stop flow studies in dogs showed that sulfate reabsorption occurred in renal proximal tubules (43). In about 1980's, studies in isolated proximal tubules found that sulfate reabsorption was dependent on Na⁺ and the activation of Na⁺/K⁺ ATPase (84). Further studies of rabbit, rat renal or ileal brush border and basolateral membrane vesicles identified two secondary active transport systems for reabsorption of sulfate: Na⁺-dependent sulfate transport across the brush border membrane and Na⁺-independent sulfate/anion exchange across the basolateral membrane (1; 7; 40; 70; 71; 72; 105; 122; 133).

Studies on Na⁺-dependent sulfate transport in rabbit renal brush border membrane vesicles (BBMVs) showed an apparent K_m from 0.6 - 0.9 mM for SO₄²⁻ in the presence of 100 mM Na⁺ and a K_m from 36 to 50 mM for Na⁺, with a Hill coefficient of 1.5 or 1.6 (122; 133). Rabbit ileal BBMVs has a similar K_m of 0.5 mM for sulfate in the presence of 100 mM Na⁺ (1). It was also found that the Na⁺/ sulfate cotransport system in rabbit renal BBMVs could absorb other similar divalent anions such as sulfite (SO₃²⁻), thiosulfate (S₂O₃²⁻), selenate

(SeO_4^{2-}), molybdate (MoO_4^{2-}), chromate (CrO_4^{2-}) and tungstate (WO_4^{2-}) but did not transport phosphate (HPO_4^{2-}) (122). Most of these studies proposed an electroneutral mechanism for Na^+ /sulfate cotransport. However, later studies of the cloned NaSi-1 found that the transport was electrogenic (19). Although kidney and small intestine are believed to be the major sulfate reabsorption or absorption sites, sulfate transport has also been found in some other organs such as liver, lung, and brain but the functional roles are still unknown (15; 76; 137).

So far there has only been one report on Na^+ / sulfate cotransport in a mammalian cell line, the OK/E cells (a clonal subline of opossum kidney cells) (132). Interestingly, properties of Na^+ /sulfate cotransport in these cells are somewhat different from renal BBMV Na^+ / sulfate cotransport. Na^+ -dependent sulfate uptake in OK/E cells had a relatively higher K_m of 2.4 mM for sulfate and a lower $K_{0.5}^{\text{Na}^+}$ of 23 mM for Na^+ with a similar Hill coefficient of 1.5 compared with the results from membrane vesicle studies (132). The transport of sulfate in OK/E cells was significantly stimulated by Na^+ and slightly stimulated by Li^+ but not by other monovalent cations (133). The most interesting observation is the sensitivity of Na^+ / sulfate cotransport in OK/E cells to inhibition by 4,4'-diisothiocyanostilbene-2,2'-disulfonic acid (DIDS, an anion-exchange inhibitor), which is usually only seen in Na^+ -independent sulfate transport (sulfate/anion exchange) but not in Na^+ -dependent sulfate transport in membrane vesicles. It is not yet clear about the difference in Na^+ / sulfate cotransport between OK/E cells and membrane vesicles.

Na⁺-coupled sulfate transporters (NaSi-1)

(i) Isolation of cDNA for Na⁺-dependent sulfate transporters

The first mammalian sulfate transporter cDNA was isolated from rat kidney by Murer's group in 1993, and some basic functional studies of the cloned transporter (rNaSi-1) expressed in *Xenopus* oocytes were also reported in the same paper (78). About two years ago, NaSi-1 was isolated from mouse and human kidney cDNA libraries and termed mNaSi-1 and hNaSi-1, respectively (8; 65). Sequence alignments show that rNaSi-1 shares 94% and 83% amino acid identity with mNaSi-1 and hNaSi-1, respectively (76). The mouse *Nas1* gene has been localized on mouse chromosome 6, spanning ~75 kb with 15 exons and 14 introns (8). The corresponding human gene (SLC13A1) has been localized on human chromosome 7 q31-q32 and also contains 15 exons and 14 introns spanning ~83 kb (65). The cDNA coding for the high affinity Na⁺-dependent sulfate transporter was isolated from human high endothelial venule (HEV) cDNA library and termed SUT-1, which shares about 50% amino acid sequence identity with rNaSi-1. The gene coding for SUT-1 mapped to human chromosome 7q33 (36). The human SUT-1 transporter has a relatively high affinity for sulfate compared with the NaSi-1 transporter and its tissue distribution is highly restricted in human HEV endothelial cells and placenta (36).

(ii) Secondary structure model of NaSi-1

All of the NaSi-1 cDNAs contain 2,200 to 3,800 nt encoding proteins of ~595 amino acid residues. The estimated molecular mass is about 66 kDa. Hydropathy analysis of the amino acid sequences of rat, mouse, and human NaSi-1 suggests a secondary structure model containing 8 - 13 transmembrane domains. The model of rat NaSi-1 contained 8 membrane-spanning domains (78; 85), whereas later studies of mouse and human NaSi-1 proposed a model containing 13 putative transmembrane segments (8; 65). To date, however, no direct experimental evidence has been shown to support above putative secondary structure models for NaSi-1. As mentioned before, studies by Pajor's group support an 11-TMD model for rbNaDC-1(95; 148). Since the hNaSi-1 transporter shares 47% sequence identity with rbNaDC-1 and also the hydropathy analysis of hNaSi-1 was similar to that of rbNaDC-1, hNaSi-1 studied in this dissertation is also predicted to contain 11 transmembrane domains.

According to protein sequence analysis of NaSi-1 transporters, there are three consensus *N*-glycosylation sequences in rNaSi-1 (Asn-140, Asn-174, and Asn-591) and mNaSi-1 (Asn-140, Asn-174, and Asn-590), and four in hNaSi-1 (Asn-140, Asn-174, Asn-207, and Asn-591). Previous studies of rNaSi-1 showed that *in vitro* translation of rNaSi-1 cRNA with rabbit reticulocyte lysate produced a protein band at 59 kDa, which was increased by 3 kDa in the presence of microsomes, indicating that at least one *N*-glycosylation site is used in rNaSi-1 transporter (78). So far this result has been the only published experimental evidence for *N*-glycosylation site in the NaSi-1 transporter. For

NaDC-1, previous studies found a single *N*-glycosylation site at Asn-578, which is located at the extracellular C-terminus of NaDC-1 (95). The residue, Asn-578, is conserved in all members of the NaDC/NaSi-1 gene family, and the counterpart residue in hNaSi-1 is Asn-591. Therefore, Asn-591 was mutated in this dissertation to determine the *N*-glycosylation site in hNaSi-1.

(iii) Functional characterization of NaSi-1

Most of the functional studies on NaSi-1 were performed in *Xenopus* oocyte expression system using radiotracer assays. All of the cloned NaSi-1 have a low affinity for both sulfate and Na⁺ with a K_m for sulfate from 0.2 to 0.6 mM and a K_{Na} from 17 mM to 24 mM for Na⁺ (8; 65; 78; 85). The Hill coefficient for Na⁺ from 2 to 3 is consistent with a stoichiometry of 3 Na⁺: 1 SO₄²⁻. Similar to the results from membrane vesicle studies, NaSi-1 has broad substrate specificity i.e. NaSi-1 can also transport substrates which have similar chemical structures to sulfate such as thiosulfate, selenate, molybdate and tungstate (65). L-arginine, L-leucine or D-glucose cannot be transported by NaSi-1 (78). Phosphate, oxalate, cholate, probenecid (an anion exchanger inhibitor) and DIDS had no significant inhibition on the transport by NaSi-1 (77; 78). These properties agree with those of the Na⁺/ sulfate cotransport in BBMVs (71; 84; 122; 133).

The rNaSi-1 has also been characterized in *Xenopus* oocytes using the two-electrode voltage-clamp technique (19). The voltage-clamp recording showed a sulfate-induced Na⁺-dependent inward current in oocytes injected with rNaSi-1 cRNA. The $K_{0.5}$ for sulfate and Na⁺ were 90 μ M and 70 mM,

respectively, at a holding potential of -50 mV, showing a higher affinity for sulfate compared with radiotracer uptake studies. The Hill coefficients for sulfate and Na^+ were 1 and 2.8, respectively, consistent with the coupling of three Na^+ ions with one sulfate anion. This was the first report to show that Na^+ -coupled sulfate transport is electrogenic rather than electroneutral, which was suggested by previous studies in membrane vesicles. In this study, thiosulfate and selenate could also induce inward-currents with $K_{0.5}$ of 85 μM and 580 μM , respectively, at a holding potential of -50 mV. In addition, the sulfate-induced inward current was not sensitive to pH (19).

The rNaSi-1 has also been expressed in cell lines including the MDCK and Sf9 cell line (34; 107). The K_m of 300 to 400 μM for sulfate in NaSi-1 expressing Sf9 cells is similar to that in NaSi-1 expressing oocytes. A recent review mentioned some unpublished results showing that OK cell lines can stably express NaSi-1 and be used for studying the sorting mechanism and posttranslational regulation of the NaSi-1 protein (76).

(iv) Tissue distribution of NaSi-1

Northern blot hybridization using full-length rNaSi-1 as a probe detected two transcripts in kidney and small intestine, respectively. Signals were stronger in kidney cortex than in medulla and also stronger in ileum than in duodenum and jejunum (78). Later studies observed expression of both rNaSi-1 related mRNA and protein in rat renal proximal tubules and medulla collecting ducts (23). However, immunofluorescence studies using antibodies

against a specific peptide of rNaSi-1 demonstrated the localization of NaSi-1 only on the apical membrane of proximal tubular cells but not in medulla (69). These two studies showed different distributions of rNaSi-1 on kidney medulla but the reason is not yet clear. Northern blotting and RT-PCR analysis detected high levels of mNaSi-1 mRNA in kidney, small intestine and colon, and lower levels of mRNA in cecum, testis, adrenal, and adipose tissues (9). In contrast, Northern blot analysis detected hNaSi-1 mRNA in kidney but not intestine (65). Further investigations are needed to explain the different pattern of NaSi-1 expression between rodents and human.

(v) Functionally-important amino acid residues and transmembrane domains of NaSi-1 and NaDC-1

So far little information has been reported on functionally important amino acids or protein domains in NaSi-1. Chimeras between rbNaDC-1 and rNaSi-1 suggest that the substrate recognition site of the two transporters is located at the carboxy terminus of the protein, past amino acid 141, and that cation binding sites might be determined by the interaction between amino and carboxy terminal portions (97). This chimera study is the only published report about substrate and cation binding of NaSi-1.

However, many detailed studies have been performed on the structure-function relationships of NaDC-1 by Pajor's group and may provide useful information to investigate the structure-function relationships of hNaSi-1. One chimeric study of rbNaDC-1 and hNaDC-1, which share 78% sequence identity but have some functional difference, suggest that transmembrane domains 7,

10 and 11 and their adjacent loops are likely to contain at least one of the cation binding sites, which is close to the substrate binding domain, and that transmembrane domain 11 is responsible for lithium inhibition in rbNaDC-1 (54). Mutagenesis studies on rabbit NaDC-1 found that two conserved amino acid residues, Asp-373 and Glu-475, in TMD 8 and 9, were important for transport activity since mutations of these two residues resulted in changed K_m for both substrate and cation (39). Also, mutations of two conserved cationic amino acid residues, Lys-84 and Arg-349, in NaDC-1, affected the K_m for the substrate (93). However, mutations of any of the 11 cysteine residues and most of the histidine residues in NaDC-1 had no effects on transport activity, suggesting that these residues may not be necessary for the function (94; 98). Cysteine-scanning mutagenesis in transmembrane domain 9 of rbNaC-1 found that cysteine replacements at four positions, Ser-478, Ala-480, Ala-481, and Thr-482, resulted in MTSET inhibition of uptakes by the protein, and that the MTSET inhibition was dependent on cation and substrate used in the buffer. These results suggest that TMD-9 is likely to be involved in the movement that mediates a conformational change from cation-binding sites to substrate-binding site, and also may form part of the translocation pathway in rbNaDC-1 transporter. Recently, another mutagenesis study performed by Yao and Pajor found that cysteine replacements at two conserved residues, Arg-349 and Asp-373, located in transmembrane domains 7 and 8 of rbNaDC-1, also resulted in cation/substrate-dependent MTSET inhibition, indicating that Arg-349 and Asp-373 are likely to be involved in the conformational changes during the transport cycle of NaDC-1(147).

(vi) Regulation of NaSi-1

Most recent studies of NaSi-1 are focused on the regulation of the transporter and indicate that NaSi-1 is highly controlled by many dietary and hormonal factors. Dietary sulfate intake and metabolic acidosis can regulate the transport activity of NaSi-1 by controlling the expression of NaSi-1 mRNA and protein (79; 106). Also, the *Nas1* gene is regulated at the transcription level by Vitamin D (29), thyroid hormone (10; 117; 131) and glucocorticoids (112; 114). In addition, NaSi-1 mRNA and protein expression are dependent on age, therefore, NaSi-1 may be regulated by growth hormones (81; 116).

Aims of studies in this dissertation

In this dissertation, two kinds of cation-dependent transporters are studied, the bacterial proton-coupled Mg^{2+} -citrate transporter (CitM) and the human Na^+ /sulfate cotransporter (hNaSi-1), and there are three study aims for these two transporters.

Aim 1: To characterize the function of CitM expressed in E. coli cells.

The function was studied using radiotracer assay method. CitM originally from *B. subtilis* transports citrate in a metal ion-citrate complex (such as Mg^{2+} -citrate) by coupling with the electrochemical gradient of proton (14). Although the functions of CitM have been studied in native membranes of *B. subtilis*, the results could have been complicated by multiple endogenous pathways of citrate transport in the bacteria. Therefore, studies in Chapter 2 of this dissertation characterized the functions of CitM expressed in *E. coli* cells,

which normally do not have an endogenous citrate transporter. Also, an electroneutral transport model was proposed for CitM in Chapter 2. Results in this study should provide a base for future studies on the structure-functional relationships of CitM.

Aim 2: To make antibodies against hNaSi-1 and to determine its tissue distribution and N-glycosylation site.

Polyclonal antibodies against hNaSi-1 were prepared using a GST fusion protein method and the tissue distribution and N-glycosylation site of hNaSi-1 were determined using Western blotting and immunofluorescence techniques.

Aim 3: To test the hypothesis that the region surrounding Ser-260 and Ser-288 in TMDs 5 and 6 are involved in cation and/or substrate binding by hNaSi-1.

This study used site-directed mutagenesis techniques to investigate the potential roles of Ser-260, Ser-288 and the surrounding residues (located in TMDs 5 and 6) in cation and/or substrate binding by hNaSi-1. Radiotracer assay and Western blotting techniques were used to measure the effect of the mutations on protein expression and transport activity.

Aims 2 and 3 in this dissertation are to characterize the hNaSi-1 transporter, including its tissue distribution, N-glycosylation site and functionally important amino acid residues and transmembrane domains. Although the cDNA coding for hNaSi-1 has been isolated (65), detailed functional studies

had not been performed, tissue distributions needed to be confirmed and *N*-glycosylation site was unknown. Also, the structure of the substrate and cation binding sites was almost completely unknown. Therefore, in this dissertation, antibodies against a specific peptide of hNaSi-1 were made and applied to determine tissue distributions and *N*-glycosylation site in hNaSi-1 (Chapter 3) and also used as a tool in later structure-function relationship studies. Mutagenesis studies were performed to investigate the substrate and cation binding sites in hNaSi-1 (Chapter 4). These studies should contribute to a better understanding of the transport mechanism of Na⁺/sulfate cotransporters as well as other transporters in the whole NaDC/NaSi-1 gene family.

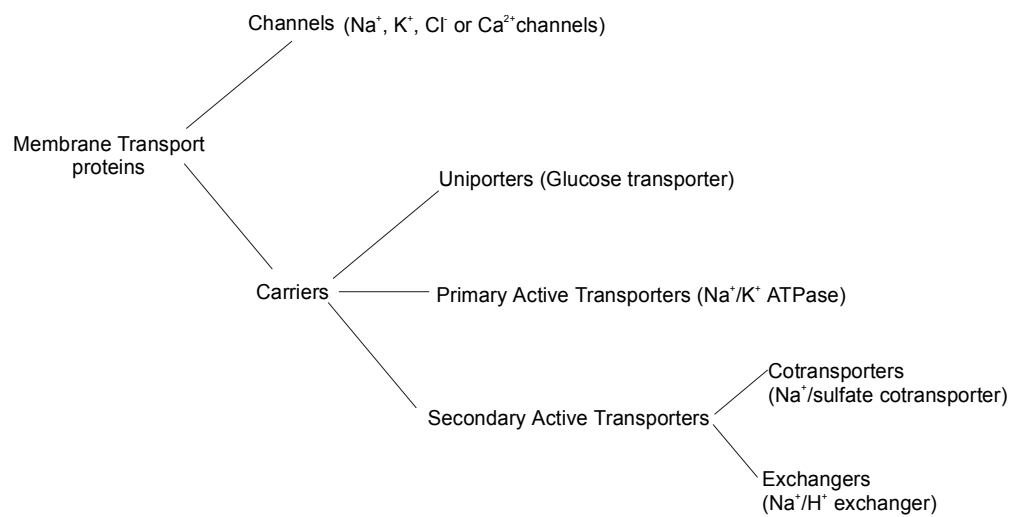
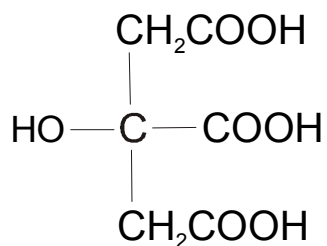
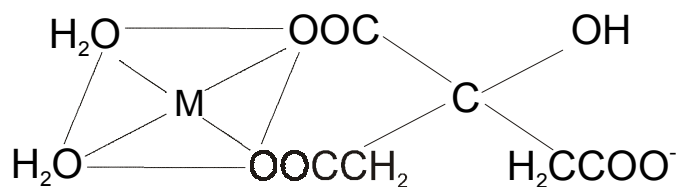


Figure 1.1 General classifications of membrane transport proteins. Transport proteins can be classified into two major types: channel proteins and transporter or carrier proteins. Transporters can be further classified into three subtypes: uniporters, primary active transporters and secondary active transporters.

A.



B.



C.

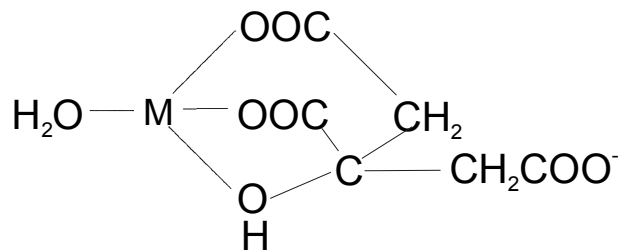


Figure 1.2 Metal citrate complexes, taken from Ref. (32). A. citrate; B. bidentate complex involving the central and one terminal carboxylate groups; C. tridentate complex involving the central carboxylate group, one terminal carboxylate group and the central hydroxyl group. M represents metal ions.

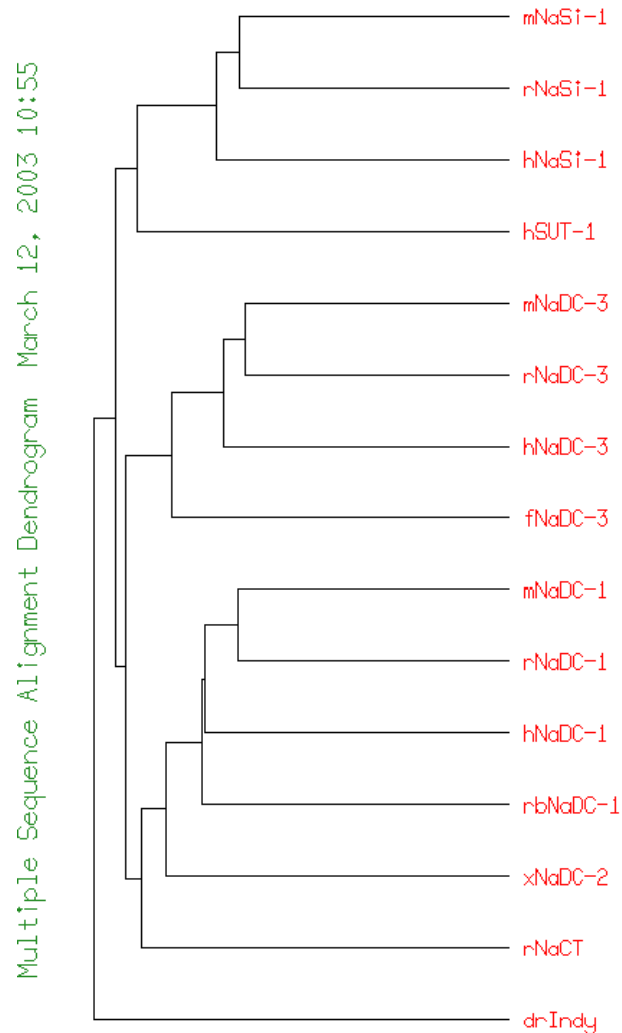


Figure 1.3 Dendrogram tree of NaDC/NaSi transporters. The dendrogram tree was constructed using the Pileup program of Genetics Computer Group (GCG). NaSi-1 transporters have a low affinity and hSUT-1 has a relatively high affinity for sulfate. NaDC-1 and NaDC-2 transporters also have a relatively low affinity for dicarboxylates whereas NaDC-3 transporters show a high affinity for substrates. The two recently identified transporters, NaCT and Indy, are also included in the NaDC/NaSi gene family. (dr: *Drosophila*; f: flounder; h: human; m: mouse; rb: rabbit; r: rat; x: *Xenopus* frog)

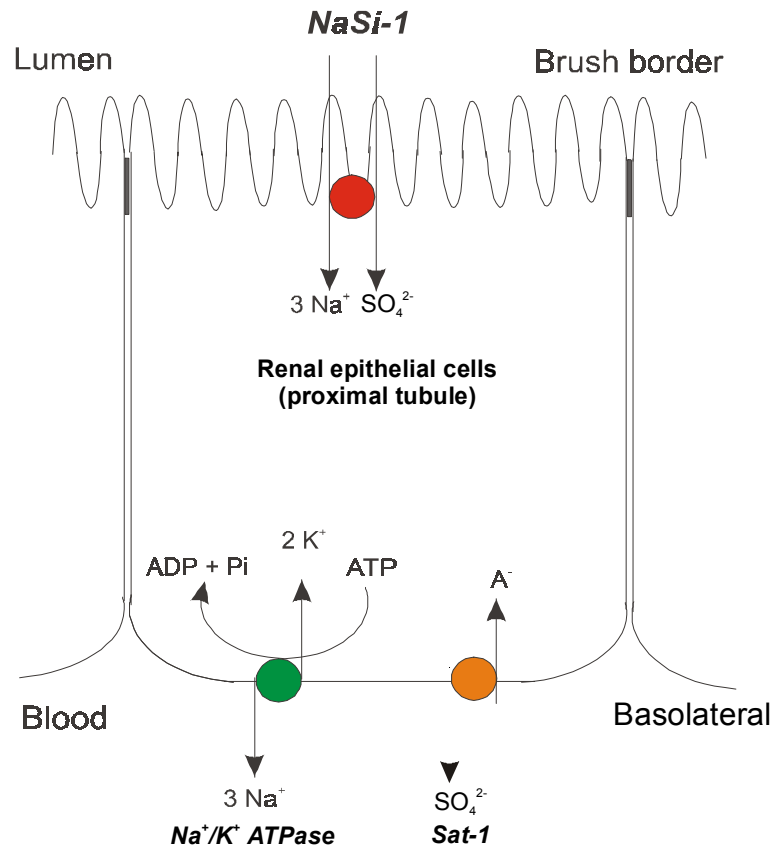


Figure 1.4 Simplified transport pathway of sulfate in renal proximal tubular epithelial cells. Sulfate is taken up from the lumen side by NaSi-1 transporters (red circle) on the apical membrane of renal epithelial cells, and then expelled into the blood side by sulfate/anion exchangers (blue circle) on the basolateral membrane. Green circle represents Na^+/K^+ ATPase. A^- represents an anion such as bicarbonate or oxalate which can be removed from the cell by Cl^- /anion exchangers.

Table 1.1 Members of the NaDC/NaSi transporter family.

Subtype	Species (prefix)	% sequence	Organs	GenBank No.	Reference
		identity with rat NaSi-1			
NaSi-1	Human (h)	100	kidney	AF260824 AK026413	(65)
	Rat (r)	83	kidney, intestine	L19102 U08031	(78; 85)
	Mouse (m)	81	kidney	AF199365	(8)
SUT-1	Human (h)	51	Endothelial venules	AF169301	(36)
NaDC-1	Rat (r)	46	kidney	AF058714	(21; 57; 125)
	Mouse (m)	46	kidney	AF201903	(99)
	Rabbit (rb)	47	kidney	U12186	(87)
	Human (h)	49	kidney	U26109	(88)
NaDC-2	<i>Xenopus laevis</i> (x)	48	intestine	U87318	(6)
NaDC-3	Rat (r)	42	placenta	AF081825	(56)
		42	kidney	AF080451	(20)
	Mouse (m)	42	brain	AF306491	(91)
	winter flounder (f)	39	kidney	AF102261	(128)
	Human (h)	44	placenta	AF154121	(128; 138)
NaCT	Rat (r)	42	brain	AF522186	(49)
INDY	<i>Drosophila</i>	37	<i>D. melanogaster</i>	AE003519	(48; 58)

CHAPTER 2: FUNCTIONAL CHARACTERIZATION OF CitM, THE Mg^{2+} -CITRATE TRANSPORTER

(Studies in this chapter have been published in the paper by H. Li and A. Pajor, titled “Functional Characterization of CitM, the Mg^{2+} -Citrate Transporter”, the *Journal of Membrane Biology*, Vol.185, 9-16, 2002, and are reprinted with permission.)

Introduction

Citrate is an important source of energy for bacteria. Most bacteria contain concentrative citrate transporters located on the cytoplasmic membrane to allow the absorption of citrate from the environment. Many of the bacterial citrate transporters carry free citrate coupled to protons or sodium (74; 80; 134; 135). However, some unusual transporters exist in *Bacillus*, *Pseudomonas* and *Klebsiella* sp. that can absorb citrate as a complex with metal ions (17; 73; 141). Citrate has three negatively charged carboxylic groups at neutral pH, two of which form stable complexes with a variety of divalent metal ions such as Mg^{2+} and Ca^{2+} (37; 129).

The citrate transporter from *Bacillus subtilis*, called CitM, is a metal ion-citrate complex transporter that prefers Mg^{2+} -citrate as a substrate (11; 141). The amino acid sequence of CitM is approximately 60% identical to the sequence of the Ca^{2+} -citrate complex transporter, CitH, also from *B. subtilis* (14; 61). Both CitM and CitH have similar predicted secondary structures

containing 12 transmembrane domains. These transporters belong to a distinct family that is not related to the other families of citrate transporters.

Although the function of CitM has been characterized in native membranes, the results could have been complicated by the multiple pathways that exist for citrate transport in *B. subtilis* (61). In this study, the cloned CitM from *B. subtilis* was expressed in *E. coli* DH5 α cells which do not have an endogenous citrate transporter. We find that CitM has a relatively low affinity for substrate and Mg²⁺. Although the transporter is very specific for citrate, other divalent metal ions, including Mn²⁺, Ba²⁺, Ni²⁺ and Co²⁺, can substitute for Mg²⁺. Transport appears to be driven by the proton electrochemical gradient. The results are similar to previous studies of CitM in native membranes and support an electroneutral transport mechanism with a coupling stoichiometry of one H⁺ and one (Mg²⁺-citrate)⁻¹ complex.

Methods

Construction of the CitM expression vector

The *citM* gene (Genbank accession number U62003) (14) was amplified from genomic DNA isolated from *B. subtilis* 168M (ATTC) using Polymerase Chain Reaction (PCR) with sequence-specific primers. The sense primer included a mutation that introduced an *Nco* I restriction site (underlined) at the start codon (in bold) to facilitate subcloning: 5'-CAG ACC **ATG** GTA GCA ATC TTA GGC TTT-3'. The introduction of the *Nco* I restriction site changed the

first and second amino acid residues from Val-Leu to Met-Val. The antisense primer was: 5'-AAT TGG ATC CTG AAT TAT **CAT** ACG GAA ATA G-3', which included a stop codon (in bold type) and a *BamH* I restriction site (underlined) to facilitate subcloning. The PCR was done using the Clontech Advantage PCR kit which contains a proofreading DNA polymerase, Klentaq, to minimize mutations. The PCR product was cloned into the pCR2.1 vector using the TopoTA cloning kit, according to manufacturer's directions (Invitrogen). The single internal *Nco* I site in the *citM* gene was removed by silent mutagenesis to facilitate subcloning (Quick change mutagenesis kit, Stratagene). The *citM* DNA was then subcloned into the *Nco* I/*BamH* I sites of the pSE380 expression vector (Invitrogen). The recombinant plasmid containing *citM* DNA in pSE380 is called pSE380/CitM. The construct was sequenced at the Sealy Center for Molecular Science (University of Texas Medical Branch, Galveston, TX). Three separate clones were sequenced and all were identical to the published sequence except for a mutation at position 256 which changes the valine to alanine. The mutation may be due to a strain variation since we used strain 168M whereas the published sequence is from *B. subtilis* strain 6GM.

Preparation of cells

The pSE380/CitM construct was transformed into *E. coli* DH5 α cells, which normally do not express a citrate transport system (59; 64). Overnight cultures of *E. coli* DH5 α cells harboring the recombinant plasmid pSE380/CitM or vector-only plasmid pSE380 were used to inoculate 100 ml TB medium

containing 50 µg/ml carbenicillin. Cells were grown at 37°C until the O.D.₆₅₀ reached ~0.8 to 0.9. Isopropyl-β-D-thiogalactopyranoside (IPTG) was added to a final concentration of 0.5 mM and the cell growth was continued for another 2 hours. The cells were harvested by centrifugation at 2000 × g (Beckman JA-25.50 rotor) for 10 minutes at 4°C. The cells were washed twice with HEPES-glucose buffer (100 mM HEPES, 0.1% D-(+)-glucose, pH 6.8 adjusted with 1M Tris) (141) and then resuspended in the same buffer to a final O.D.₆₅₀ of ~10. For experiments using different pH values, cells were washed with HEPES-glucose buffer at pH 6.8 and then resuspended in HEPES-glucose buffer adjusted to the appropriate pH. In experiments using potassium-phosphate buffer, the cells were washed and resuspended in 50 mM K-phosphate, pH 7.0.

Transport assay

Cells were preincubated for 10 minutes at room temperature with MgCl₂ by combining 80 µl of cell suspension with 10 µl of 100 mM MgCl₂ stock solution prepared in HEPES-glucose buffer. Transport was initiated by adding 10 µl of substrate solution in which radioactive ¹⁴C-citrate (0.1 µCi/µl, Moravek Biochemicals) was mixed with different concentrations of non-radioactive citrate. Transport was stopped with ice-cold HEPES glucose buffer. In pilot experiments, we compared HEPES-glucose and 100 mM LiCl stop solutions (results not shown). The radioactivity retained by the filters was the same using both stop solutions but there appeared to be leakage from the cells in LiCl

(tested by waiting 30 sec before filtration). Therefore, uptakes were stopped by the addition of 1 ml of ice-cold HEPES-glucose buffer. For the measurement of uptake at time 0, the stop solution was added to the cell suspension before adding the radioactive substrate. The mixture was immediately filtered through a nitrocellulose filter (HAWP Millipore, 0.45 μm) using suction. The filter was washed twice, first with 1ml and then with 4ml of ice-cold HEPES-glucose buffer and immediately submerged in scintillation liquid. The radioactivity retained on the filter was counted. For experiments testing the inhibition of citrate transport by potential substrates such as isocitrate, *cis*-aconitate and tricarballic acid, a final concentration of 1 mM of the test inhibitor was added together with the radiolabelled citrate. For experiments testing the effect of different metal ions, cells were preincubated for 10 minutes with a final concentration of 5 mM different divalent metal ion solutions prepared in HEPES-glucose buffer.

In experiments testing the effects of ionophores, the 80 μl of cell suspension was preincubated together with 10 μl MgCl_2 and 1 μl of ionophore stock solution dissolved in 100% ethanol. Control groups were preincubated in ethanol without ionophore. The final concentration of carbonyl cyanide p-trifluoromethoxyphenylhydrazone (FCCP) was 25 μM . In experiments involving trichlorocarbanilide (TCC), a final concentration of 100 μM was used and the cells were suspended in 100 mM choline chloride, 10 mM HEPES, pH 6.8 to provide a source of anions for the TCC (2). In experiments involving nigericin or valinomycin, the cells were first permeabilized with EDTA as described

below and final concentrations of 50 μ M for nigericin or 10 μ M for valinomycin were used (2).

Permeabilization of cells

The outer membrane of *E. coli* prevents access of some large or hydrophobic molecules to the inner membrane where CitM is located. Therefore, in experiments involving the ionophores, nigericin or valinomycin, the *E. coli* cell wall was first permeabilized using EDTA (2; 121). Briefly, the cells were grown and washed as described above and resuspended in 1/30 the original culture volume. The cells were then equilibrated to 37°C and an equal volume of resuspension buffer containing 2 mM EDTA was added. The cells were then incubated exactly 3 minutes at 37°C before being diluted 100-fold with resuspension buffer containing 100 mM MgSO₄. The cells were then washed and resuspended in 100 mM HEPES buffer without glucose, since the cells can repair the permeabilization of the outer membrane in the presence of glucose (66). For the experiments involving valinomycin, the cells were resuspended in 60mM HEPES buffer containing 20 mM KCl or CholineCl.

Protein assay

The total membrane protein was measured using the DC Protein Assay kit (BioRad), according to the manufacturer's directions. The protein standard used was bovine plasma gamma globulin dissolved in HEPES-glucose buffer.

Data analysis

Each data point represents the mean of 4 replicate samples. For most experiments, the counts in cells transformed with control vector pSE380 have been subtracted from the counts in cells expressing CitM. For citrate kinetic calculations, the initial uptake rate of citrate was fit by non-linear regression using Sigma Plot 2000 (SPSS) to the Michaelis-Menten equation: $v = V_{max} * [S] / (K_m + [S])$, where v is the initial uptake rate, $[S]$ is the concentration of the substrate, V_{max} is the maximum uptake rate at saturating substrate concentrations, and K_m is the substrate concentration producing one half of V_{max} and is also called the Michaelis-Menten constant. In some experiments the data were fitted to the Hill equation: $v = (V_{max} * [S])^n / (K_{0.5}^n + [S]^n)$ with an additional constant, C , which represents the uptake or binding of citrate in the absence of added Mg^{2+} . The n represents the Hill coefficient.

In some of the experiments, the concentrations of free Mg^{2+} and the Mg^{2+} -citrate complex were calculated using the MaxChelator program (Winmaxc v.2.05, <http://www.stanford.edu/~cpatton/maxc.html>) (12). Although both divalent ($citrate^{2-}$) and trivalent ($citrate^{3-}$) forms of citrate are able to form complexes with Mg^{2+} , the complex with trivalent citrate ($Mg-citrate^{1-}$) is more abundant. For example, under the conditions used in many of our experiments (pH 6.8, 500 μM total citrate and 10 mM total Mg^{2+}), the concentration of the $Mg-citrate^0$ complex is only 1.2 μM whereas the concentration of $Mg-citrate^{1-}$ is 468 μM .

Results

Time course of citrate uptake

The time course of citrate uptake in the presence of saturating concentrations of Mg^{2+} was measured in whole cells of *E. coli* DH5 α transformed with the pSE380/CitM construct or with the pSE380 vector alone (Figure 2.1). Transport studies in bacteria often use potassium phosphate buffer to resuspend the cells and LiCl buffer to stop the reaction. However, previous studies of citrate transport in *B. subtilis* suggested that HEPES might be a better transport buffer than phosphate because the phosphate can form complexes with divalent metal ions (22; 38; 141). Therefore, the time course of citrate transport was compared in potassium phosphate buffer and HEPES-glucose buffer.

In both buffers, the transport of citrate in *E. coli* cells transformed with the control plasmid, pSE380, was very low, verifying that *E. coli* DH5 α do not express a native citrate transporter (Figure 2.1A, B). The transport activity in cells expressing CitM was approximately tenfold higher when measured in HEPES-glucose buffer (Figure 2.1B) than in potassium-phosphate buffer (Figure 2.1A), in agreement with previous reports that phosphate may interfere with the transport assay. The linear range of transport measured in HEPES-glucose was in about the first 30 seconds. There appeared to be some binding or rapid uptake in cells expressing CitM (Figure 2.1B). In four experiments, the

uptakes measured at time 0 were $10 \pm 2\%$ (mean \pm SEM) of the uptakes measured at 30 seconds. The HEPES-glucose buffer was used for the following studies and 15 or 30 second time points were measured.

Citrate uptakes as a function of citrate concentrations

The kinetics of citrate uptake in *E. coli* expressing CitM is shown in [Figure 2.2](#). At saturating magnesium concentrations (10 mM), the K_m for citrate was 339 μ M and the V_{max} was 252 nmol/mg-min ([Figure 2.2A](#)). In three experiments, the mean K_m was 274 ± 51 μ M and the V_{max} was 222 ± 47 nmol/mg-min (mean \pm SEM). The native transporter expressed in *B. subtilis* has a K_m of 550 μ M (141). The data were also analyzed by calculating the Mg-citrate concentrations instead of total citrate since the transported species is the Mg-citrate complex ([Figure 2.2B](#)). Since the Mg^{2+} concentration was 10 mM, the concentration of Mg-citrate was similar to the total citrate concentration and there was very little difference in the kinetic values. For example, the K_m for Mg-citrate in [Figure 2.2B](#) is 320 μ M.

Substrate specificity of CitM

The substrate specificity of CitM was tested by measuring the inhibition of uptake of radiolabelled citrate in the presence of saturating Mg^{2+} concentrations. Four tricarboxylic acids (citrate, isocitrate, *cis*-aconitate and tricarballic acid) and one dicarboxylic acid (succinate) were tested. Only

citrate inhibited the transport of radiolabelled citrate whereas there was no inhibitory effect of the other test substrates (Figure 2.3). The uptake of ^3H -succinate was also tested directly in DH5 α cells expressing CitM but there was no difference from control cells transformed with pSE380 alone (data not shown). Therefore, CitM is highly specific for citrate.

Cation effects on citrate uptakes by CitM

Previous studies have shown that CitM transports citrate as a complex with Mg^{2+} (14; 141). In this study, we examined the effect of increasing total Mg^{2+} concentrations while keeping total citrate concentrations constant. This would result in changing both Mg-citrate and free Mg^{2+} concentrations. As shown in Figure 2.4A, the uptake of radiotracer citrate was appeared to be a sigmoidal function of the Mg-citrate concentrations in the medium. The apparent half saturation constant ($K_{0.5}$) for Mg-citrate was 271 μM and the Hill coefficient was 2.6 (Figure 2.4A). When the data were replotted as a function of free Mg^{2+} concentrations, the curve fit was still sigmoidal but the Hill coefficient decreased to 1.6 (Figure 2.4B). There was also measurable uptake of citrate in the absence of added Mg^{2+} in *E. coli* expressing CitM compared with controls. The citrate uptake in the absence of added Mg^{2+} was about 20 nmol/mg-min (Figure 2.4).

CitM can carry complexes of citrate with divalent metal ions other than Mg^{2+} . As shown in Figure 2.5, the substitution of Mg^{2+} with Mn^{2+} produced 76%

of the citrate transport rate. Substitution with Ba^{2+} , Ni^{2+} and Co^{2+} was less effective, producing citrate uptake rates between 50% and 30% of that observed in Mg^{2+} . The uptake of citrate in the presence of Ca^{2+} was similar to the uptake in the absence of added metal ions. It is likely that the transport solutions contain some residual divalent cations since the addition of the divalent cation chelator, EGTA, reduced the uptake further. There was no significant uptake of citrate in the presence of Zn^{2+} when compared with the EGTA-containing solution. The uptake of radiotracer citrate in this experiment was not necessarily related to the concentration of the citrate-metal ion complex. For example, the concentration of the Ba^{2+} -citrate complex was 63% of the total citrate compared with Mg-citrate (88% of total) which could account for the decreased uptake activity in the presence of Ba^{2+} . However, Zn^{2+} and Ca^{2+} , which produced the lowest transport activity, had the highest percentage of metal ion-citrate complex (Zn-citrate 99% and Ca-citrate 91% of total citrate).

Effect of pH on citrate uptakes by CitM

Previous studies have suggested that citrate transport by CitM is coupled to protons (11; 14). Therefore, we examined the effect of pH on citrate uptakes in *E. coli* expressing CitM. As shown in [Figure 2.6](#), there was little effect of pH on citrate transport between pH 5 and 6.8, whereas at pH 7.5 and 8.0 the transport was greatly reduced to only about 30% of the average uptake at pH 5 to 6.8. Since the intracellular pH of *E. coli* is normally between 7.5 to

8.0 (47), extracellular pH values above 7.5 should abolish the transmembrane pH gradient. The inset of [Figure 2.6](#) shows that the concentration of the Mg-citrate complex is not affected much by changes in pH. The decrease in concentration of Mg-citrate occurs at acidic pH, which is different from the decrease in transport activity. Therefore, the results suggest that citrate transport by CitM is likely to be dependent on an inwardly-directed pH gradient or an outwardly directed OH^- gradient.

Effect of ionophores on citrate uptakes in CitM

Ionophores were tested to examine the effect of chemical and electrical gradients of ions on the transport activity of CitM ([Figure 2.7](#)). Two of the ionophores (FCCP and TCC) cross the cell wall readily and were used directly on the *E. coli* cells, whereas nigericin and valinomycin require prior permeabilization of the cell wall with EDTA. Carbonyl cyanide p-(trifluoromethoxy) phenylhydrazone (FCCP) is an electrogenic proton ionophore, which can dissipate the transmembrane H^+ gradient (104). Citrate uptakes in the presence of FCCP in CitM were reduced to about 47% of uptakes without FCCP ([Figure 2.7](#)). Trichlorocarbanilide (TCC) is an anion/ OH^- exchanger that produces a change in intracellular pH without affecting membrane potential (2). The addition of TCC also inhibited transport by Cit M ([Figure 2.7](#)). Nigericin is an electroneutral K^+/H^+ exchanger which also dissipates the transmembrane pH gradient without changing membrane potential (2; 104). Nigericin reduced uptakes of citrate in CitM by 86% ([Figure](#)

2.7). Finally, valinomycin was used to test whether the membrane potential affects citrate transport by CitM. Valinomycin is an electrogenic K^+ ionophore that produces a diffusion potential of K^+ . In bacteria the addition of valinomycin can also change intracellular pH depending on the concentration of extracellular K^+ (2). However, extracellular K^+ concentrations below 25 mM affect the membrane potential without changing pH. Intracellular K^+ concentrations in bacteria are approximately 350 mM (47). The combination of valinomycin and an outward gradient of K^+ should produce a hyperpolarization of the membrane potential, but there was no change in citrate transport under these conditions (Figure 2.7). Therefore, CitM activity does not appear to be affected by membrane potential. Based on these results, the coupling stoichiometry is likely to be one proton coupled to one complex of $(Mg^{2+}$ -citrate) $^{1-}$, with no net movement of charge across the membrane.

Discussion

The CitM transporter carries a complex of Mg^{2+} and citrate across the cytoplasmic membrane of *B. subtilis*. The major findings of this study are that CitM expressed in *E. coli* DH5 α cells is an electroneutral proton-coupled transporter for the Mg^{2+} -citrate complex. Furthermore, CitM is very specific for citrate as a substrate. Other di- or tricarboxylic acids, including succinate, isocitrate, cis-aconitate and tricarballic acid are not substrates of CitM. However, the divalent metal ion carried by CitM is not limited to Mg^{2+} . The transporter also accepts Mn^{2+} , Ba^{2+} , Ni^{2+} and Co^{2+} .

The apparent K_m for citrate in CitM expressed in *E. coli* is around 270 μM . This agrees well with the K_m of 550 μM reported in previous studies of whole cells of *B. subtilis*, also measured in HEPES-glucose buffer with saturating Mg^{2+} concentrations (141). However, there is some variability reported in the literature on the K_m for citrate in CitM. Some of the variability is due to the use of phosphate buffer for assays, which typically results in a much larger apparent K_m . One exception is the study by Bergsma and Konings which reported a K_m of 40 μM in phosphate buffer using membrane vesicles from *B. subtilis* (11). Vesicle experiments should provide a more accurate measurement of K_m because they do not contain the cell wall found in whole cell studies, which could add complications of unstirred layers to the kinetic measurements. Interestingly, a recent study done with the cloned CitM expressed in whole cells of *E. coli* DH5 α reported a K_m for citrate of about 60 μM using PIPES buffer (61). At the moment it is not clear why there are such large differences in measured K_m between studies.

The CitM transporter is very specific for the complex of citrate with a divalent cation. Citrate has three carboxyl groups that can form a stable complex with metal ions. In the case of magnesium, citrate forms a tridentate complex involving two of the carboxyl groups and the central hydroxyl group. The central hydroxyl group and carboxyl group are very important for the stability of the complex (37). Although the tricarboxylic acids that were tested as potential substrates, isocitrate, *cis*-aconitate and tricarballic acid, also form complexes with metal ions they lack the central hydroxyl group necessary for

the formation of the tridentate complex (37), which may result in structures that are not recognized by the CitM substrate binding site. The dicarboxylic acid succinate is not a substrate of CitM, presumably also because it does not form the appropriate complex with divalent metal ions. Alternately, the concentration of the metal ion-test substrate complex may be very low compared with the Mg-citrate concentration.

Although Mg^{2+} is the preferred metal ion transported by CitM, other metal ions including Mn^{2+} , Ba^{2+} , Ni^{2+} , Co^{2+} , and Ca^{2+} (in order of preference) can substitute for Mg^{2+} . The order of cation preference seen in our study is similar to that observed previously in *B. subtilis* cells (11). However, as in the other measurements of CitM function, there have been reports of different cation preferences of CitM. The same order of cation preference was measured in whole cells of *B. subtilis* in a recent study (61). Surprisingly, the same study reported a different order of cation preference for the cloned CitM expressed in *E. coli*, with the highest transport rate in Ni^{2+} , followed by Co^{2+} , Mg^{2+} , Mn^{2+} , and finally Zn^{2+} . It is not clear why such large differences between the cloned CitM and whole cells of *B. subtilis* were found in the same study. The highest transport rate for citrate was seen with Mg^{2+} , and *B. subtilis* has only two transporters for citrate-metal ion complexes, CitM and CitH. Since CitH does not transport Mg^{2+} (61) one would expect that the activity of CitM would account for the high transport rate measured in Mg^{2+} .

In the experiments reported here, there was measurable uptake of citrate by CitM in the absence of added divalent metal ions. This is likely due to the presence of residual metal ions in the transport buffer since the transport in the presence of EGTA was lower than in its absence. Similar results were observed in recent whole cell studies of CitH expressed in *E. coli*. The uptake of citrate in the absence of added metal ions was reduced to background levels by the addition of EGTA (61).

The transport activity of CitM in the Mg^{2+} -activation experiment appears to be a sigmoidal function of the Mg-citrate concentration. One explanation for this is that Mg^{2+} may have two functions in CitM, much like the Mg^{2+} in Mg-ATP requiring enzymes (123). It is possible that the Mg^{2+} is not only a transported substrate, as part of the Mg-citrate complex, but it may also act as an essential activator of transport by binding to the CitM transport protein at an allosteric site. However, the uptake rate at the same concentration of Mg-citrate was similar in the kinetic experiment shown in [Figure 2.2](#) (with free $[\text{Mg}^{2+}]$ close to 10 mM) and in [Figure 2.4](#) (at low free $[\text{Mg}^{2+}]$). This raises the possibility that the residual divalent cations in the medium might have complicated the results by introducing uncertainty into the calculations of the Mg-citrate concentrations at low free $[\text{Mg}^{2+}]$. Therefore, more experiments are needed to distinguish these possibilities.

The mechanism of transport by CitM is likely to involve proton cotransport (or countertransport of OH^-). In our study, the transport of citrate by

CitM was likely to be dependent on an inwardly-directed proton gradient. Transport was reduced when the extracellular pH was greater than 7.5 or in the presence of ionophores that disrupt the transmembrane pH gradient, including FCCP, nigericin and TCC. Valinomycin is an electrogenic K^+ ionophore, and under the conditions used in this study, the addition of valinomycin should change the membrane potential without affecting the pH (2). However, valinomycin treatment had no effect on the transport of citrate by CitM in our studies. In previous studies of CitM activity in membrane vesicles of *B. subtilis*, the addition of valinomycin resulted in an inhibition of uptake, although the phosphate transport buffer used could complicate the results (11). A second study reported little effect of valinomycin on the cloned CitM expressed in *E. coli*, but the experiments were not done using permeabilized cells, so it is unclear whether the valinomycin reached the inner membrane (14). Furthermore, the experiments were done in the presence of 50 mM extracellular K^+ , which should inhibit transport by the large decrease in the transmembrane pH gradient since valinomycin changes the pH in *E. coli* at extracellular K^+ concentrations above 25 mM (2). The insensitivity of CitM to changes in membrane potential produced by valinomycin indicates that the transporter is electroneutral. Since the complex of Mg^{2+} and citrate contains one net negative charge, it is likely that one proton is coupled to the movement of one $(Mg^{2+}\text{-citrate})^{1-}$ complex.

In conclusion, we have characterized the function of CitM expressed in *E. coli*. Although the endogenous CitM activity has been characterized in *B.*

subtilis, the results could have been complicated by multiple transport pathways for citrate in those membranes. However, we find that the cloned CitM expressed in *E. coli* has very similar properties to the native transporter. CitM is a low-affinity transporter that carries the complex of citrate with metal ions such as Mg^{2+} or other divalent metal ions. The transporter is very specific for the citrate-metal ion complex and other tricarboxylic acids are not substrates. Finally, the transporter appears to be electroneutral with a likely coupling stoichiometry of 1 H^+ : 1 (Mg^{2+} -citrate) $^{1-}$.

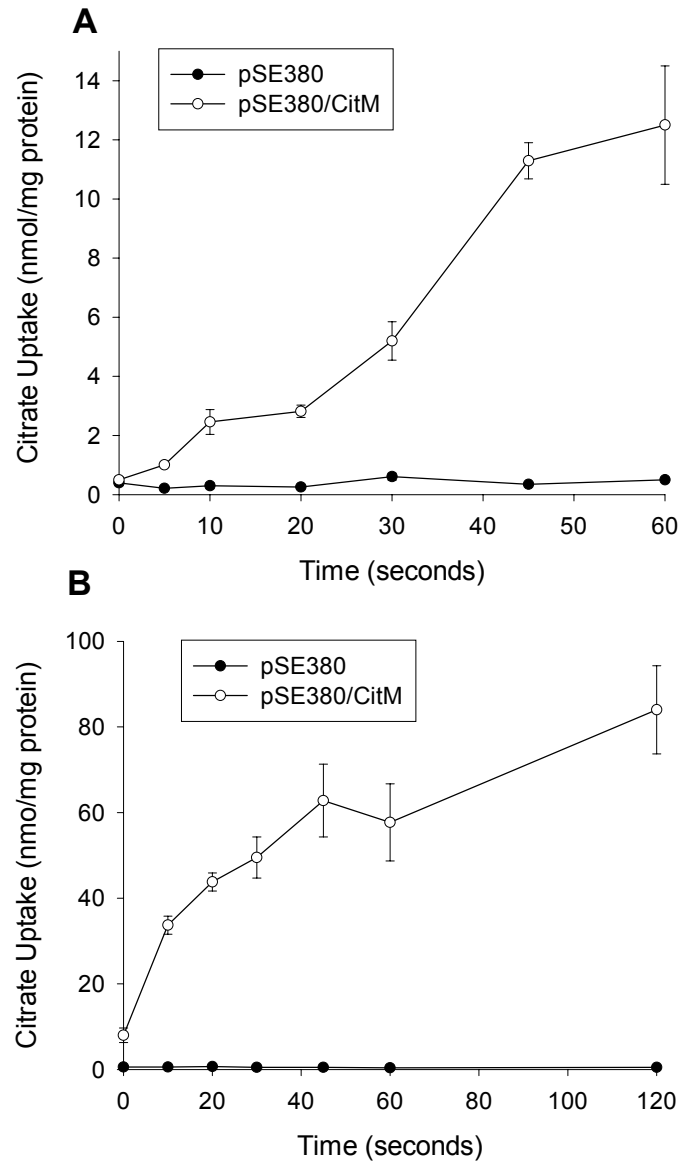


Figure 2.1 Time course of the uptake of 1 mM citrate by CitM expressed in *E. coli*. Citrate uptakes were measured in whole cells of *E. coli* transformed with pSE380/CitM or with pSE380 vector. Cells were first preincubated with 10 mM MgCl₂ for 10 minutes and then ¹⁴C-citrate was added to activate the transport. (A) The uptakes were measured in 50mM potassium phosphate buffer (pH = 7.0) and stopped with 100 mM LiCl buffer. (B) The uptakes were measured and stopped with 100 mM HEPES-glucose buffer (pH = 6.8). The data shown are means \pm SEM of four replicate measurements.

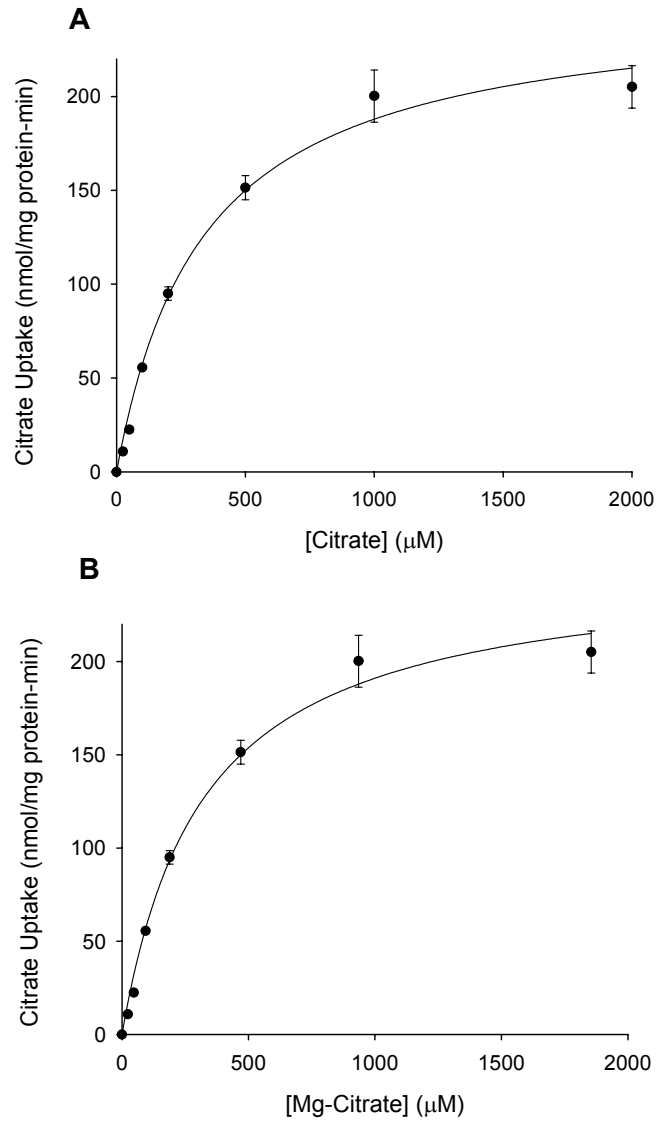


Figure 2.2 (A) Citrate kinetics of CitM expressed in *E. coli* DH5 α cells. 30-second uptakes of different concentrations of citrate (50 μM to 2 mM) were measured in the presence of 10 mM MgCl_2 in HEPES-glucose buffer, pH = 6.8. The K_m for citrate is 339 ± 46 μM and the V_{max} is 252 ± 12 nmol/mg protein-min (the error represents SE of the regression). The data shown are means \pm SEM of four replicate measurements. (B) The same uptake data (shown in A) were expressed as a function of the Mg-citrate concentration. The K_m for citrate is 320 ± 44 μM and the V_{max} is 252 ± 12 nmol/mg protein-min (the error represents SE of the regression).

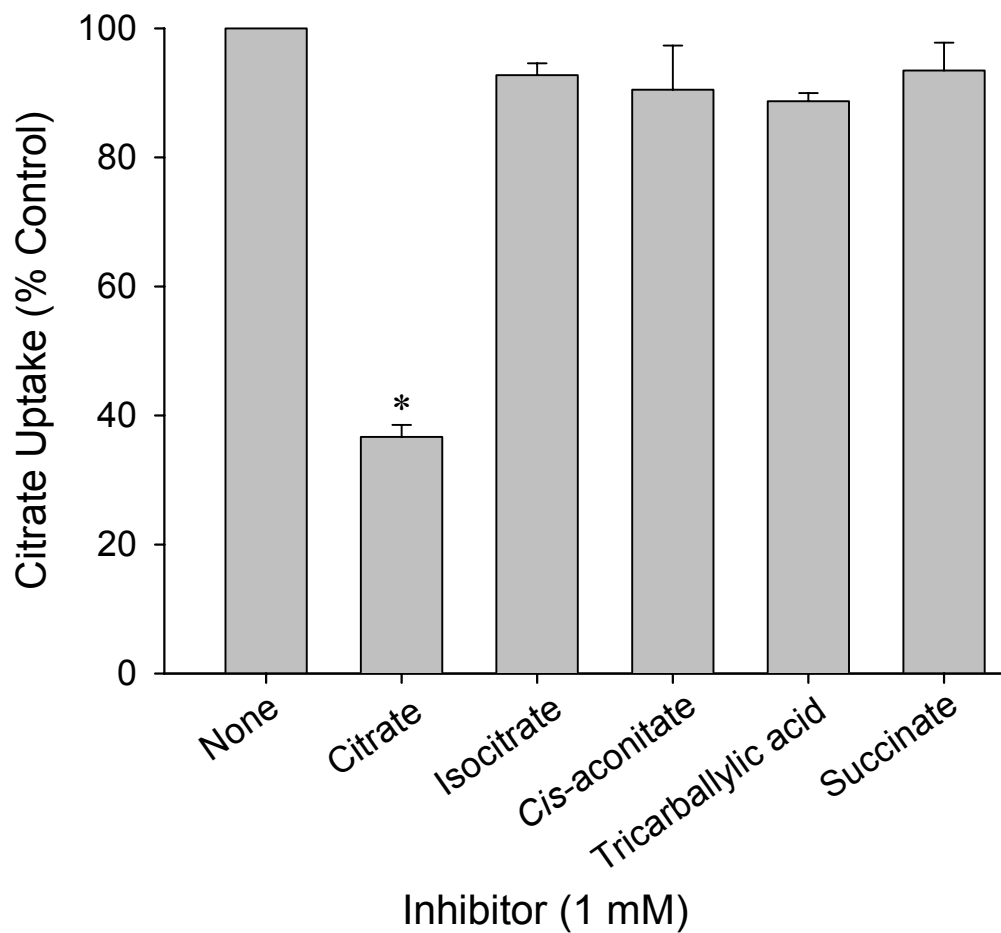


Figure 2.3 Substrate specificity of CitM expressed in *E. coli*. 30-second uptakes of 10 μM ^{14}C -citrate was measured in the presence of 10 mM MgCl_2 and 1 mM test inhibitors or in the absence of test inhibitors. The results shown are the mean \pm range of two separate experiments. The uptake of citrate in the absence of inhibitors was 1.0 ± 0.1 nmol/mg protein-min ($n = 2$). (* significantly different from uptake in absence of inhibitor, $P < 0.001$).

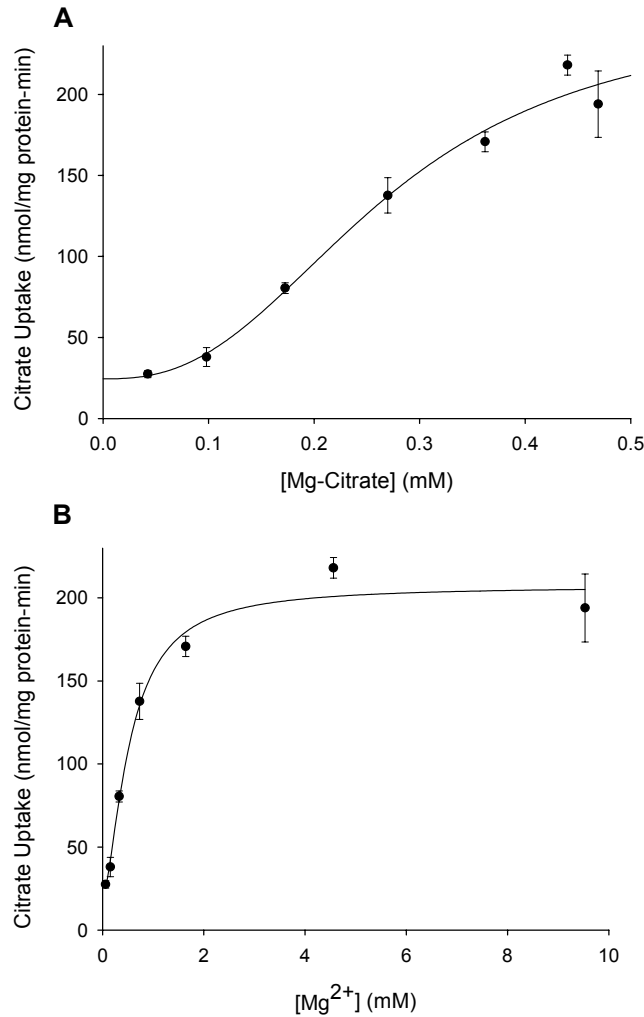


Figure 2.4 Effects of varying Mg^{2+} concentrations on citrate transport in CitM expressed in *E. coli* DH5 α cells. 15-second uptakes of 500 μM ^{14}C -citrate were measured in HEPES-glucose buffer, pH = 6.8 in the presence of different concentrations of total $MgCl_2$ (0 - 10 mM). (A) The uptake data expressed as a function of Mg-citrate concentration in the medium. The $K_{0.5}$ for Mg-citrate is $271 \pm 68 \mu M$, the V_{max} is 226 ± 72 nmol /mg protein-min and the Hill coefficient n is 2.6. (B) The same uptake data as in A expressed as a function of the free Mg^{2+} concentration in the medium. The $K_{0.5}$ for Mg^{2+} is $541 \pm 113 \mu M$, the V_{max} is 187 ± 24 nmol /mg protein-min, the Hill coefficient is 1.6. The uptake in the absence of added Mg^{2+} is 20 ± 17 nmol/mg-min (the errors represent SE of regression). The data shown are the mean \pm SEM of four replicate measurements.

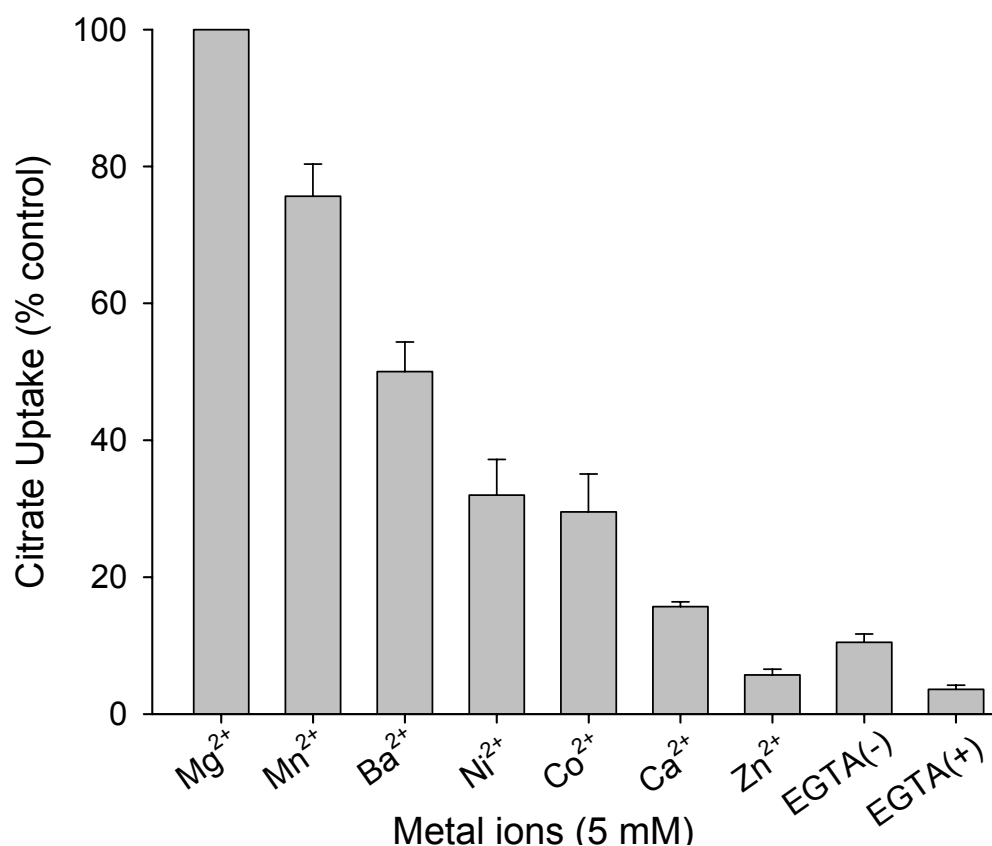


Figure 2.5 Cation specificity of CitM expressed in *E. coli*. 30-second uptakes of 500 μM ^{14}C -citrate were measured in the presence of 5 mM concentrations of different metal ions as shown in the figure. The uptakes were also measured in the absence of added metal ions, without EGTA (-) or with 1 mM EGTA (+). The data are expressed as a percentage of control uptake of citrate measured in Mg^{2+} (82 ± 12 nmol /mg protein-min, mean \pm SEM, $n = 4$). The data shown are the means \pm SEM of 2-4 separate experiments.

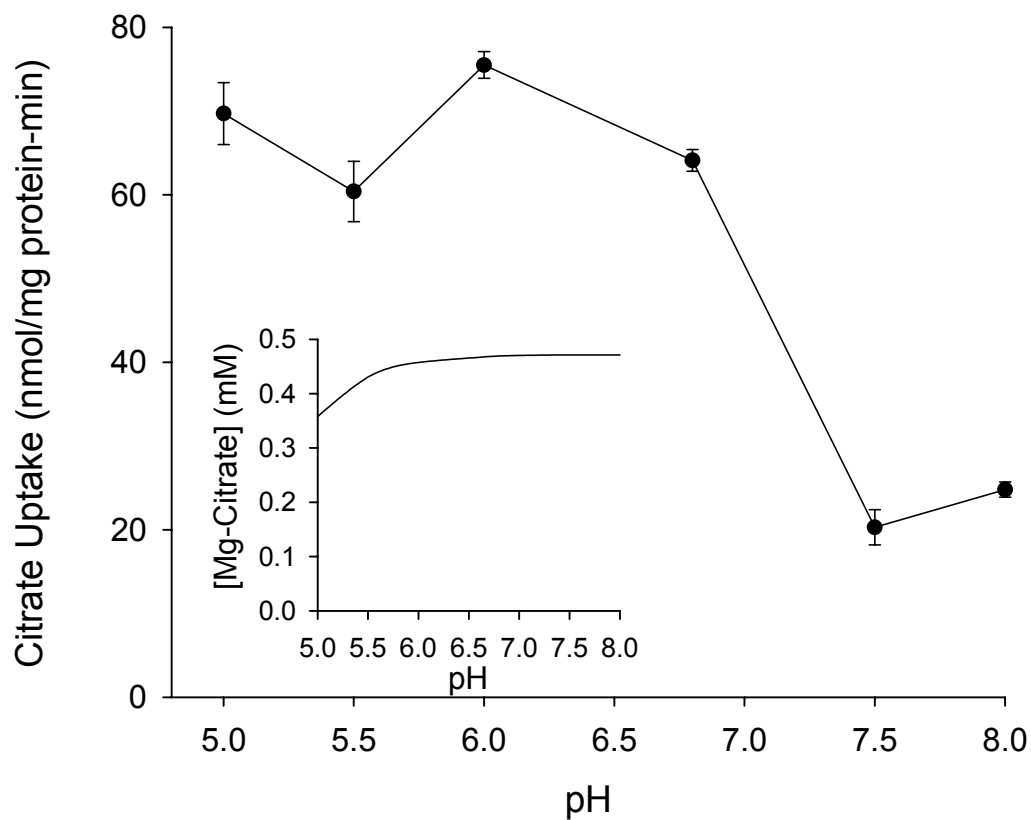


Figure 2.6 Effect of external pH on uptake of citrate by CitM expressed in *E. coli*. Cells were resuspended in HEPES-glucose buffer at different pH values as shown in the figure and 30-second uptakes of 500 μ M citrate were measured in the presence of 10mM MgCl_2 . Inset, the concentration of the Mg-citrate complex in the medium as a function of pH.

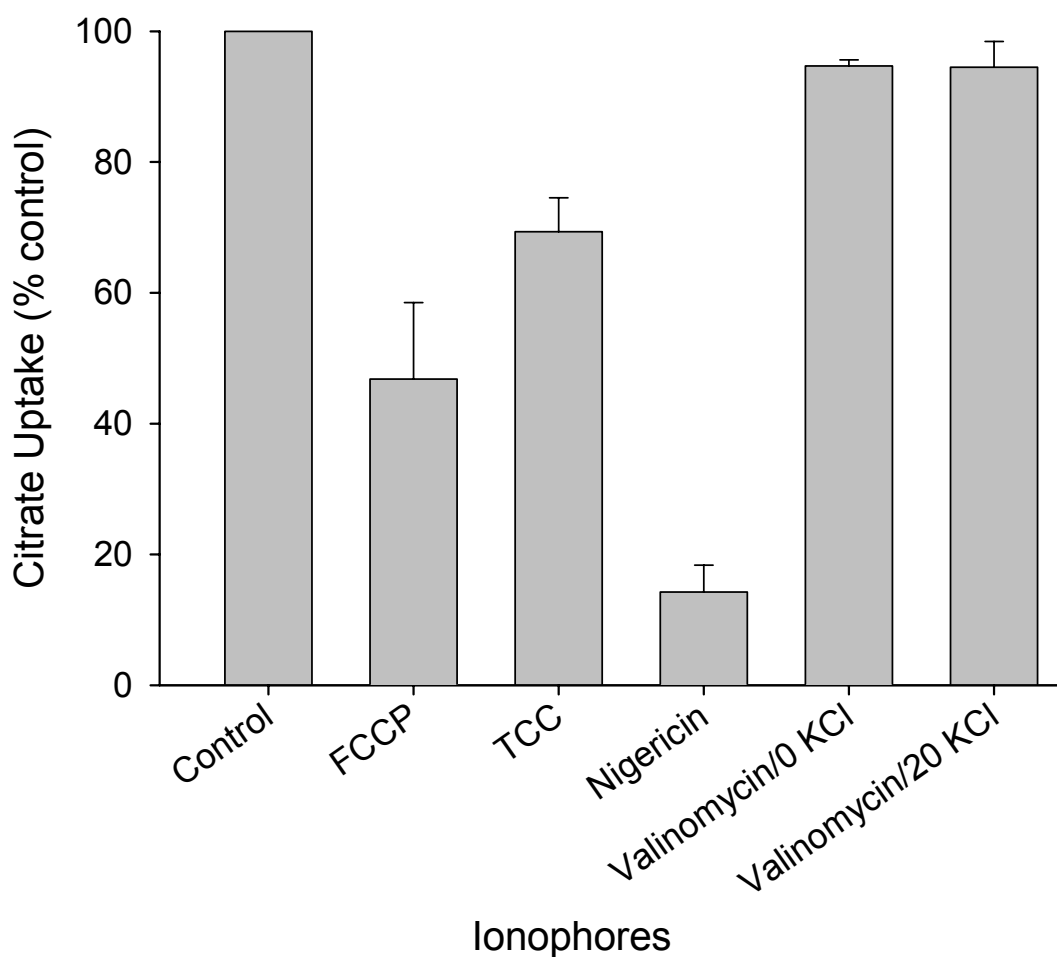


Figure 2.7 Effect of ionophores on citrate uptake by CitM expressed in *E. coli*. 30-second uptakes of 500 μ M citrate were measured in HEPES-glucose buffer in the presence of 10 mM $MgCl_2$ and ionophores: FCCP, TCC, nigericin and valinomycin. The valinomycin experiment was done in 20 mM extracellular KCl (20 KCl) or in 20 mM choline chloride (0 KCl). The data shown are the means \pm range of two separate experiments.

CHAPTER 3: ANTIBODIES AGAINST hNaSi-1 FUSION PROTEIN: TISSUE DISTRIBUTION AND N- GLYCOSYLATION

Introduction

As mentioned in the introduction, the Na^+ -dependent sulfate transporter (NaSi-1) is located mainly on the apical membrane of renal proximal tubule epithelial cells and plays an important role in sulfate reabsorption. Early stop-flow studies of the dog kidney suggested that sulfate uptakes occurred in proximal tubules (43). Later studies with renal membrane vesicles in rats and rabbits further indicated that the transport of sulfate is a secondary active transport process, which is dependent on Na^+ gradient (7; 71; 122; 133). The first mammalian Na^+ /sulfate cotransporter (rNaSi-1) was cloned from rat kidney and small intestine cDNA libraries (78; 85). In later studies using RT-PCR and polyclonal antibodies against the C-terminus of rNaSi-1, it was observed that both NaSi-1-related mRNA and protein were expressed in renal proximal tubules and papillary collecting ducts (23). Immunofluorescence studies and Western blots using proximal tubule apical and basolateral membranes isolated by free-flow electrophoresis confirmed the expression of rNaSi-1 in renal proximal tubules and further restricted the expression to the apical membrane (69). Recent studies of the mouse NaSi-1 showed relatively high levels of mNaSi-1 mRNA expression in kidney, small intestine, and colon, and low levels of expression in cecum, testis, adrenal and adipose tissue (8). In studies of the human NaSi-1 (hNaSi-1), however, the transporter message

seemed to be restricted to kidney (65), suggesting that there is difference in the NaSi-1 distribution between rodents and humans. This species difference has not yet been verified at the protein level. Results of tissue distributions shown in this chapter provided experimental evidence to verify the difference.

Most membrane proteins are glycoproteins which commonly have an oligosaccharide attached to the side-chain NH_2 group of an asparagine residue (called *N*-glycosylation). Glycoproteins may also be glycosylated at the OH group of the side chain of a serine, threonine, or hydroxylysine amino acid residue (called *O*-glycosylation). All transporter proteins of the NaDC/NaSi gene family are predicted to have one or two *N*-glycosylation sites in the C-terminus. Site-directed mutagenesis studies of the rabbit NaDC-1 protein showed that Asn-578, located near the COOH-terminal, is glycosylated (95). *In vitro* translation of rNaSi-1 cRNA with rabbit reticulocyte lysate produced a protein signal at 59 kDa, which was increased to 62 kDa in the presence of microsomes, also consistent with one *N*-glycosylation site (78). The sequences of the cloned NaSi-1 transporters have three or four consensus *N*-glycosylation sites (8; 65; 78). However, no experimental evidence has been reported about which consensus site is used for *N*-glycosylation in NaSi-1 transporters. Furthermore, the functional role of *N*-glycosylation in NaSi-1 is not yet known. The role of *N*-glycosylation in transporter proteins seems to be diverse. Generally, *N*-linked oligosaccharides may affect the biosynthesis, folding, sorting, or trafficking of the protein to the membrane and may also play a role in maintaining the conformational stability and charge, and in resisting

proteolysis (101). Mutagenesis studies of the rabbit Na^+ /dicarboxylate cotransporter, which belongs to the same gene family as NaSi-1 and has ~40% sequence identity with NaSi-1, suggested that *N*-glycosylation is not essential for transport activity (95). Similar results were also observed for Na^+ /glucose cotransporters (42; 45; 126). However, studies of the glucose transporter, GLUT, showed that mutations at *N*-glycosylation site resulted in an increased K_m value, indicating an important functional role of *N*-glycosylation in transport activity (5). Also, the results from mutagenesis and electrophysiology studies of the neuronal GABA transporter suggested that a local conformation at Asn-181 is essential for transport activity (68). No direct experimental evidence, however, has been reported to elucidate the role of *N*-glycosylation in NaSi-1 transporters. Mutagenesis studies in this chapter provided direct experimental evidence for *N*-glycosylation site and the functional role of *N*-glycosylation in hNaSi-1.

In this chapter, a glutathione-S-transferase fusion protein (called GST-Si65) containing a 65 amino acid peptide of hNaSi-1 was used to raise polyclonal antibodies in rabbits. The antibodies were then used to study the tissue distribution as well as location of the *N*-glycosylation site in hNaSi-1. The antibodies were also used to detect the expression of hNaSi-1 mutants (described in Chapter 4). Results in this chapter showed that the antibodies recognized native proteins (rat and pig brush border membrane vesicles) as well as recombinant proteins expressed in oocytes. The hNaSi-1 protein was probably distributed in human kidney, small intestine and colon. Sequence

alignment of SLC13 gene family showed that the putative *N*-glycosylation site at the C-terminal tail is conserved in all members of the gene family and used for *N*-glycosylation in NaDC-1 (95). Therefore, Asn-591 was mutated to tyrosine and alanine, and then the mutants were expressed and studied in *Xenopus* oocytes. The results from Western blotting suggested that hNaSi-1 contains only one *N*-glycosylation site at Asn-591, which is located in the extracellular C-terminus, similar to other members of the SLC13 gene family. Immunofluorescence images showed that cell-surface expression of the two *N*-glycosylation site mutants, N591Y and N591A, was more abundant than the wild-type, indicating that the removal of the *N*-glycosylation site does not reduce the protein trafficking to the membrane. However, kinetic experiments showed a pronounced reduction in the maximum uptake rate of N591Y and N591A, with no change in K_m . Therefore, Asn-591 or *N*-glycosylation in hNaSi-1 seems to be required for transport activity.

Methods

Isolation of hNaSi-1 cDNA

A routine sequence search of GenBank found a human sequence of unknown function (GenBank accession number AK026413), which had a high sequence identity with rat NaSi-1. Therefore, it was likely that this sequence might code for the human NaSi-1. At that time, the paper describing the cloning of human NaSi-1 (GenBank accession number AF260824) was not published

yet (65). The hNaSi-1 was amplified from human kidney cDNA by polymerase chain reaction (PCR) using the Advantage cDNA PCR kit (Clontech). Two gene-specific primers were designed: 5'-ATT GTC GAC ACC TGC CCA GGA CAA **TGA** AAT TCT TC-3', which included the start codon (in bold) and a *Sa*/I restriction site (underlined), and 5'-TAT GGC CAA GCA AGT TGC AGA TGG TTC ATG AGC-3', located ~240 bp downstream of the stop codon and included a *Msc* I restriction site (underlined) to facilitate subcloning. The PCR product was ligated into the pCR2.1 vector using a TOPO TA cloning kit according to manufacturer's directions (Invitrogen). The hNaSi-1 cDNA was then subcloned into the *Sa*/I / *Msc* I sites of the pSPORT1 expression vector (Gibco) containing the 3' UTR from NaDC-2, which facilitates expression of transporter proteins in oocytes (6). The plasmid construct, called pSPORT/hNaSi-1, was sequenced at the Sealy Center for Molecular Science (University of Texas Medical Branch at Galveston, TX). The secondary structure model of hNaSi-1 was predicted using a combination of Kyte-Doolittle and Rao-Argos hydropathy analysis (63; 111).

Site-directed mutagenesis of N-glycosylation site

Site-directed mutagenesis was performed using the oligonucleotide-directed method of Kunkel {Kunkel 1985 161 /id}. *E. coli* CJ236 bacteria transformed with pSPORT/hNaSi-1 were grown in uridine-containing medium to produce double-stranded plasmids which contain uracil in place of thymine. Single stranded DNA was rescued using M13K07 helper phage and then used

as a template for mutagenesis performed by an *in vitro* mutagenesis kit (Muta-gene, BioRad). The mutations were introduced with the following antisense primers (the mutated nucleotides are highlighted in bold): (1) Asn-591 to Tyr: 5'-CAT GGT CTC **ATA** ACT CAT AGC AGG-3' and (2) Asn-591 to Ala: 5'-CAT GGT CTC **AGC** ACT CAT AGC AGG-3'. The sequences of the mutated plasmids were verified by the Sealy Center for Molecular Science (UTMB).

Preparation of GST-Si65 fusion protein

PCR amplification of cDNA coding for a specific peptide in hNaSi-1 Amino acid residues (173-237) of hNaSi-1, located in an intracellular loop between putative TMDs 4 and 5, were amplified by PCR using the pSPORT/hNaSi-1 construct as a template. The reaction was performed with the following two primers, which contained restriction sites for *BamH* I and *EcoR* I (underlined) to facilitate subcloning: 5'- CGT GGA TCC TTC AAC GGA TCA ACC AAC -3', and 5'-ATG AAT TCC GTG GCC CTT CTT TGT -3'. A touch-down PCR reaction was performed using the Advantage cDNA PCR kit (Clontech) with the following conditions: denaturation at 95°C for 3 minutes followed by 5 cycles: 94°C for 30 seconds, 72°C for 30 seconds, 5 cycles: 94°C for 30 seconds, 70°C for 30 seconds, and another 25 cycles: 94°C for 30 seconds, 68°C for 30 seconds. The PCR product was ligated into the pCR2.1 vector using the TOPO TA cloning kit (Invitrogen) and then subcloned into the *BamH* I and *EcoR* I sites of the pGEX-2T vector (Amersham Biosciences Corp.). This vector is designed to produce a fusion protein of the inserted cDNA sequence at the C-

terminal end of glutathione S-transferase (GST). The new construct is called pGEX/hNaSi-1 and the fusion protein is called GST-Si65 since it contains a peptide of 65 amino acid residues of the hNaSi-1 protein fused to GST. The sequence of the pGEX/hNaSi-1 recombinant plasmid was verified by the Sealy Center for Molecular Science (UTMB).

Expression and purification of the fusion proteins The methods used here were as described previously (95). *E. coli* DH5 α cells were transformed with the pGEX/hNaSi-1 recombinant plasmid or only pGEX-2T vector and then cultured in rich medium (120). Protein synthesis was induced by the addition of isopropyl- β -D-galactopyranoside (IPTG). After 2-hour growth, the cells were harvested, lysed, centrifuged and then purified using affinity chromatography with a glutathione Sepharose 4 B column (Amersham Biosciences Corp.). The bound proteins (GST-Si65 or GST) were eluted from the columns using elution buffer containing 10 mM glutathione. The eluted proteins were then concentrated and desalted into phosphate-buffered saline (PBS) through a Centricon-10 column (Amicon Inc.) according to the manufacturer's instruction. The protein samples were tested on 10% sodium dodecyl sulfate (SDS)-polyacrylamide gel and stained with Coomassie blue. The mass of the protein was estimated by comparison with BenchMark Prestained Protein Ladder (Invitrogen).

Preparation and purification of the antibodies

The purified fusion protein was sent to Covance Research Products Inc. (Denver, PA) to raise polyclonal antibodies in 2 rabbits. The immune sera were tested using Western blots of fusion proteins. Titers of the immune sera were tested with Enzyme-Linked Immunosorbent Assay (ELISA) by the Covance company one and three months after immunization. The final immune serum with the highest titer was purified through a GST affinity column to remove anti-GST antibodies. The GST affinity column was prepared using the Aminolink Immobilization Kit (Pierce) with 20 mg of purified GST protein. The purified immune serum containing the anti-hNaSi-1 antibodies was then used for Western blotting and immunofluorescence experiments.

Western blotting

Membrane proteins were separated by SDS-polyacrylamide gel electrophoresis (SDS-PAGE) on 8% or 6% tricine gel and then transferred to nitrocellulose membranes (0.45 μm , Schleicher & Schuell Inc.) by electrotransfer (100 volts for 1 hour) (95). For some experiments, a preparative gel with a single sample well was run and the membrane was cut into strips. The membranes or strips were blocked with 0.5% Carnation instant dried milk and 0.05% Tween 20 dissolved in PBS (called PBS-TM) at room temperature for 1 hour or at 4°C overnight. Then the blots were incubated with 1:1000 dilution of the primary antibodies in PBS-TM at room temperature for 2 hours

and then washed three times with PBS-TM. For fusion-protein blocking experiments, the immune serum was pre-incubated with 2 mg/ml of fusion protein or GST at 37°C for 1 hour and then applied to the blot. The secondary antibodies, anti-rabbit IgG horseradish peroxidase linked whole antibody from donkey (Amersham Biosciences Corp.), were diluted to 1:5000 in PBS-TM and applied at room temperature for 1 hour. Antibody binding was detected using a Supersignal West Pico Chemiluminescent Substrate kit (Pierce) and images were acquired using a Kodak Image Station 440CF (Eastman Kodak Company) with overlapping 6 captures (exposure time is 5 minutes per capture without saturating). The mass of hNaSi-1 was estimated by comparison with chemiluminescent protein size standards (MagicMark Western Standard, Invitrogen).

Preparation of brush border membrane vesicles

Brush border membranes of rat and pig kidneys were prepared using a Mg^{2+} precipitation method as described previously (92). The kidneys were perfused and removed, and then the cortex was dissected from medulla. The dissected kidneys were homogenized with a polytron in 300 mM mannitol, 1 mM EDTA, 20 mM MES-Tris (pH 6) and 0.1 mM PMSF. Then 100 mM $MgCl_2$ stock solution was added to a final concentration of 10 mM and the sample was mixed in the cold for 20 minutes. The samples were then centrifuged 4 times at $6,000 \times g$ for 10 minutes, taking the supernatant each time. The supernatant was then centrifuged at $35,000 \times g$ for 10 minutes. The pellet

from this centrifugation was homogenized in 300 mM mannitol, 1 mM EDTA, 20 mM HEPES-Tris (pH 7.4) and 0.1 mM PMSF. Then the mixture was centrifuged again at $35,000 \times g$ for 10 minutes and the supernatant was discarded. The pellet was resuspended and centrifuged again in the same way. The final pellet was resuspended in 300 mM mannitol, 20 mM HEPES-Tris (pH 7.4), 0.1 mM Mg^{2+} -sulfate and then stored at $-80^{\circ}C$ until use. The concentrations of the brush border membrane vesicles were measured using a protein assay kit (Bio-Rad). The SDS-PAGE gels for Western blots contained 20 μg (rat) or 24 μg (pig) of the vesicle proteins in each lane.

Transcription of cRNA

The pSPORT/hNaSi-1 plasmid construct was linearized with *Xba* I and then purified using RNase-free Chroma-spin 1000 columns (Clontech). This linearized RNase-free DNA was used as a template for *in vitro* cRNA transcription, using the T7 mMessage mMachine kit (Ambion). The cRNA was resuspended in RNase-free water to a final concentration of $\sim 1 \mu g / \mu l$ and stored at $-80^{\circ}C$.

Preparation and injection of Xenopus oocytes

Healthy adult female *Xenopus laevis* (Xenopus I) were anesthetized by submersion in 0.1% 3-aminobenzoic acid ethyl ester (MS-222) solution and a portion of the ovary was surgically removed. The oocytes were then placed in

Barth's solution (88 mM NaCl, 2.4 mM NaHCO₃, 10 mM HEPES, 1 mM KCl, 0.33 mM Ca(NO₃)₂, 0.41 mM CaCl₂, and 0.82 mM MgSO₄, pH 7.4) and separated using forceps. The follicular layer was removed by incubating oocytes first in collagenase solution (0.2% collagenase from Roche and 0.1% trypsin inhibitor type III-0 dissolved in Ca²⁺-free Barth's solution) for 60 minutes and then in 100 mM potassium phosphate/0.1% BSA solution for another 45 minutes. Stage V and VI oocytes (~1mm diameter) were sorted and then placed at 18°C overnight in Barth's solution with 100 µg/ml gentamycin sulfate, 50 µg/ml of tetracycline, 2.5 mM Na⁺-pyruvate, and 5% heat inactivated horse serum at 18°C. The next day, oocytes were sorted again before injection. The tip of the glass needle (Drummond) used for injection was made to about 20-30 µm. Each oocyte was injected with 50 nl of hNaSi-1 cRNA (1 µg/ µl). The medium and culture vials were changed daily.

Biotinylation of Xenopus oocytes

Groups of 5 oocytes were washed three times with PBS (pH 9) then incubated in 0.5 ml of 0.5 mg/ml of Sulfo-NHS-LC-Biotin (Pierce) for 10 minutes at room temperature. The oocytes were rinsed with Quench buffer (100 mM glycine in PBS) at room temperature followed by incubation in the same Quench buffer for 20 minutes on ice. The oocytes were then incubated on ice for 30 minutes with lysis buffer (1% Triton X-100, 20 mM Tris and 150 mM NaCl, pH 7.6), which contained protease inhibitors (10 µg/ml pepstatin, 10 µg/ml leupeptin and 0.5 mM phenylmethylsulfonyl fluoride or PMSF). The

solubilized oocytes were centrifuged in a microcentrifuge (Model 5415C, Brinkmann Instruments, Inc.) at full speed for 15 minutes and the supernatants were incubated with 50 μ l Immunopure Immobilized Streptavidin (Pierce) at 4°C overnight. The next day, the samples were washed and pelleted in the following buffers: the same lysis buffer as before but without protease inhibitors, high-salt buffer (0.1% Triton X-100, 20 mM Tris and 50 mM NaCl, pH 7.5) and no-salt buffer (50 mM Tris, pH 7.5). The washed streptavidin-biotin complexes were then used in Western blots.

Preparation and deglycosylation of *Xenopus* oocyte plasma membranes

The plasma membrane was prepared from oocytes by the method of Geering and colleagues (35). Each group of 50 oocytes was washed twice with homogenization buffer (83 mM NaCl, 1 mM MgCl₂ and 10 mM HEPES-Tris, pH 7.9) and then homogenized 20 passes with a glass-teflon homogenizer. The samples were centrifuged twice at 1, 000 \times g for 10 minutes, discarding the pellet each time. The supernatants were transferred to a microcentrifuge tube and spun down at maximum speed (Model 5415C, Brinkmann Instruments, Inc.) for 20 minutes. The supernatants were removed and the pellets were resuspended in homogenization buffer containing protease inhibitors (0.5 mM PMSF, 50 μ g/ μ l leupeptin and 16.7 μ g/ μ l pepstatin) and then stored at -20°C until use. The concentrations of the protein samples were measured using a protein assay kit (Bio-Rad). For deglycosylation, 4 μ g of the plasma membranes were denatured in 0.5% SDS and 1% β -mercaptoethanol and

boiled for 10 minutes, and then incubated in 50 mM sodium phosphate buffer (pH 7.5), 1% NP-40 and 1 μ l Peptide:N-glycosidase F, PNGaseF (500,000 U/ml, New England BioLabs) at 37°C for 1 hour (95). Controls were incubated with water instead PNGase F. The samples were then used in Western blots.

Immunofluorescence of *Xenopus* oocytes and human tissue array

Oocytes were injected with cRNA of wild-type hNaSi-1 and two glycosylation mutants, N591Y and N591A. Four days after injection, the oocytes were washed three times with PBS and then incubated, at room temperature for 30 minutes, with 25 μ g/ml of Alexa Fluor 594 conjugated Wheat Germ Agglutinin, WGA, (Molecular Probes, Inc.) to label the plasma membrane. After incubation, the oocytes were washed three times with PBS and then frozen and cut into sections (5 μ m) by the Histopathology Core Facility (UTMB). The human tissue array slides were paraffin sections purchased from Imgenex (San Diego, CA). Before immunoblotting, the paraffin was removed and then the slides were treated with antigen retrieval method by the Histopathology Core Facility UTMB). Either frozen oocyte section or human tissue array slides were then incubated with blocking buffer of 1% goat serum in PBS at room temperature for 1 hour. The primary antibodies were diluted to 1:100 in the same blocking buffer and then applied at room temperature for 1 hour. The slides were washed 3 times with PBS. The secondary antibodies (Alexa Fluor 488 goat anti-rabbit IgG, 2mg/ml, Molecular Probes) were diluted to 1:500 for oocyte or 1:750 for human tissue array and then applied to the

samples at room temperature for 1 hour. The slides were washed again three times with PBS. The optimal concentrations of the primary and secondary antibodies were determined in preliminary experiments. Vectashield mounting medium (Vector) was added to the slides, which were then covered with microscope cover glass (22 x 50-1, thickness range 0.13-0.17 mm, Fisher Scientific), and the edges were sealed with nail polish. The immunofluorescence was observed with 10x (Plan Fluor, 0.3 NA), 20x (Plan Fluor, 0.5 NA) or 60 x (Plan Apo, 1.4 NA Oil) objectives on a Nikon Eclipse E800 upright epifluorescence microscope. Standard bandpass emission filter sets for tetramethylrhodamine-isothiocyanate (TRITC) and fluorescein-isothiocyanate (FITC) were used to observe the red (Alexa Fluor 594) and green (Alexa Fluor 488) fluorescent dyes, respectively. Images were acquired by a digital camera (Roper Scientific CoolSNAP FX cooled CCD monochrome 12 bit), recorded with Metavue 4.67 and analyzed with MetaMorph 5.0 imaging software (Universal Imaging Corporation, Downingtown, PA). These experiments were done with the help of the Optical Imaging Laboratory (UTMB).

Radiotracer uptake assay

The transport of [^{35}S]-sulfate (Perkin Elmer Life Science) was measured in *Xenopus* oocytes 3 or 4 days after cRNA injection. Each group of 5 oocytes was incubated at room temperature for about 15 minutes and then rinsed with room temperature choline buffer (100 mM cholineCl, 10 mM HEPES, 2 mM

KCl, 1 mM MgCl₂ and 1 mM CaCl₂, pH 7.5). Transport buffer (0.4 ml) containing [³⁵S]-sulfate in Na⁺ buffer (100 mM NaCl in place of cholineCl), was added to initiate the uptake. After a timed period of incubation, 4 ml ice-cold choline buffer were added to stop the reaction. Then the oocytes were washed 3 times using the same buffer. Individual oocytes were transferred to scintillation vials and 0.25 ml of 10% SDS was added to dissolve the oocytes. Then 3 ml of scintillation cocktail was added to each vial and the radioactivity was counted in a scintillation counter.

Transport data analysis

In kinetic experiments, sulfate uptakes in individual cRNA-injected oocytes have been corrected for background uptakes by subtracting the mean uptakes in control uninjected oocytes. The uptake rates were fitted to the Michaelis-Menten equation: $v = V_{max} * [S] / (K_m + [S])$, where [S] is the concentration of sulfate, V_{max} is the maximum uptake rate and K_m is the concentration of sulfate that produces $\frac{1}{2} V_{max}$. The non-linear regression of the data to the equation was done using Sigma Plot 2000 (SPSS).

Results

Preparation of the GST-Si65 fusion protein and anti-hNaSi-1 antibodies

The hNaSi-1 protein (595 amino acid residues) is predicted to have 11 transmembrane domains (TMD) and 4 putative *N*-glycosylation sites as shown

in [Figure 3.1](#). This model is based on hydropathy analysis of the hNaSi-1 amino acid sequence (63) and comparison with other members of the SLC13 gene family (95; 148). Amino acid residues (173 to 237) of hNaSi-1, which are located in an intracellular loop between putative transmembrane domains 4 and 5, have a high antigenic index (50). Also, the sequence alignments of the members in the NaDC/NaSi gene family have a very low amino acid sequence identity in this region. Therefore, this part of the sequence was selected as an immunogenic peptide in a GST fusion protein to reduce the possible cross-reactions with other members in the gene family. In addition, GST was chosen to make a fusion protein because it is easy to purify with a GST affinity chromatography column. The cDNA sequence coding for the 65 amino acid peptide was amplified by PCR and then subcloned into the pGEX-2T vector. The recombinant plasmid, pGEX-2T/hNaSi-1, codes for the GST-Si65 fusion protein consisting of 65 amino acid residues of hNaSi-1 fused to the C-terminal end of GST.

[Figure 3.2](#) shows a Coomassie stained gel of samples taken during the purification of GST and GST-Si65 fusion protein. The expression of the proteins in *E. coli* cells reached a maximum level two hours after IPTG induction. The soluble fraction containing the GST or GST-Si65 fusion protein was purified through a GST affinity chromatography column. The two proteins, GST (28 kDa) and GST-Si65 (34 kDa), differ in mass by approximately 6 kDa, which is close to the predicted mass of 7 kDa for the hNaSi-1 peptide. The purified GST-Si65 fusion protein was injected into two rabbits (TX122 and

TX123) to raise antibodies. Three months after the first injection, ELISA tests of the immune sera from the two rabbits showed titers of 56, 000 x and 36, 000 x. The final immune serum with the highest titer was purified by removing anti-GST antibodies and used in all of the subsequent experiments. The immune serum recognized the purified GST-Si65 fusion protein in Western blots (data not shown).

Western blots of renal brush border membranes

Brush border membrane vesicles (BBMVs) prepared from rat or pig renal cortex were tested by Western blotting as shown in [Figure 3.3](#). There was no signal obtained for either rat or pig with the preimmune serum. An immunoreactive protein signal centered at 79 kDa (rat) or 73 kDa (pig) was detected with the crude (unpurified) or purified immune serum. These two signals disappeared after blocking the immune serum with the GST-Si65 fusion protein but did not show change with GST-blocked immune serum. The predicted mass of the rat NaSi-1 is estimated to be 66 kDa (78). Therefore, these two protein signals are most likely to represent glycosylated NaSi-1 transporters in rat and pig renal brush border membranes.

Tissue distribution of hNaSi-1

Preliminary experiments showed that the purified immune serum containing anti-hNaSi-1 antibodies worked well on formalin-fixed paraffin embedded sections from rat kidney (data not shown). Therefore, commercially

available formalin-fixed human tissue array slides containing more than 50 human normal tissues were purchased to study the tissue distribution of hNaSi-1. Immunofluorescence experiments were performed on the slides using purified immune serum or preimmune serum (control).

Figure 3.4 shows some representative tissues having a positive signal: kidney cortex, kidney medulla, small intestine (jejunum/ileum) and colon. In these tissues, no immunofluorescent signals were seen with preimmune serum. When probing the slide with purified immune serum, some relatively weak signals were detected on the apical membrane of epithelial cells but much stronger immunofluorescence signals were observed in the nuclei. Since previous immunofluorescence studies detected the rat NaSi-1 on the apical membrane of renal proximal tubules (69), the hNaSi-1 transporter was also expected to have the same distribution. It is not clear whether the signal in nucleus represents cross-reactivity with other proteins or not.

Positive immunofluorescence signals were also observed in other tissues and organs on the human tissue array slides: skin, breast, liver, urinary bladder, lymph node, tonsil, thymus, spleen, salivary gland, pancreas, thyroid, adrenal gland cortex and medulla, bronchus, lung, brain white matter, brain gray matter and cerebellum, prostate, testis, ovary, uterine cervix, endometrium and placental villi (data not shown). The signals are also seen primarily in nucleus. Several tissues did not show positive immunofluorescence: subcutaneous fat, heart, skeletal muscle, ureter, salpinx,

esophagus, duodenum, epididymis and seminal vesicle, myometrium, and placenta amniochorion and cord (data not shown).

N-glycosylation of hNaSi-1 expressed in *Xenopus* oocytes

Based on the secondary structure model of hNaSi-1 shown in [Figure 3.1](#), the conserved residue, asparagine 591, located at the extracellular C-terminal tail, is the most likely candidate for *N*-glycosylation. This residue is conserved in all members of the NaDC/NaSi gene family. The counterpart of Asn-591 in rabbit NaDC-1, Asn-578, was used for *N*-glycosylation (95). Therefore, this residue was mutated to tyrosine or alanine (N591Y or N591A) in order to determine whether Asn-591 is also the *N*-glycosylation site in hNaSi-1. Plasma membranes prepared from control uninjected oocytes or oocytes expressing wild-type hNaSi-1 or N591Y were incubated with PNGase F to remove *N*-linked oligosaccharides (75). Control samples were incubated with water. The samples were then analyzed on Western blots using anti-hNaSi-1 antibodies ([Figure 3.5](#)). For the water treated wild-type hNaSi-1 protein, the antibodies recognized two protein bands at 53 kDa and 64 kDa. After treatment with PNGase F, only a single protein of 49 kDa was detected. The mass of the wild-type protein decreased by 4 or 15 kDa after the enzyme treatment. The 53 kDa and 64 kDa proteins are likely to represent the core and mature glycosylated forms of hNaSi-1 protein, respectively. The N591Y mutant had a smaller apparent mass than the wild-type, about 52 kDa, which was not

affected by PNGase F treatment. Therefore, Asn-591 is most likely to be the residue used as the single *N*-glycosylation site in hNaSi-1.

It is somewhat surprising that the apparent mass of N591Y (about 52 kDa) is not identical to that of the deglycosylated wild-type hNaSi-1 (49 kDa). Therefore, in order to determine whether the 3 kDa difference might be due to a difference in migration rate of the protein in the gel between the wild-type and tyrosine-containing mutant, a second mutant using alanine at position 591 (N591A) was tested and compared with N591Y on Western blots of the cell-surface biotinylation of intact oocyte plasma membrane. The N591A mutant had the same apparent mass as N591Y (50 kDa) ([Figure 3.6](#)), suggesting that the replacement residue does not alter the protein's migration rate in SDS-PAGE gel.

Many of the Western blots with wild-type or mutant hNaSi-1 have larger immunoreactive protein signals at about 100-110 kDa, which may represent dimeric forms of hNaSi-1 ([Figure 3.5](#) and [Figure 3.6](#)). Different treatments were tried to dissociate these dimers including the addition of 100 mM DTT or 8 M urea in the sample buffer, increasing the percentage of SDS in the sample buffer from 4% to 6%, boiling the sample for 4 minutes or heating at 55°C for 15 minutes. However, the aggregation seemed very stable and none of the treatments had effect on it (data not shown).

In control experiments, I found that it is not possible to do cell-surface biotinylation with hNaSi-1 expressed in oocytes. It appears that the streptavidin agarose beads bind non-specifically to hNaSi-1. Streptavidin and neutravidin gels were also tested but had the similar results (data not shown). This is in contrast to oocytes expressing NaDC-1, which have no protein signals when incubated without Sulfo-NHS-LC-biotin (Ana M. Pajor, unpublished data). Therefore, immunofluorescence experiments of frozen sectioned oocytes were performed to compare the cell-surface expression level of the mutant proteins with the wild-type hNaSi-1.

Immunofluorescence of Xenopus oocytes expressing wild-type hNaSi-1 and mutants N591Y and N591A

In this study, the red fluorescent dye (Alexa Fluor 594) conjugated WGA was used to label the plasma membrane of oocytes. Preliminary experiments showed that the dye did not penetrate to the intracellular side of oocytes and can also survive the freezing and sectioning process (data not shown). As shown in [Figure 3.7](#), the immunofluorescence of the wild-type and two *N*-glycosylation mutants was predominantly distributed on the plasma membrane but some signals were also observed intracellularly. The red fluorescent WGA labeled membrane of each oocyte was used as a mask to outline the green immunofluorescence area of the same oocyte. The average intensity of the green immunofluorescence signals located in the overlapped area (yellow area in the color combination as shown in [Figure 3.7](#)) was analyzed with 11 to 16 individual oocytes from the same batch. The average intensity of the

overlapped green immunofluorescence on plasma membrane of oocytes expressing the wild-type hNaSi-1 was considered as a positive control ($100\% \pm 11$, $n = 11$). Compared with the wild-type, the two mutants, N591Y and N591A, showed significantly stronger average intensity with $137\% \pm 11$ ($n = 16$) and $206\% \pm 14$ ($n = 16$) of the control, respectively. Preliminary experiments showed that there were no significant immunofluorescence signals in uninjected oocytes. These results indicate that the two non-glycosylated mutants, N591Y and N591A, have more abundant cell-surface expression than the wild-type.

Kinetics of sulfate uptakes by N591Y and N591A expressed in oocytes.

To test the functions of the N591Y and N591A mutants, 15-minute uptakes of $100 \mu\text{M}$ sulfate were measured and then compared in oocytes expressing the wild-type and mutant hNaSi-1 (data not shown). It was found that uptakes in the two mutants were decreased to about 30% of the wild-type. To further study the functional role of the *N*-glycosylation in hNaSi-1, the kinetic properties of the two mutants were assessed. Preliminary studies showed that uptakes of 1 mM sulfate by oocytes expressing wild-type hNaSi-1 were linear up to 60 minutes, therefore, 10 minutes were used in the kinetic experiments. [Figure 3.8](#) shows the results from a single kinetic experiment. The two mutants both showed a similar affinity for sulfate as the wild-type but the maximum uptake rates were greatly reduced compared with the wild-type. In three separate experiments, the mean K_m was $376 \pm 122 \mu\text{M}$ (wild-type), $466 \pm 295 \mu\text{M}$ (N591Y) and $258 \pm 66 \mu\text{M}$ (N591A), and the maximum uptake rate V_{max}

was 1135 ± 282 pmol/oocyte-hr (wild-type), 298 ± 113 pmol/oocyte-hr (N591Y) and 391 ± 88 pmol/oocyte-hr (N591A), mean \pm SEM. Since N591Y and N591A were both expressed on the plasma membrane of oocytes (Figure 3.7), the mutations affect the transport activity rather than targeting of hNaSi-1 proteins. Since V_{max} is the product of protein expression and turnover number, removal of either the asparagine residue at 591 or the *N*-glycosylation results in a decrease in hNaSi-1 turnover number.

Discussion

This chapter discussed the preparation of the anti-hNaSi-1 antibodies which were used to determine the tissue distribution and *N*-glycosylation site of hNaSi-1. A peptide containing 65 amino acids (from 173 to 237) of the hNaSi-1 protein was chosen to prepare a GST fusion protein (called GST-Si65). Polyclonal antibodies against the GST-Si65 fusion protein were raised in rabbits. The purified antibodies recognize the native NaSi-1 transporters in rat and pig renal brush border membranes as well as recombinant proteins in oocytes. Based on the secondary structure model of hNaSi-1, there are four putative *N*-glycosylation sites in hNaSi-1 and Asn-591 is the only one that is located at the extracellular C-terminal thus this residue is the most likely candidate for *N*-glycosylation. Therefore, asparagine at 591 was mutated to tyrosine or alanine, and the wild-type and two mutants were expressed and studied in *Xenopus* oocytes. PNGase F treatment resulted in up to 15 kDa shifting of protein band for wild-type hNaSi-1 but no change for the mutant, N591Y, indicating that the extracellular C-terminal residue, Asn-591, is the one

single *N*-glycosylation site in hNaSi-1. Furthermore, mutations of Asn-591 did not decrease the expression of the protein on the plasma membrane of oocytes but resulted in a decrease of about 70% of the maximum uptake rate compared with the wild-type protein. Therefore, Asn-591 or its glycosylation plays an important role in the transport activity but not cell-surface expression of hNaSi-1. Since the maximum uptake rate is related with the turnover rate and the number of proteins expressed on the membrane, it is most likely that Asn-591 or *N*-glycosylation are involved in changing the turnover number thus reducing the transport activity of the protein.

Specificity of the anti-hNaSi-1 antibodies

Since it is difficult to obtain renal brush border membrane vesicles from human, rat and pig renal BBMVs were used in this chapter to test the specificity of the anti-hNaSi-1 antibodies. The results showed a 79 kDa protein band in rat and a 73 kDa protein band in pig. Based on the protein sequence, the mass of rat NaSi-1 was predicted to be 66 kDa (78). Several previous studies provided experimental evidence for the mass of the rat NaSi-1 transporter. The *in vitro* translation of rat NaSi-1 cRNA resulted in a ~59 kDa protein band (78). Also, rat NaSi-1 antibodies detected a 68 to 69 kDa protein signal on Western blots of rat renal brush border membrane proteins (69; 115). Western blotting of Sf9 cells expressing rat NaSi-1 detected proteins at 55-60 kDa (34). In this chapter, the protein band detected in rat renal BBMVs by anti-hNaSi-1 antibodies is about 79 kDa, which is not exactly the same as previous reports. The difference in the apparent mass of the protein is probably because

the migration rate of a membrane protein is related to the percent of acrylamide used in the gel (45). In this chapter, 8% SDS-polyacrylamide gel was used to separate protein samples, whereas the previous study used 15% polyacrylamide gels (115). Despite the difference, the 79 kDa protein band is likely to be a glycosylated form of the native NaSi-1 transporter in rat renal brush border membranes. Also, in this chapter, the 73 kDa protein band detected on the Western blots is likely to represent the glycosylated form of NaSi-1 in pig renal brush border membrane. No studies have yet been reported on the mass of the pig NaSi-1.

The anti-hNaSi-1 antibodies identified two protein bands at 53 kDa and 64 kDa on Western blots of biotinylated plasma membranes of intact oocytes expressing wild-type hNaSi-1 (Figure 3.5 and Figure 3.6). These two protein bands may represent different glycosylation states of the protein. Previous studies of rbNaDC-1 also showed various mature forms between 57 to 66 kDa (95). Based on the primary amino acid sequence, the predicted mass of hNaSi-1 is 66 kDa. However, the nonglycosylated form of hNaSi-1 shown here is about 49 kDa and the glycosylated form is between 53 kDa and 64 kDa. The mass of rNaSi-1 in native renal BBMV is from 68 to 69 kDa (69; 115). Similar difference between the apparent and predicted mass was also observed for rbNaDC-1 (95) and the Na⁺-glucose cotransporter (45). One explanation is possibly because NaSi-1 is expressed in the heterologous system, *Xenopus* oocytes, which have a different sorting process than the native mammalian cells. Another explanation is that membrane proteins migrate differently in

SDS-PAGE than the protein standards, which are soluble proteins. Therefore, it is not possible to obtain an accurate estimate of mass of membrane proteins from a single gel (45).

Tissue distribution

Although there are several reports of tissue distribution of NaSi-1 transporters, some discrepancies exist between studies. Northern blot analysis of rat NaSi-1 showed mRNA transcripts in kidney cortex, kidney medulla/papilla and small intestine but not in other tissues (proximal colon, lung, liver, brain, heart, and skeletal muscle) (78). However, later immunofluorescence studies of the rat kidney using polyclonal antibodies observed NaSi-1 protein signals throughout the superficial and deep cortex but not in the medulla (69). Further observations found that the distribution of rat NaSi-1 proteins was on the brush border membrane of the proximal tubular cells (69). RT-PCR studies of mouse NaSi-1 found higher levels of mNaSi-1 mRNA expression in kidney, small intestine, and colon, and lower levels of expression in cecum, testis, adrenal, and adipose tissue (8). Northern blot analysis of the hNaSi-1 mRNA and also PCR analysis detected hNaSi-1 only in human kidney (65). However, RT-PCR reactions performed in our lab produced amplified hNaSi-1 fragments in both kidney and small intestine (A. M. Pajor, unpublished data). Furthermore, the immunofluorescence experiments detected possibly positive signals in human kidney cortex, human medulla, small intestine, and colon (Figure 3.4).

As mentioned before, sulfate is an essential inorganic ion for many physiological activities in the human body. Therefore, sulfate transport systems should be expected not only in kidney but also in many other tissues (76). Furthermore, the distribution of hNaSi-1 should be consistent with its functions in different tissues. In this chapter, the localization of hNaSi-1 in kidney indicates that this transporter is responsible for sulfate reabsorption. The hNaSi-1 related immunofluorescence signal was also observed on the brush border membrane of small intestine villus epithelial cells, indicating that the hNaSi-1 protein may be responsible for absorbing sulfate from the lumen side into the cytoplasmic side of the enterocyte. Also, positive immunofluorescence signal signals were observed on the plasma membrane of columnar cells in colon. Previous studies also showed a higher sulfate content in normal colonic mucosa (26; 30). The main function of the columnar cells in colon is to absorb water and salts to concentrate the feces. It is possible that NaSi-1 proteins might be involved in the absorption of Na^+ and sulfate thus facilitating water absorption in the colon.

In the human tissue array, the immunofluorescence signals were not only distributed on the apical membrane but also in the nucleus. Since the energy of hNaSi-1 transporters is dependent on the electrochemical gradient of Na^+ ions (from outside to inside of the cell), it is unlikely that the protein signals observed in the nucleus could represent the hNaSi-1 protein. Since the immune serum has been purified through a GST column to remove anti-GST antibodies, the protein signals observed in the nucleus should not be GST

proteins. Also, the slides were treated using antigen retrieval method in order to reduce non-specific binding. In addition, the control experiment using preimmune serum did not show positive immunofluorescence signals in the nucleus, ruling out another possibility that the secondary antibodies may react with some non-specific proteins on the nucleus membrane. It is possible that the anti-hNaSi-1 antibodies cross-react with some other proteins located in the nucleus. The sequence of the hNaSi-1 peptide (from amino acid residue 173 to 237) used in the GST-Si65 protein was compared with proteins in Genbank via Blast search. Two proteins, tetratricopeptide repeat Down syndrome (TPRD) protein (110) and Down's syndrome critical region (DCR) protein (28), were found to have 36% sequence identity with the hNaSi-1 peptide. However, the subcellular localization of these proteins are yet unknown. More experiments are still required to explain the immunoreaction with nuclear proteins.

N-glycosylation of hNaSi-1

N-glycosylation site in hNaSi-1 So far little direct experimental evidence has been reported for the *N*-glycosylation site in NaSi-1 transporters. There is only one previous study reporting that the *in vitro* translation of rat NaSi-1 cRNA with rabbit reticulocyte lysate resulted in a major protein at 59 kDa, which was shifted to 62 kDa in the presence of microsomes, suggesting one possible *N*-glycosylation site in rat NaSi-1 (78). One previous study of the NaDC-1 transporter, which belongs to the same gene family as hNaSi-1, also suggested one *N*-glycosylation site, asparagine 578, located at the extracellular C-terminus. In this chapter, the mass of the recombinant wild-type

hNaSi-1 protein expressed in oocytes was decreased by 15 kDa after PNGase F treatment. Furthermore, the mutant N591Y had the same apparent mass before and after PNGase F treatment suggesting that Asn-591, at the C-terminal tail, is likely to be the only *N*-glycosylation site in hNaSi-1 protein.

The functional role of N-glycosylation in hNaSi-1 The role of *N*-glycosylation in the function of transporter proteins is poorly understood. Previous studies of the NaDC-1 transporter found that succinate uptakes and protein expression of a non-glycosylated mutant both decreased 50% compared with the wild-type, suggesting that *N*-glycosylation was required for expression but not succinate transport function (95). Studies of Na⁺/glucose transporters also reported that *N*-glycosylation appeared not to be required for transport activity (42; 45; 126). However, other studies of the glucose transporter, GLUT1, and the GABA transporter suggested that *N*-glycosylation may play a functional role in transport (5; 68). Mutations of Asn-45 in GLUT1 resulted in a greater K_m value for the substrate than the wild-type, suggesting that *N*-glycosylation is involved in the structure of GLUT1 for the high substrate affinity (5). Also, mutations of *N*-glycosylation sites of the GABA transporter caused a reduction in turnover number (68). However, no published data have been reported for the functional role of *N*-glycosylation in NaSi-1 transporters.

A recent review about mammalian sulfate transporters mentioned unpublished preliminary data which showed that mutations at Asn-140 and Asn-591 in rNaSi-1 resulted in a total loss of transport activity, and the loss of function was thought to be due to defective trafficking of the protein to the

plasma membrane (76). Previous studies of the Na^+ -phosphate cotransporter NaPi-2 observed intracellular immunofluorescence signals only in the *N*-glycosylation mutant but not the wild-type, suggesting that the mutation may result in retention of the protein in cell thus reducing surface delivery of the protein and leading to decreased transport activity (41). However, according to the results shown in [Figure 3.7](#), intracellular immunofluorescence signals were observed in both of the wild-type and two mutants, N591Y and N591A. Furthermore, the average intensity of cell-surface immunofluorescence in both N591Y and N591A was stronger than the wild-type. It seems that the mutations are not likely to be the cause of the retention of the protein in cell. Therefore, the functional deficiency of the mutants should not be due to the defective protein trafficking to the plasma membrane or the protein abundance on the plasma membrane.

The mutations at Asn-591 only changed the V_{max} of hNaSi-1 without a change in K_m for sulfate, suggesting that Asn-591 or *N*-glycosylation is involved in the substrate turnover rate. Previous studies of the mannose 6-phosphate-specific receptor suggested that *N*-glycosylation was required for the ligand-binding conformation of the receptor (44). Later structure studies of *N*-glycopeptides suggested that *N*-glycosylation can affect the conformation through changing the type of a specific secondary structure (such as beta-turn) in the carrier peptide, and also may change the covalent bond as well as the hydrogen bond formed between the backbone and side chain atoms (102). Chimera studies of rabbit NaDC-1 and rat NaSi-1 suggested that the substrate

recognition site of the two transporters is located at the carboxy terminus of the protein, past amino acid 141, from transmembrane domains 5 to 11 (97). Since Asn-591 is also located at the C-terminal tail, it is likely that this residue or the sugar group may participate in forming the translocation pathway of hNaSi-1, thus changing the turnover number of the protein.

In summary, anti-hNaSi-1 polyclonal antibodies were prepared against a GST fusion protein and then applied to investigate the tissue distribution and *N*-glycosylation of the hNaSi-1 protein. The antibodies recognized a 79 kDa or 73 kDa protein in rat or pig brush-border membrane vesicles, respectively. The hNaSi-1 protein might be distributed in kidney, small intestine and colon. PNGase F treatment of the wild-type hNaSi-1 resulted in up to 15 kDa shifting of protein band, whereas the apparent mass of the N591Y mutant had no change before and after the enzyme treatment, indicating that Asn-591 is the one single site used for *N*-glycosylation in hNaSi-1. The tyrosine and alanine replacements at Asn-591 did not reduce the cell-surface expression but resulted in much less maximum uptake rates of the protein than the wild-type, suggesting that Asn-591 or *N*-glycosylation play an important role in transport activity but not protein expression. Furthermore, the maximum uptake rate is related with the turnover rate and the number of proteins expressed on the membrane, therefore, it is most likely that Asn-591 or *N*-glycosylation are involved in changing the turnover number thus reducing the transport activity of the protein.

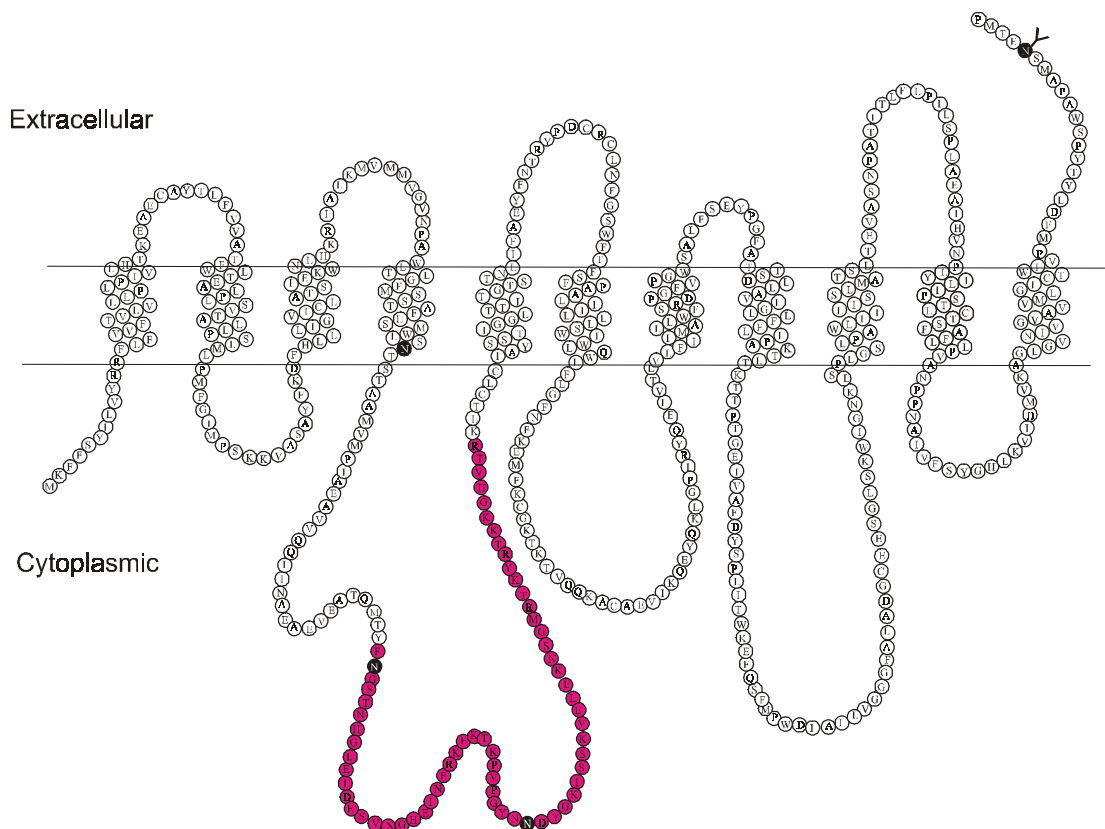


Figure 3.1 Secondary structure model of hNaSi-1 containing 11 transmembrane domains. The amino terminus is located inside of the cell, and the carboxy terminus is located extracellularly. The four consensus *N*-glycosylation sites are highlighted in black (Y: Asn-591). The amino acid residues (173-237) used for producing antibodies were highlighted in magenta.

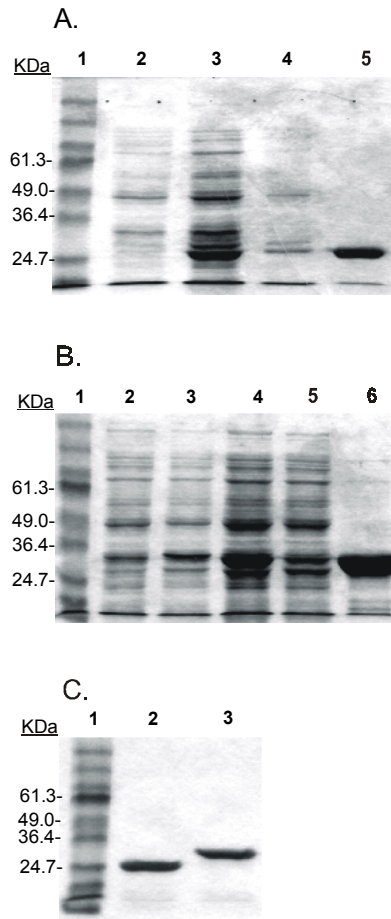


Figure 3.2 Expression and purification of GST and GST-Si65 fusion protein. Expressions of the protein in *E. coli* cells were induced by isopropyl- β -D-galactopyranoside (IPTG) and then the protein was extracted and purified through a glutathione Sepharose 4 B column. Protein samples taken from each step were separated on a 10% SDS-polyacrylamide gel and stained with Coomassie blue. Size standards (in kDa) are shown in Lane 1 in each panel. In (A) and (B), Lane 2 and 3 show the uninduced and induced protein samples, respectively. In (A), Lane 4 shows the flow-through protein sample from the column and the eluted fusion protein is shown in Lane 5. In (B), Lane 4 shows the extracted soluble fraction, the flow-through and eluted samples are shown in Lane 5 and 6, respectively. In (C), the purified GST and GST-Si65 fusion protein were separated on the same 10% SDS-polyacrylamide gel. There is a difference of ~ 6 kDa between the two proteins.

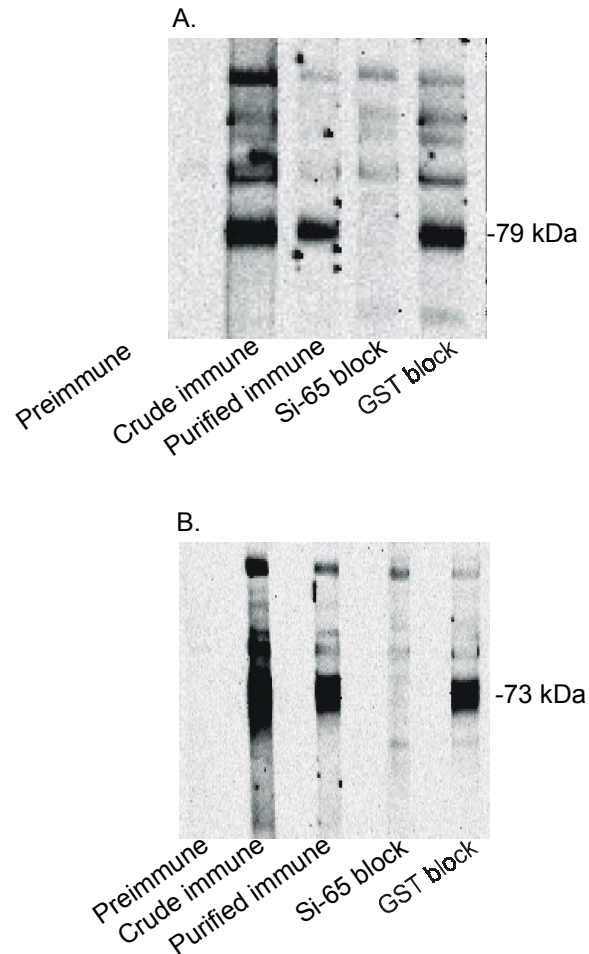


Figure 3.3 Western blots of rat and pig renal brush border membrane vesicles. Rat (A) or pig (B) renal brush border membrane vesicles were separated on 8% tricine SDS gels and then transferred to nitrocellulose membranes, cut into strips, which were then blocked in PBS-TM at room temperature for 1 hour. The primary antibodies and secondary antibodies were diluted to 1:1000 and 1:5000 respectively in PBS-TM and then applied as described in the Methods. The blocked immune serum was prepared by incubating the purified immune serum with GST (GST block) or GST-Si65 fusion protein (Si-65 block). The immunoreactive protein at ~79 kDa or ~73 kDa disappeared when the strips were incubated with the fusion protein blocked immune serum.

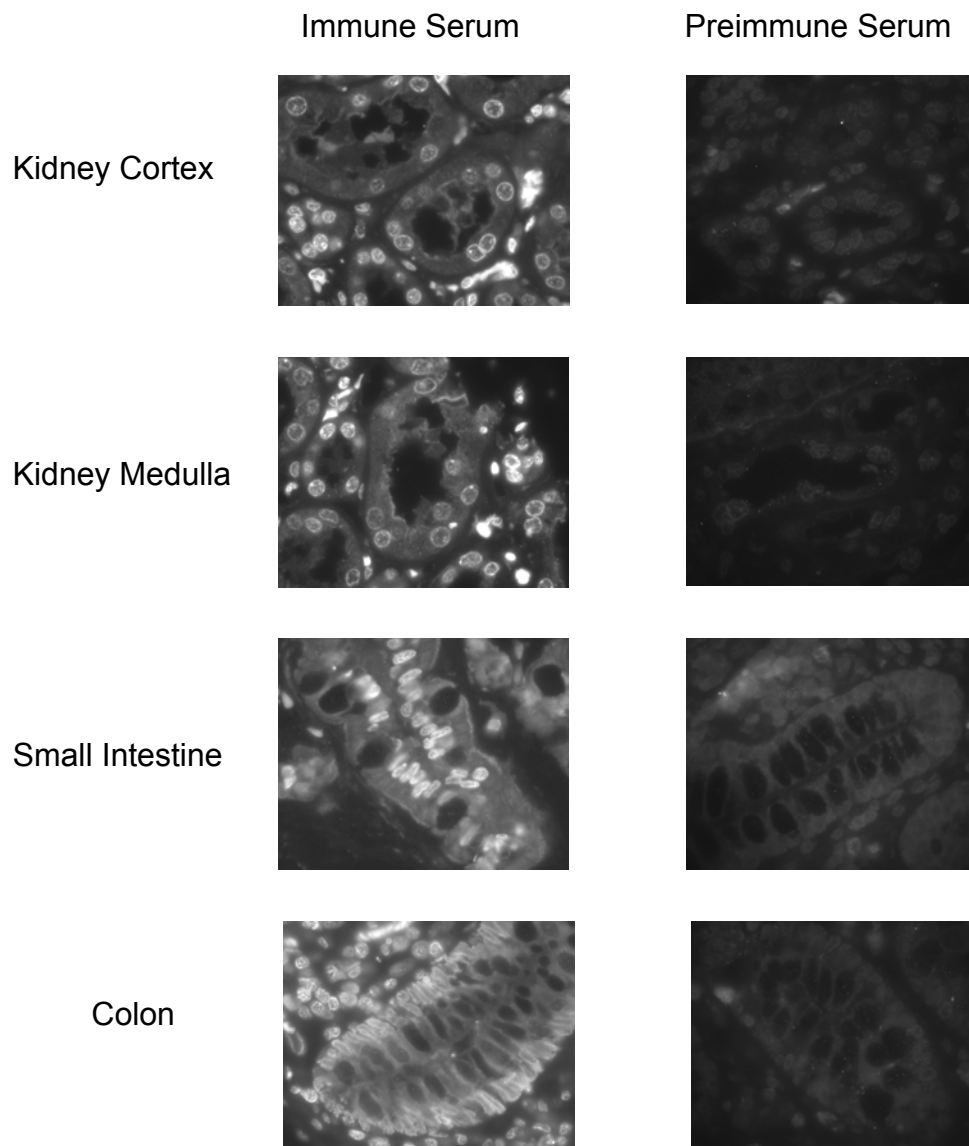


Figure 3.4 Immunofluorescence of human tissues. The human tissue array slides (Imagenex, CA) were incubated with 1:100 dilution of anti-hNaSi-1 antibodies (left column) or preimmune serum (right column) and then probed with 1:750 dilution the fluorescent secondary antibodies. Some positive tissues were selected to show in this figure. The photos were taken at a magnification of 60 X.

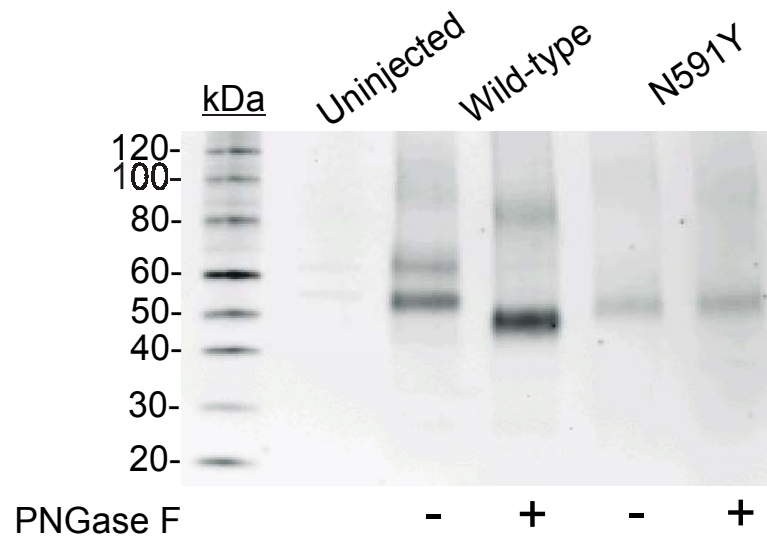


Figure 3.5 Western blot of deglycosylation of plasma membranes from *Xenopus* oocytes expressing wild-type hNaSi-1 and the glycosylation site mutant, N591Y. The plasma membranes were deglycosylated using PNGase F or incubated with water as control. The samples were used in Western blots with 1:1000 dilution of antifusion protein antibodies and 1:5000 dilution of secondary antibodies. (+: PNGase F, -: water)

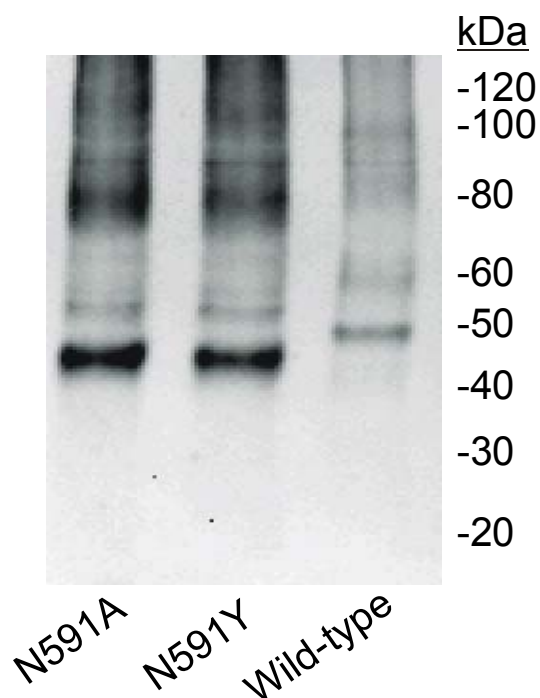


Figure 3.6 Western blot of biotinylated *Xenopus* oocytes expressing wild-type hNaSi-1 and the glycosylation site mutants, N591Y and N591A. The plasma membranes of the oocytes were biotinylated with Sulfo-NHS-LC-Biotin. The biotinylated samples were then separated on 6% tricine SDS gel and then transferred to nitrocellulose membrane. The Western blotting was performed using antifusion protein antibodies as described in the Methods.

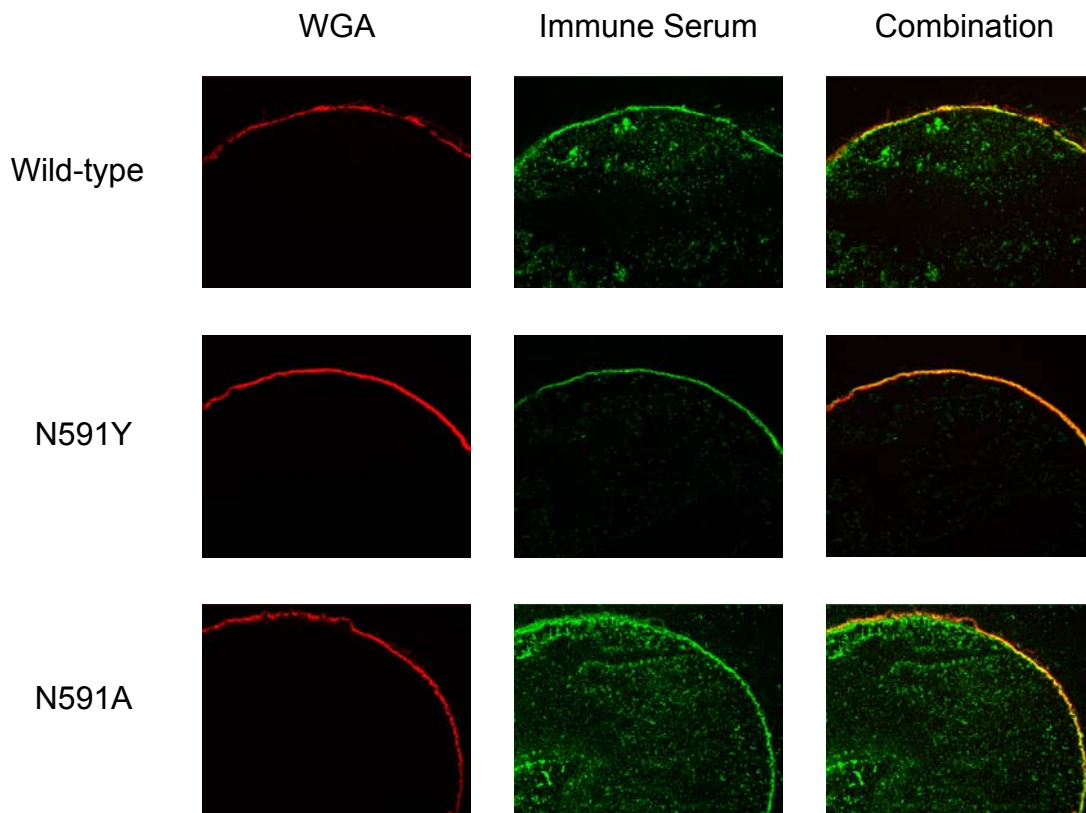


Figure 3.7 Immunofluorescence of *Xenopus* oocytes expressing wild-type hNaSi-1 and the glycosylation site mutants, N591Y and N591A. Oocytes were first stained with the red-fluorescent dye, Alexa Fluor 594 conjugate of Wheat Germ Agglutinin (WGA), and then frozen and cut into sections. The frozen sections were probed with the antifusion protein antibodies followed by the green fluorescent secondary antibodies, Alexa Fluor 488 conjugate of goat anti-rabbit IgG. The sections in the first column show the red fluorescent WGA-stained membranes of oocytes expressing wild-type hNaSi-1, N591Y and N591A. The sections in the middle show oocytes probed with the antifusion protein antibodies and green fluorescent secondary antibodies. The right-side sections are color combinations of the first two images. The images were acquired using standard filter sets (band pass emission) for TRITC (Alexa Fluor 594) and FITC (Alexa Fluor 488) at the same magnification using a 10 X / 0.3 NA Plan Fluor objective.

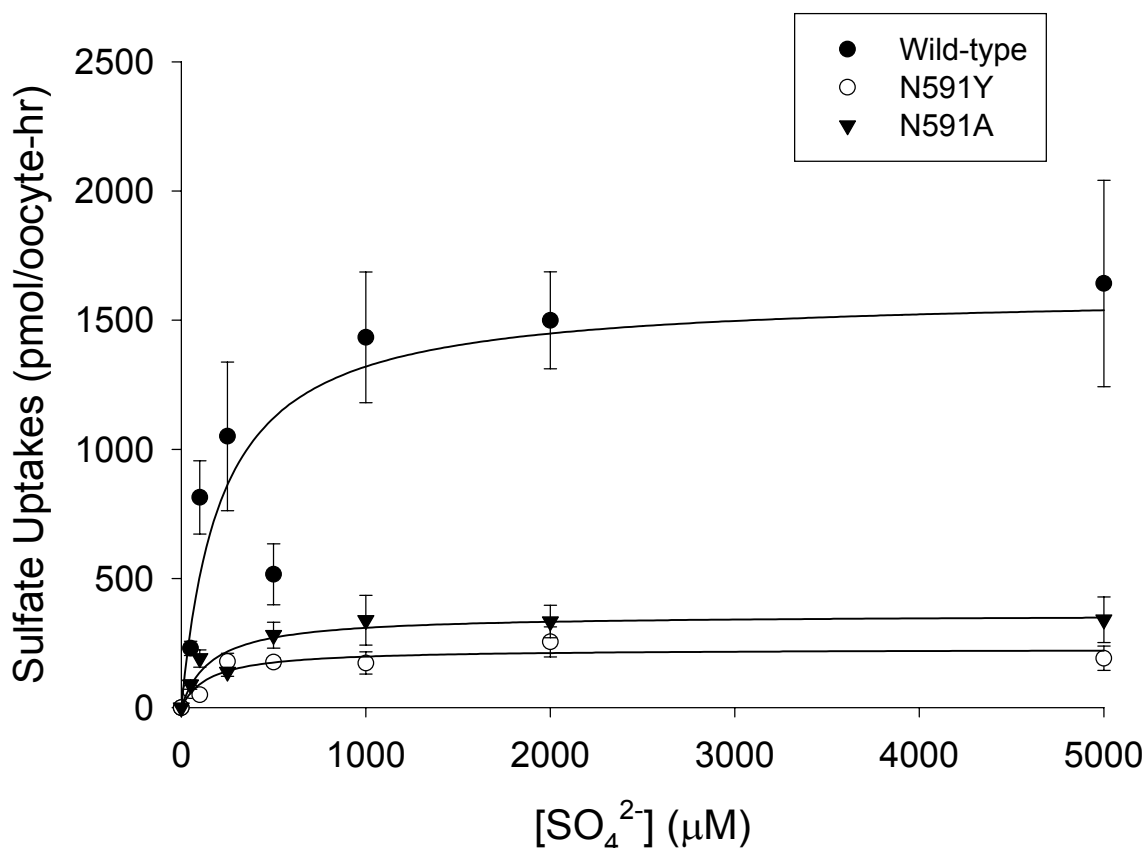


Figure 3.8 Kinetics of sulfate uptakes by *Xenopus* oocytes expressing wild-type hNaSi-1 and the glycosylation site mutants, N591Y and N591A. 10-minute uptakes of increasing concentrations of sulfate were measured in the presence of 100 mM Na⁺. Each data point represents the average of 5 oocytes. This figure represents a single experiment, the half saturation constant K_m : 215.4 μM (wt), 151.0 μM (N591Y), and 164.4 μM (N591Y), the maximum uptake rate V_{max} : 1604.2 pmol/oocyte-hr (wt), 227.2 pmol/oocyte-hr (N591Y), and 359.6 pmol/oocyte-hr (N591A).

CHAPTER 4: THE ROLES OF SERINE 260 AND SERINE 288 IN THE TRANSPORT FUNCTION OF hNaSi-1

Introduction

As mentioned before, the low affinity human Na^+ /sulfate cotransporter (hNaSi-1) belongs to the SLC13 gene family, which also includes the high affinity Na^+ -dependent sulfate transporter (hSUT-1) and the Na^+ -dependent dicarboxylate transporter (NaDC-1). The transport mechanism of hNaSi-1 has not yet been investigated. In contrast, the structure of the cation and substrate binding sites of NaDC-1 has been studied in more detail. Previous chimera studies of NaDC-1 and rat NaSi-1 showed that the substrate recognition site of these two transporters was located in the C-terminal portion of the protein, past amino acid 141 from TMD 5 to 11 (97). Another chimera study of rabbit and human NaDC-1 further found that at least one of the three Na^+ binding sites is close to the substrate binding site in TMD 7, 10 and 11 (54). Mutagenesis and electrophysiology studies provided more direct evidence to propose that at least one of the cation binding sites and the substrate binding site are close together in the C-terminal portion of NaDC-1, and that TMD 8 and 9 are likely to be involved in the formation of the translocation pathway (39). Recently, cysteine scanning mutagenesis experiments indicated that TMD 9 may be involved in transducing conformational changes between the cation-binding sites and the substrate-binding site in NaDC-1 (90). Site-directed mutagenesis in TMD 7 and 8 also suggested that these two transmembrane domains might

be involved in the conformational change during the transport cycle of NaDC-1 (147).

One of the most widely used methods to study the structure-function relationship of a membrane transporter is the site-directed mutagenesis of residues conserved in the transporter family. The side chain of serine residues contains a hydroxyl group, which is easy to form hydrogen bond. This special feature makes serine an interesting residue to be studied. Although there has been no information reported about mutations of conserved serines of transporters in the NaDC/NaSi gene family, previous studies of many other transporters have reported important roles of serine residues in the transport function. For example, studies of Na^+/K^+ ATPase provide the evidence that Ser-775 is probably involved in the cation binding pocket (13). Studies of the Na^+/Cl^- -dependent serotonin transporter found that Ser-545 in TMD 11 is important for the cation dependence of substrate transport (130). Site-directed mutagenesis studies of glucose transporter in COS-7 cells suggested that Ser-294 is involved in the conformational change during the transport process (27). Previous studies of the glutamate transporter found two serines, Ser-440 and 443, which are important for the cotransport of Na^+ and substrate (149). Site-directed mutagenesis studies of two serines (Ser-354 and Ser-357) in TMD 7 of the human norepinephrine transporter found that the mutations at these two serines resulted in different effects on substrate binding and transport (24). The combination of chimera and site-directed mutagenesis studies of two subtypes of Na^+ -nucleoside transporters suggested that Ser-318 is likely to be

located in the substrate transport pathway and important for substrate selectivity (139). In this chapter, site-directed mutagenesis studies of two conserved serines, Ser-260 and Ser-288, in hNaSi-1 are described.

Another powerful tool to study the structure-function relationship of a membrane transporter is the substituted-cysteine modification method which is used to determine the membrane topology and the role of a specific residue in conformational changes of membrane transporters. Amino acid residues are mutated to cysteine one at a time by site-directed mutagenesis. The mutants are then exposed to a thiol-reactive compound and the effect on the function is tested and compared with wild-type. The methanethiosulfonate (MTS) derivatives are widely used thiol-reactive compounds, including 2-aminoethylmethane thiosulfonate (MTSEA) (16), 2-trimethylammonioethylmethane thiosulfonate (MTSET) and 2-sulfonatoethylmethane thiosulfonate (MTSES) (3; 127). MTSET and MTSES are negatively charged and membrane impermeant whereas MTSEA is positively charged and somewhat membrane permeant (46). Compared to other thiol-reactive compounds, the MTS derivatives are the most rapidly reacting reagents. These sulfhydryl-specific reagents can chemically modify a cysteine by covalently reacting with the side chain sulfhydryl (-SH) group of the cysteine (55). If the substituted cysteine can be accessible to the impermeant MTSET and chemically modified by it (MTSET inhibition of transport activity), the residue mutated to cysteine is most likely to be exposed to the extracellular side or water transport pathway of membrane transporters.

In this chapter, the structure-function relationship of hNaSi-1 has been investigated from two conserved serine residues, Ser-260 and Ser-288, and their 12 surrounding residues using site-directed mutagenesis and substituted-cysteine modification methods. There are a total of 42 serines in hNaSi-1. Based on the sequence alignment of members in the NaDC/NaSi transporter gene family, only two serine residues, Ser-260 and Ser-288, are conserved in all Na⁺-coupled sulfate transporters but not in NaDC transporters. Results showed that the cysteine mutants around Ser-288 were either inactive or had altered transport activity. Three out of seven mutants surrounding Ser-260, G258C, S260C, and N262C, were completely inactive, whereas another four mutants, T257C, T259C, T261C, and L263C had decreased sulfate uptakes. Western blotting analysis showed that all 14 mutants were expressed well on the plasma membrane of oocytes, indicating that functional changes are not due to defective expression of the proteins. Most of the mutants around Ser-288 except the inactive ones were insensitive to MTSET inhibition. However, the four mutants around Ser-260, T257C, T259C, T263C and L263C, were all sensitive to MTSET inhibition and exhibited substrate protection in Na⁺ but not choline buffer. The dependence of MTSET inhibition on the cations and substrate used suggests that the modification of these substituted cysteines is related to conformational changes in the transport cycle of hNaSi-1. Since the four residues are located in TMD-5, this transmembrane domain is also likely to participate in the conformational movement during the transport cycle of hNaSi-1.

Methods

The cloning and subcloning of hNaSi-1, site-directed mutagenesis, transcription of cRNA, preparation and injection of oocytes, cell-surface biotinylation of oocytes, Western blots, the radiotracer assay and data analysis for kinetic experiments are the same as the methods described in Chapter 3. The primers used for site-directed mutagenesis are listed in [Table 4.1](#) and the mutated codons are shown in bold.

For Na⁺-activation experiments, different concentrations of Na⁺ were prepared by replacing Na⁺ with choline. The data from this experiment were fitted to the Hill equation: $v = V_{max} * [S]^n / (K_{0.5}^n + [S]^n)$, where [S] is the concentration of Na⁺, $K_{0.5}$ is the half-saturation constant for Na⁺ and n is the Hill coefficient. The non-linear regression of the data to the equation was done using Sigma Plot 2000 (SPSS).

For the cation selectivity experiments, uptakes in Li⁺, Cs⁺, K⁺ or choline buffer were measured by completely replacing 100 mM of Na⁺ with 100 mM of Li⁺, Cs⁺, K⁺ or choline while keeping other components in the buffer as the same. For substrate specificity experiments, uptakes of 10 μ M [³⁵S]-sulfate were measured in the absence or presence of 1 mM tested inhibitors. Uptakes in the presence of inhibitors were presented as a percentage of uptakes in the absence of inhibitors. The statistical analysis was performed using SigmaStat statistic software (Jandel, Version 1.0).

In the MTSET inhibition experiments, the MTSET solution was prepared in Na⁺ or choline buffer immediately prior to use. Oocytes were preincubated in the absence or presence of MTSET dissolved in 0.4 ml of Na⁺ or choline buffer with or without 5 mM of sulfate added. After 10 minutes, the MTSET solution was washed away with four washes of 4 ml of choline buffer (room temperature). Then the oocytes were incubated in the transport buffer containing 100 μM [³⁵S]-sulfate and uptakes were measured by radiotracer assay as described in the Methods in Chapter 3. The data are presented as a percentage of uptakes of oocytes preincubated in the absence of MTSET.

Table 4.1 Oligonucleotide primers used for preparing cysteine mutants of Ser-260, Ser-288 and the 12 surrounding residues in TMDs 5 and 6 of the hNaSi-1 transporter.

Mutation	Name	Sequence of oligonucleotide primer (5' to 3')
Ser-260 to Ala	S260A	CAA GTT GGT GGC CGT ACC AGT GAT TG
Ser-288 to Ala	S288A	G GGC AGC GGG GAA GGC AAA CGT AAA CCA TG
Thr-257 to Cys	T257C	GTT GGT GGA CGT ACC ACA GAT TGT TGT CAG
Gly-258 to Cys	G258C	GTT GGT GGA GGT ACA AGT GAT TGT TG
Thr-259 to Cys	T259C	A GTT GGT GGA GCA ACC AGT GAT TGT TG
Ser-260 to Cys	S260C	AT CAA GTT GGT GCA CGT ACC AGT GAT TG
Thr-261 to Cys	T261C	AA GAT CAA GTT GCA GGA CGT ACC AGT GAT TG
Asn-262 to Cys	N262C	C AAA GAT CAA GCA GGT GGA CGT ACC AGT GAT TG
Leu-263 to Cys	L263C	CTC TGC AAA GAT ACA GTT GGT GGA GGT
Phe-285 to Cys	F285C	GGC AGC GGG GAA GGA AAA CGT ACA CCA TGA TC
Thr-286 to Cys	T286C	TGG GAA GGA AAA ACA AAA CCA TGA TCC
Phe-287 to Cys	F287C	G GGC AGC GGG GAA GGA ACA CGT AAA CCA TG
Ser-288 to Cys	S288C	G GGC AGC GGG GAA GCA AAA CGT AAA CCA TG
Phe-289 to Cys	F289C	AAG GGC AGC GGG GCA GGA AAA CGT AAA CC
Pro-290 to Cys	P290C	AAG GGC AGC GCA GAA GGA AAA CGT AAA C
Ala-291 to Cys	A291C	GAT AAG GGC ACA TGG GAA GGA AAA CG

Results

Location of the mutated residues in the secondary structure model of hNaSi-1

In [Figure 4.1](#), the secondary structure model of hNaSi-1 shows that two serines 260 and 288 and the 12 surrounding residues are located close to the extracellular surface of putative transmembrane domains 5 and 6, respectively. The sequence alignment of the NaDC/NaSi gene family shows that the two serines are conserved in all Na⁺-dependent sulfate transporters but not in Na⁺-dependent dicarboxylate transporters. Also, most of the surrounding residues of these two serines are highly conserved in all members of the NaDC/NaSi gene family.

Functional characterization of S260A and S288A mutants

Transport activity and cell-surface expression of S260A and S288A mutants Since the Na⁺/dicarboxylate cotransporters contain alanine or threonine in place of Ser-260 and Ser-288, these two serines were first mutated to alanine, Ser-260-Ala (S260A) and Ser-288-Ala (S288A). Then the two mutants were expressed and studied in *Xenopus* oocytes. As shown in [Figure 4.2](#), S260A and S288A remained $23 \pm 4 \%$ and $79 \pm 23\%$ (mean \pm SEM, n = 6) of the wild-type transport activity, respectively. Expression of the two mutants on the plasma membrane of oocytes was tested using cell-surface

biotinylation with the anti-hNaSi-1 antibodies prepared in Chapter 3. Protein signals of the two mutants were both more abundant on the plasma membrane than the wild-type, indicating that the alanine replacement did not reduce the cell-surface expression of these proteins. There was no signal detected in uninjected oocytes. Since the alanine replacement at least did not decrease expression of the mutants, the decreased transport activity is not likely due to defective expression of the proteins.

Kinetic properties Preliminary experiments showed that uptakes of 1 mM sulfate by wild-type hNaSi-1 were linear to at least 60 minutes (data not shown). Therefore, 10 minute uptakes were used for kinetic experiments. [Figure 4.3](#) shows a single experiment comparing the kinetic properties of the S260A and S288A mutants with wild-type hNaSi-1. Based on repeated kinetic experiments for wild-type hNaSi-1, the average values of K_m and V_{max} were $379 \pm 66 \mu\text{M}$ (100 mM) and $3069 \pm 679 \text{ pmol/oocyte-hr}$ (100 mM) (means \pm SEM, n=6), respectively. The kinetic measurements of the mutants were repeated three times. S260A had an increased apparent K_m of $1123 \pm 228 \mu\text{M}$ (mean \pm SEM, n=3), whereas S288A had a K_m of $429 \pm 144 \mu\text{M}$ (mean \pm SEM, n=3) similar to the wild-type. Both of the mutants had a similar value of V_{max} to the wild-type, $2539 \pm 252 \text{ pmol/oocyte-hr}$ for S260A and $3651 \pm 492 \text{ pmol/oocyte-hr}$ for S288A. Therefore, alanine replacement at Ser-260 resulted in a decreased affinity of hNaSi-1 for substrate, whereas alanine replacement at Ser-288 did not affect the substrate binding affinity.

Na⁺-activation of sulfate uptakes Figure 4.4 represents a single experiment to compare the sodium activation of sulfate transport of the two mutants with that of the wild-type. There was a sigmoidal dependence of sulfate uptakes on Na⁺ concentration. Two experiments were repeated for the wild-type. The average K_{Na} of these two experiments was 26 ± 3 mM and the average Hill coefficient was 1.8 ± 0.4 (mean \pm regression error). Compared with the wild-type, S288A had a 2-fold decreased K_{Na} of 15 ± 2 mM, indicating an increased Na⁺ affinity. However, S260A showed a greatly decreased sodium affinity but it was not possible to obtain an accurate kinetic constant because the kinetic curve for S260A did not show saturation. It seemed that replacements of alanine at Ser-260 and Ser-288 resulted in an opposite effect on the cation affinity of hNaSi-1. Similar results were also seen in previous studies of the human norepinephrine transporter in which alanine replacements at two serines, Ser-354 and Ser-357, in TMD 5 resulted in different effect on substrate binding (24).

Cation selectivity Cation selectivity of the two mutants and wild-type hNaSi-1 was measured by replacing the 100 mM Na⁺ buffer with Li⁺, Cs⁺, K⁺ or choline buffer (Figure 4.5). Wild-type hNaSi-1 has a strict cation selectivity with transport activity only in the presence of Na⁺ but not other monovalent ions. Sulfate uptakes of wild-type hNaSi-1 in Li⁺, Cs⁺, K⁺ or choline buffer were decreased to less than 1% of uptakes in Na⁺ buffer. S260A has a similar cation selectivity to the wild-type, with almost no transport in the presence of the other tested cations. However, S288A seemed to have altered cation selectivity with increased sulfate uptakes in the presence of other cations, particularly Li⁺,

which stimulated about 28% of sulfate uptakes in Na^+ . Previous mutation studies of the glutamate transporter also showed a broadened ion specificity, which was resulted from mutation of Ser-440 to glycine (149).

Substrate specificity The substrate specificity of the wild-type and mutant hNaSi-1 was studied by measuring the inhibition of 10 μM sulfate uptakes with 1 mM test inhibitors (Figure 4.6). My experiments showed that wild-type hNaSi-1 has a broad substrate specificity. In addition to sulfate, anions with similar structures such as chromate (CrO_4^{2-}), thiosulfate ($\text{S}_2\text{O}_3^{2-}$), selenate (SeO_4^{2-}), and sulfite (SO_3^{2-}), also resulted in more than 50% inhibition of transport in the wild-type. Markovich's studies of cloned hNaSi-1 also showed broad substrate specificity for hNaSi-1 (65). However, there is somewhat difference between my studies and Markovich's studies on hNaSi-1. Results from my studies showed that succinate, phosphate and probenecid did not inhibit sulfate uptakes in the wild-type whereas Markovich's studies showed that succinate could also inhibit sulfate uptakes by hNaSi-1. Two NaDC-1 inhibitors, furosemide and flufenamate (96), were also tested in my experiments and only flufenamate produced ~40% inhibition of sulfate uptakes by hNaSi-1. Comparing with the wild-type, however, both S260A and S288A showed somewhat different inhibition results of sulfate uptakes. Sulfate and all of the four compounds having similar structures to sulfate also resulted in inhibition for the two mutants, however, the inhibition caused by sulfate or sulfite was significantly reduced in S260A, whereas the inhibition by sulfite for S288A seemed to be significantly increased compared with the wild-type. The reduced

inhibition by sulfate and sulfite for S260A is probably due to the decreased substrate binding affinity of S260A as shown in [Figure 4.4](#). Thiosulfate resulted in the same amount of inhibition for both of the mutants as for the wild-type. Succinate, phosphate, probenecid and furosemide did not result in any inhibition for either S260A or S288A, which is the same as wild-type hNaSi-1. Flufenamate caused about the same amount of inhibition for S260A as for the wild-type but had no significant effect on S288A.

Substituted-cysteine mutagenesis surrounding Ser-260 and Ser-288 in hNaSi-1

Preliminary studies tested the sensitivity of wild-type hNaSi-1 to MTSEA, MTSES and MTSET. Wild-type hNaSi-1 is sensitive to inhibition by MTSEA and MTSES but insensitive to MTSET (data not shown), indicating that the endogenous cysteine residues of hNaSi-1 are not reactive to MTSET. Therefore, wild-type hNaSi-1 can be used as a parent protein in studies using cysteine substitution and chemical modification with MTSET. Cysteine replacement at Ser-260 (S260C) resulted in a total loss of transport activity and S288C had a very low transport activity (data not shown). Therefore, a total of 12 residues surrounding Ser-260 or Ser-288 were mutated to cysteine one at a time, including T257, G258, T259, T261, N262, L263, F285, T286, F287, F289, P290, and A291, which are illustrated as filled gray circles in [Figure 4.1](#).

Transport activity and cell-surface expression of the 14 mutants The sulfate transport activity of the 14 mutants (S260C, S288C and the 12 surrounding cysteine mutants) was tested and compared with the wild-type as shown in [Figure 4.7](#). Five of the mutants, G258C, S260C, N262C, F285C, and P290C were completely inactive. Another eight of the mutants, T257C, T259C, T261C, L263C, T286C, F287C, S288C and F289C had decreased uptakes, which were only from 4% to 39% of sulfate uptakes by the wild-type. Sulfate uptakes by A291C were quite variable in three separate experiments. In one experiment, the activity of A291C was almost twice that of the wild-type whereas the activity in another two experiments was the same as the wild-type. The expression of the mutants on the plasma membrane of oocytes was tested using cell-surface biotinylation and anti-hNaSi-1 antibodies ([Figure 4.8](#)). All 14 mutants were found on the plasma membrane and as abundant as or more abundant than the wild-type, indicating that the cysteine replacement at least did not decrease the cell-surface expression of the mutant proteins.

MTSET sensitivities of the active mutants The sensitivity of the active mutants to MTSET was tested using a relatively high concentration of 1 mM ([Figure 4.9](#)). Only four mutants surrounding Ser-260, T257C, T259C, T261C and L263C, were sensitive to MTSET. After preincubation with MTSET, the remaining uptakes of these four mutants were only about 4% (T257C), 45% (T259C), 9% (T261C) and 0.9% (L263C) of the control. In contrast, S288C and the surrounding mutants, T286C, F287C, and F289C, were all insensitive to MTSET inhibition.

MTSET concentration dependence of T257C, T259C, T261C and L263C The concentration dependence of MTSET inhibition for the four mutants, T257C, T259C, T261C, and L263C, was tested by measuring sulfate uptakes of each mutant after 10-minute preincubation with increasing concentrations of MTSET (Figure 4.10). The results in Figure 4.9 showed that T259 is less sensitive to MTSET inhibition because more transport activity was remained after preincubation with 1 mM MTSET. In this experiment, therefore, concentrations of MTSET up to 1 mM were used for T259C whereas concentrations up to 10 μ M were used for T257C, T261C and L263C. The results showed that T259C had the highest K_i of about 630 μ M and L263C had the lowest K_i of less than 0.1 μ M. T257C had a relatively low K_i of less than 2 μ M whereas T261C had a relatively higher K_i of 90 μ M. The value of K_i represents the concentration of MTSET required to label a cysteine, and also reflects the MTSET accessibility of the residue (25). Therefore, the substituted cysteines at positions 257, 261, and 263 seem to be more sensitive to the MTSET modification, whereas the substituted cysteines at position 259 is relatively less sensitive to MTSET.

Cation and substrate dependence of MTSET inhibition The effect of cations and substrates on the MTSET modification to substituted cysteines at the four positions are shown in Figure 4.11. The concentration of MTSET was selected for each mutant based on the K_i values: 2.5 μ M for T257C, 500 μ M for T259C, 250 μ M for T261C, and 1 μ M for L263C. Three of the four mutants, T257C, T261C, and L263C, are more sensitive to MTSET inhibition in Na^+ than choline buffer. After preincubation with MTSET in Na^+ buffer alone, 46% of the control

uptakes remained for both T257C and T261C, and only 1% of the control uptakes remained for L263C. In contrast, after preincubation with MTSET in choline buffer, more transport activity was remained for T257C (73%), T261C (79%), and L263C (27%). These results indicate that the substituted cysteines at positions 257, 261 and 263 are more sensitive to MTSET modification in Na^+ than choline buffer. Furthermore, all of these three mutants showed substrate protection in Na^+ but not choline buffer, i.e. MTSET inhibition was prevented by adding sulfate in Na^+ buffer. When preincubating these mutants with MTSET in the buffer containing both of Na^+ and sulfate compared with Na^+ alone, the average transport activity increased to 118%, 129% and 43% of the control uptakes for T257C, T261C, and L263C, respectively. However, preincubation of the three mutants with MTSET in the buffer containing choline and sulfate together did not result in significant increase of transport activity compared with preincubation with MTSET in choline buffer alone. These results suggest that sulfate can protect the substituted cysteine from being modified by MTSET. Compared with T257C, T261C, and L263C, T259C has equally sensitivity to MTSET inhibition in both Na^+ and choline buffer (about 40% of the control transport activity remained after preincubation with MTSET in either of the two cation buffers), indicating that the cysteine at position of 259 can be modified by MTSET in either Na^+ or choline buffer. T259C also exhibited substrate protection in Na^+ but not choline buffer, suggesting that the cysteine at position of 259 can be protected from MTSET modification in the presence of both Na^+ and sulfate. Based on these results, it seems that MTSET modification of the

substituted cysteines at these four residue positions is dependent on cation and/or substrate used in the buffer.

Cation selectivity of the four mutants One possible explanation for the accessibility of substituted cysteine to MTSET in the presence of choline is because the mutation may increase the cation binding affinity. Therefore, the cation selectivity for each mutant was tested as shown in [Figure 4.12](#). The results showed that all four mutants had the same cation specificity as the wild-type (see wild-type cation specificity shown in [Figure 4.5](#)). It seemed that the cysteine replacements of these four residues did not increase the binding affinity for other cations including choline.

Effect of Na⁺ on kinetics of sulfate uptakes

A transport model for hNaSi-1 is required to explain the results of cation and substrate dependence of MTSET inhibition of sulfate uptakes by the four mutants, T257C, T259C, T261C and L263C. Previous studies proposed a 6-state ordered binding transport model for NaDC-1 (144, 146), which belongs to the same gene family as hNaSi-1, therefore, here a similar ordered transport model (see [Figure 4.16](#)) was proposed and tested for hNaSi-1.

In order to test the cation and sulfate binding order in the transport cycle of hNaSi-1, the dependence of the wild-type kinetic properties on different Na⁺ concentrations was studied as shown in [Figure 4.13](#) and [Figure 4.14](#). Sulfate

uptakes by wild-type hNaSi-1 with increasing sulfate concentrations in the presence of 20, 40, or 100 mM Na⁺ are shown in [Figure 4.13](#). The experiments which both have a K_m with a regression error of more than 50% and a V_{max} with a regression error of more than 15% were omitted. The mean K_m s for sulfate were 707 ± 70 μ M (20 mM), 687 ± 23 μ M (40 mM), and 379 ± 66 μ M (100 mM) (mean \pm SEM, n = 2, 3 and 6, respectively). The mean values of V_{max} were 2705 ± 1515 pmol/oocyte-hr (20 mM), 5451 ± 2379 pmol/oocyte-hr (40 mM), and 3069 ± 679 pmol/oocyte-hr (100 mM) (mean \pm SEM, n = 2, 3 and 6, respectively). The values of K_m and V_{max} were replotted as a function of Na⁺ concentrations as shown in [Figure 4.14](#). Results from statistical analysis show that the K_m in 100 mM Na⁺ buffer is significantly decreased relative to that in 20 mM Na⁺ buffer. The K_m in 40 mM Na⁺ buffer was between the values in 20 and 100 mM Na⁺ buffer. Therefore, it seemed that the values of K_m increased with decreasing Na⁺ concentrations. In contrast, the V_{max} did not show significant changes at different Na⁺ concentrations.

Discussion

In this chapter, the functional roles of the two serines, Ser-260 and Ser-288, and the 12 surrounding mutants in TMDs 5 and 6 of hNaSi-1 were investigated. The major finding is that MTSET accessibility of the substituted-cysteine residues at positions Thr-257, Thr-259, Thr-261 and Leu-263, is dependent on cation and substrate. The MTSET sensitivity of these cysteines is high in the presence of Na⁺ alone but decreased in the absence of Na⁺ or presence of both of Na⁺ and sulfate. Since these residues are located in TMD-

5, the results may indicate that TMD-5 is involved in the conformational changes during the transport cycle of hNaSi-1.

Ser-260 and Ser-288 were chosen for mutagenesis for several reasons. First of all, as mentioned in the introduction, previous studies of other transporters suggested that serine residues are likely to be involved in the substrate and cation binding process. Chimera studies of NaDC-1 and rat NaSi-1 indicated that the substrate recognition site of these two transporters was located in the C-terminal portion, past amino acid 141, from TMD-5 to 11 (97). In hNaSi-1 transporter, there are a total of 42 serine residues. Amino acid sequence alignment of transporters in the NaDC/NaSi gene family showed that only serines 260 and 288 were conserved in Na⁺/sulfate cotransporters but not in NaDC transporters. Therefore, these two serine residues, Ser-260 and Ser-288, were chosen from the total of 42 serines in hNaSi-1 to perform site-directed mutagenesis. Since alanine or threonine replaces these two serines in the same position in the other members of the family, serines 260 and 288 were first mutated to alanine one at a time.

Results from site-directed mutagenesis of Ser-260 showed that alanine replacements at Ser-260 resulted in a decreased K_m value for both substrate and Na⁺. One possible explanation is that Ser-260 is directly involved in the structure of the substrate and cation binding sites i.e. Ser-260 is located at or close to the substrate and cation binding sites. Another possibility is that Ser-260 is a key residue to support the optimal conformation for substrate and

cation binding although it is not directly located at or close to the binding sites. The K_m value reported here can reflect not only the real binding affinity for substrate or cation but also other factors (such as the translocation rate) which are also involved in the whole transport cycle (100). Therefore, besides substrate- or cation-binding process, the changed K_m may also suggest that Ser-260 plays a role in other steps during the transport cycle including the translocation of the loaded transporter, the release of Na^+ and sulfate into the cytoplasmic side of the cell or the reorientation of the unloaded transporter.

Compared with S260A, the K_m value of S288A for substrate is similar to that of the wild-type, however, the K_m value for Na^+ decreased almost two fold and cation selectivity was broadened especially for Li^+ . It might be possible that the oxygen of the hydroxyl group in the side chain of Ser-288 directly forms part of cation binding sites. If this possibility is true, the neutral alanine replacement at Ser-288 should be expected to reduce cation binding affinity, however, the results showed a decreased K_m for Na^+ as well as a broadened cation selectivity. Therefore, it is more likely that the hydroxyl group in the side chain of Ser-288 may form a hydrogen bond with other residues to support the structure of cation binding sites rather than be directly part of the sites. Alanine replacement at the position 288 may loosen the cation-binding structure and thus making it also fit to other cations especially Li^+ . Previous studies of the Na^+/K^+ -coupled glutamate transporter observed that glycine replacement at Ser-440 produced a broadened ion specificity but did not affect the K_m for transportable substrates and also suggested that Ser-440 was likely to be near

the substrate binding site thus the changed ion specificity may also be related to a small change in substrate binding produced by the mutation (149). It is not completely sure whether Ser-288 could also be involved directly or indirectly in substrate binding although alanine replacement at Ser-288 did not significantly affect the K_m for substrate. More experiments are required to explain these results.

In order to further investigate how Ser-260 and Ser-288 are involved in the structure of substrate and cation binding sites, these two serines and their surrounding residues were mutated to cysteine. Radiotracer assay results showed that two out of seven cysteine mutants around Ser-288, Phe-285 and Pro-290, were inactive, and the rest of them had altered transport activity. Three out of seven mutants around Ser-260 (G258C, S260C and N262C) completely lost transport activity, whereas another four mutants (T257C, T259C, T263C and L263C) showed a decreased transport activity. Since the 14 mutants were all expressed well on the plasma membrane, changed transport activity is most likely because cysteine replacements at these residues changed the optimal conformation for the transport. Therefore, not only the two serines but also all of the surrounding residues are important for the transport function of hNaSi-1.

The membrane-impermeant cysteine-specific reagent, MTSET, was used to determine the topological localization of the cysteine-substituted residues. Since the substrate and cation binding sites are usually located in the

hydrophilic transport pathway of the transporter, if these substituted cysteine residues are located in or near the transport pathway or exposed to the extracellular side of the membrane, they would be modified by MTSET and thus producing inhibition. MTSET sensitivity of all the active mutants was tested and only the four mutants around Ser-260 (T257C, T259C, T263C and L263C) were sensitive to MTSET inhibition. Moreover, MTSET inhibition of these mutants was found to be dependent on the cation and substrate used. In order to explain these results, a transport model will be explained first.

The transport model of NaDC-1, the same family member as NaSi-1, has been well studied. Previous membrane vesicle studies of the sodium succinate cotransport across renal brush-border membrane proposed an ordered binding kinetic model in which three Na^+ ions first bind to the carrier in order to increase the substrate affinity for the following substrate binding (144). This model was based on an important experimental observation that decreasing external sodium concentrations increased the apparent K_t for succinate transport without affecting the maximum uptake rate J_{max} . Based on the equation for an ordered rapid equilibrium enzyme system in which an activator binds prior to substrate binding, the V_{max} is not affected by concentrations of the activator but the apparent K_m for substrate increases with decreasing concentrations of the activator (124). Therefore, the most likely reaction mechanism to fit the observation is an ordered rapid equilibrium system in which 3 Na^+ ions (activators) must bind to the transporter prior to succinate binding (substrate) (124). Recent voltage-clamp studies of human

Na^+ /dicarboxylate cotransporter (hNaDC-1) also suggested a similar kinetic model based on the observation that the K_m for succinate increased with decreasing Na^+ concentrations, whereas the maximum succinate-induced current I_{max} was independent of different Na^+ concentrations (146). Electrophysiological analysis of rat NaSi-1 transporter showed an electrogenic cotransport of three Na^+ ions and one sulfate (19), but no experimental evidence has been reported about whether the NaSi-1 cotransport also fits into a similar ordered binding model to that for NaDC-1.

In this chapter, results of the Na^+ effect on the kinetics of sulfate transport by hNaSi-1 suggested an ordered rapid equilibrium transport model for this transporter. The dependence of K_m and V_{max} for sulfate on different Na^+ concentrations showed that the K_m increased with decreasing Na^+ concentrations, whereas the V_{max} did not show a significant change at different Na^+ concentrations. This observation is the same as that for the NaDC-1 transporter (144; 146), therefore, a 6-state ordered binding model is proposed for hNaSi-1 in which 3 Na^+ ions bind prior to sulfate binding (see [Figure 4.16](#)). In this model, hNaSi-1 in state 1 exists in unloaded form, in which the cation and substrate binding sites are accessible from the outside of the cell. When Na^+ binds to hNaSi-1 (state 2), a conformational change is triggered to increase the affinity for substrate binding and then sulfate binds to hNaSi-1 (from state 2-3). To simplify the model, the binding of three Na^+ ions is assumed to be a simple step. The fully loaded transporter (state 3) then translocates cations and sulfate into inside of the cell (from state 3-4). Cations

and sulfate are then released into the cell (from state 4-6). The unloaded transporter (state 6) is reoriented to expose cation and substrate binding sites to extracellular side of the cell again (from state 6-1) and thus the whole transport cycle is finished. The following explanation will be based on this 6-state ordered kinetic model for hNaSi-1.

Firstly, in order to exclude the possibility that the conformational changes during the transport cycle may expose the endogenous cysteine residues to MTSET, preliminary experiments were performed to test the cation and substrate dependence of MTSET inhibition of wild-type hNaSi-1. The results showed that the wild-type was insensitive to MTSET inhibition in either Na^+ or choline buffer with or without sulfate added, indicating that the conformational changes during the transport cycle do not expose the endogenous cysteine residues of hNaSi-1 to MTSET. Therefore, the cation and substrate dependence of MTSET inhibition of the four mutants should only reflect features of the substituted cysteine but not endogenous cysteine residues.

MTSET modification of substituted cysteines in the four mutants, T257C, T259C, T261C, and L263C, is dependent on the cation and/or substrate used. The two mutants, T257C and T261C, are more sensitive to MTSET modification in Na^+ (state 1) than choline buffer (state 2), indicating that the substituted cysteines at positions 257 and 261 are originally less accessible to MTSET in state 1 and then the conformational change induced

by Na^+ binding in state 2 makes these cysteines more accessible to MTSET. After adding sulfate in Na^+ buffer (state 3), transport activity of the two mutants increased to even more than 100% of the control uptakes, suggesting that sulfate binding triggers another conformational change which makes the substituted cysteines almost completely inaccessible to MTSET. For L263C, although MTSET inhibition in choline buffer was also less than in Na^+ buffer, the remaining activity in choline buffer was very low (only 27% of the control uptakes) compared with T257C and T261C (73% to 79% of the control uptakes). These results may suggest that the cysteine at position 263 is probably somewhat accessible to MTSET in choline buffer (state 1) and the conformational change induced by Na^+ binding makes the cysteine even more accessible to MTSET. In the presence of both Na^+ and sulfate, transport activity of L263 recovered to only 40% of the control uptakes compared with T257C and T261C (more than 100%), indicating that conformational change caused by sulfate binding makes the cysteine at 263 less accessible to MTSET. T259C shows MTSET inhibition in both Na^+ (state 2) and choline (state 1) buffer, suggesting that the cysteine at position 259 is most likely to be exposed to the cell-surface or a water-filled pore of hNaSi-1 and thus accessible to MTSET without requiring any conformational change. T259C also showed substrate protection in Na^+ buffer, indicating that the conformational change induced by sulfate binding makes the cysteine at position 259 less accessible to MTSET. In brief, based on the ordered kinetic binding model proposed for hNaSi-1, MTSET modification of these four substituted cysteines at positions 257, 259, 261 and 263 seems to be related to the conformational

changes in the transport cycle of hNaSi-1. In addition, the result of the sulfate protection which occurred only in Na⁺ but not choline buffer in turn provide another evidence to support that Na⁺ binding is required to be prior to sulfate binding.

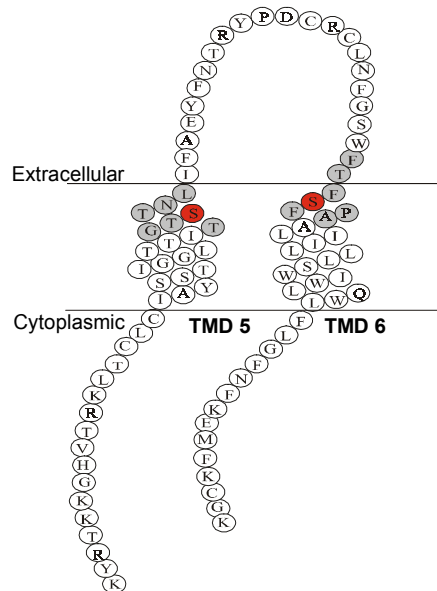
Since the four residues, Thr-257, Thr-259, Thr-261, and Leu-263, are located in TMD-5, this transmembrane domain is also likely to be involved in the conformational changes during the transport cycle. The location of Ser-260 and its 6 surrounding residues are summarized in [Figure 4.15](#). Thr-257, Thr-261 and Leu-263 are located on one side whereas Thr-259 is on the opposite side of TMD-5 but very close to Leu-263. The cysteine at position 259 seems equally sensitive to MTSET modification in both Na⁺ and choline buffer. One possible explanation is that the side of TMD-5 containing residue at position 259 is most likely to define part of the water-filled pore of hNaSi-1 and thus accessible to MTSET in both Na⁺ and choline buffer, and Leu-263 is likely to be partially exposed to the pore. Or it is likely that TMD-5 stays in the membrane in some angle and thus residues at positions 259 and 263 are somewhat exposed to the extracellular side. In contrast, residues at positions 257 and 261 in TMD-5 are likely to be buried in the hydrophobic side and thus inaccessible to MTSET in choline buffer. The conformational change triggered by Na⁺ binding resulted in a movement of TMD-5, which exposes residues at positions 257 and 261 to the hydrophilic environment. Therefore, MTSET inhibition of sulfate uptakes by the mutants, T257C and T261C, was seen only in Na⁺ but not choline buffer. However, adding sulfate in Na⁺ buffer more or

less reduced MTSET inhibition for all four mutant, indicating that sulfate binding triggers another movement of TMD-5, which makes residues at the four positions 257, 259, 261, and 263 less exposed to hydrophilic environment. Pajor's group also reported similar observation that MTSET accessibility of substituted cysteines in TMD-9 of NaDC-1 was dependent on cations and substrate used in the buffer suggesting that TMD-9 is likely to be involved in the conformational changes during the transport cycle of NaDC-1(90).

In conclusion, the main findings of this chapter are that the regions surrounding two serine residues, Ser-260 and Ser-288, in TMDs 5 and 6 are functionally important for hNaSi-1, and that TMD-5 is likely to be involved in conformational changes during the transport cycle of hNaSi-1. Alanine replacement at Ser-260 resulted in decreased substrate and cation binding affinity, indicating Ser-260 is likely to be involved in the substrate and/or cation binding of hNaSi-1. In contrast, alanine mutation of Ser-288 resulted in increased cation binding affinity and broadened cation selectivity, suggesting that Ser-288 is probably directly or indirectly involved in the cation binding sites of hNaSi-1. Cysteine replacements for Ser-260 and Ser-288 and the 12 surrounding residues produced inactive mutants or mutants with altered transport activity, however, cell-surface expression of these mutants was not affected. These results indicate that these residues are functionally required for hNaSi-1. The four mutants, T257C, T259C, T261C, and L263C, were sensitive to MTSET inhibition and exhibited substrate protection in Na⁺ buffer. MTSET modification of the substituted cysteines at positions 257, 259, 261, and 263 is dependent on transported cations and substrate, suggesting that these

residues are likely to be involved in the conformational changes triggered by Na^+ and sulfate binding. Since these four residues are located in TMD-5, this transmembrane domain may also be involved in the conformational changes during the transport cycle of hNaSi-1.

A.



B.

	253					295
hNaSi-1	LTTI	TGT	STNLIFA	EYFNTRYPD.	CRCLNFGSWF	TFSFPAALII
rNaSi-1	LTTI	TGT	STNLIFS	EHFNTRYPD.	CRCLNFGSWF	LFSFPVAVIL
mNaSi-1	LTTI	TGT	STNLIFS	EHFNTRYPD.	CRCLNFGSWF	LFSFPVALIL
hSUT-1	LTTI	IGT	STSLIFL	EHFNQYPA.	AEVVNFGTWF	LFSFPISLIM
rbNaDC-1	IATL	TGTT	PNLVLQ	GQMTSLFPQN	PNVVNFASWF	GFAFPIMVIL
hNaDC-1	IATL	TGT	APNLVLQ	GQINSLFPQN	GNVVNFASWF	SFAFPTMVIL
rNaDC-1	IATL	TGTT	PNLVLQ	GQVNSLFPQN	GNVVNFASWF	GFAFPTMIIL
mNaDC-1	IATL	TGTT	PNLVLQ	GQVNSIFPEN	SNVVNFASWF	GFAFPTMVIL
xNaDC-2	IATL	TGTT	PNLVMK	GQMDLFPEN	NNIINFASWF	GFAFPTMLVL
rNaDC-3	TATL	TGT	APNLILL	GQLKSFFPQ.	CDVVNFGSWF	IFAFPLMLLF
fNaDC-3	TATL	TGT	APNLILI	GQLKSYFPD.	CDLINFGSWF	AFAPPLMLIF
hNaDC-3	TATL	TGT	APNLILL	GQLKSFFPQ.	CDVVNFGSWF	IFAFPLMLLF
mNaDC-3	TATL	TGT	APNLILL	GQLKSFFPQ.	CDVVNFGSWF	IFAFPLMLLF

Figure 4.1 The amino acid residues of hNaSi-1 mutated in this chapter. (A) Secondary structure model of transmembrane domains 5 and 6 of hNaSi-1. The amino acid residues mutated are highlighted in red (Ser-260 and Ser-288) or gray (6 residues surrounding Ser-260 or Ser-288). (B) Multiple sequence alignment of members in the NaDC/NaSi transporter family (from amino acid residue 253 to 295 in hNaSi-1). The sequence alignment was performed using the GCG Pileup program. The two serine residues (red) are conserved only in sulfate transporters but not in any of other members of the family. Most of the residues (light gray) surrounding the two serines are highly conserved in all members of the family.

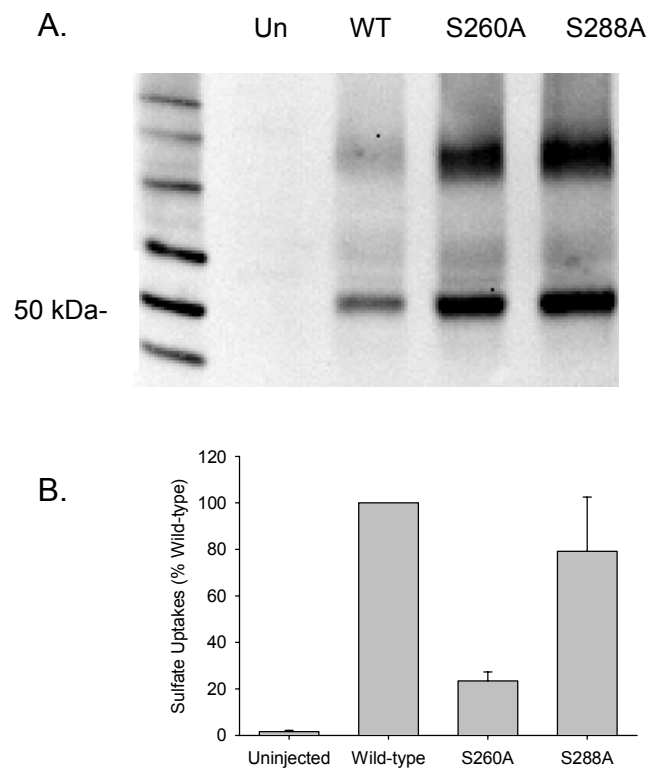


Figure 4.2 Western blot and uptakes of *Xenopus* oocytes expressing wild-type hNaSi-1 and the mutants, S260A and S288A. (A) Western blot of biotinylated oocytes. Intact uninjected (Un) oocytes or oocytes injected with cRNA of wild-type (WT) hNaSi-1 or mutants S260A and S288A were biotinylated with Sulfo-NHS-LC biotin. The biotinylated proteins were then separated on 6% tricine SDS gel and used for Western blotting analysis with anti-hNaSi-1 antibodies. Size standards are shown in the first lane from the right. (B) Uptakes of oocytes expressing the wild-type and mutant hNaSi-1. 15-minute uptakes of 100 μ M [35 S]-sulfate were measured in the presence of 100 mM Na $^{+}$. The data are presented as a percentage of the uptakes of wild-type hNaSi-1. The data shown here are means \pm SEM of three or four separate experiments.

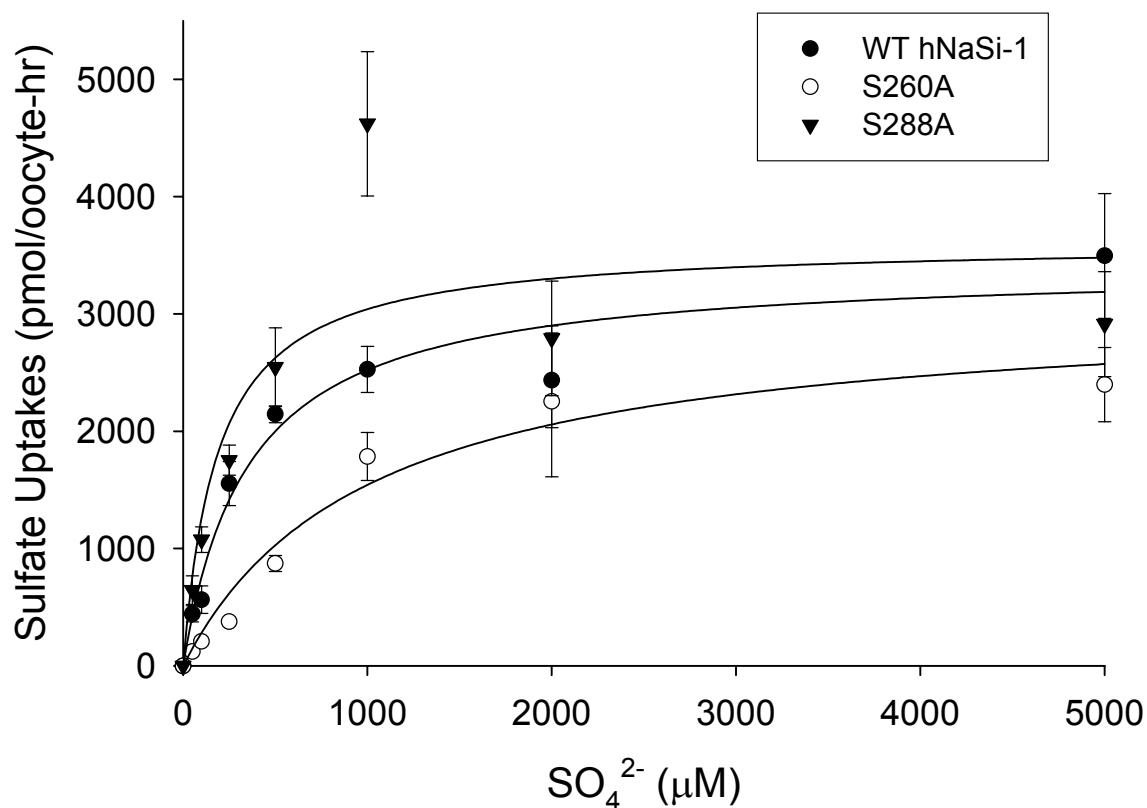


Figure 4.3 Kinetics of sulfate uptakes by *Xenopus* oocytes expressing wild-type hNaSi-1 and the mutants, S260A and S288A. 10-minute uptakes were measured with increasing concentrations of [^{35}S]-sulfate in the presence of 100 mM Na^+ . Each data point represents the mean \pm SEM of uptake rates of 4 or 5 oocytes. The data were fit to the Michaelis-Menten equation. The K_m values are (in μM): 354 (wild-type), 1002 (S260A) and 188 (S288A). The maximum uptake rates, V_{max} , are (in pmol/oocyte-hr): 3414 (wild-type), 3088 (S260A) and 3611 (S288A).

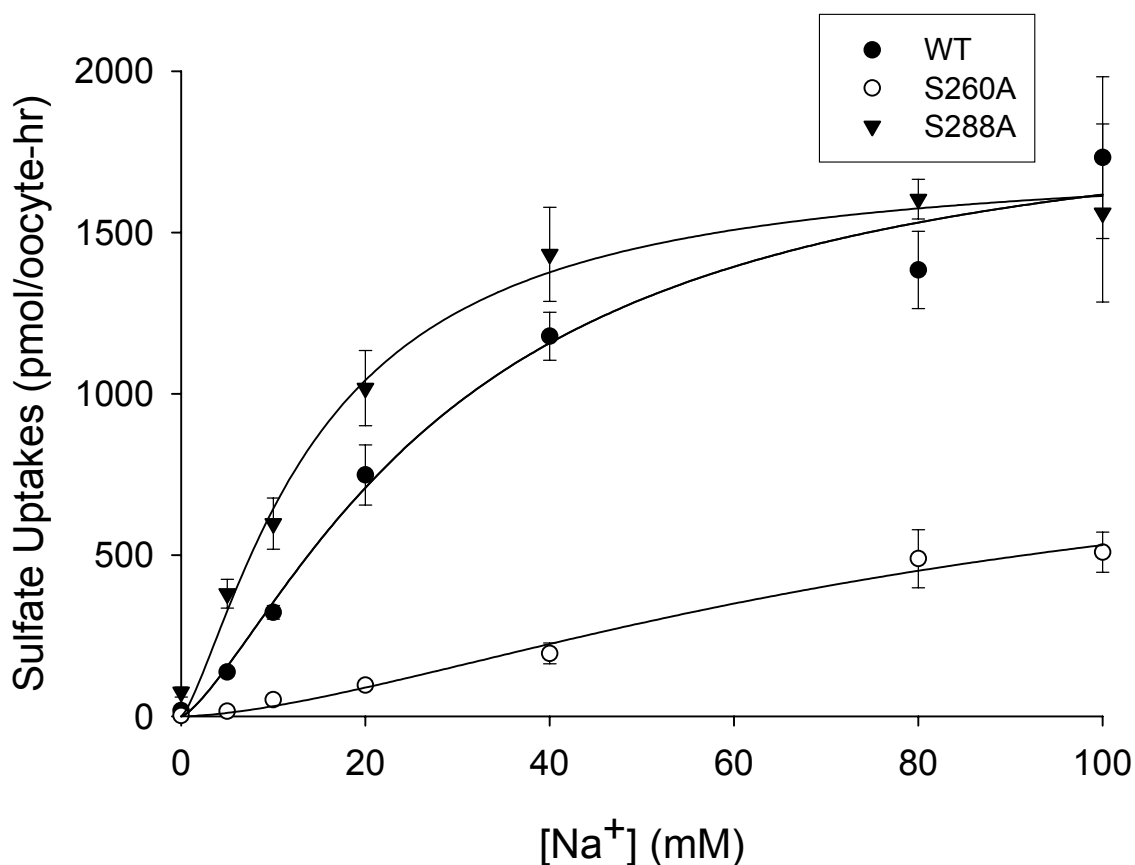


Figure 4.4 Na⁺-activation of sulfate uptakes by *Xenopus* oocytes expressing wild-type hNaSi-1 and the mutants, S260A and S288A. 10-minute uptakes of 100 μ M [³⁵S]-sulfate were measured in the presence of increasing concentrations of Na⁺. Each data point represents the mean \pm SEM of uptake rates of 5 oocytes. The data were fit to the Hill equation. The half saturation concentration constants for Na⁺ are (in mM): 30 (wild-type), 80 (S260A) and 15 (S288A). The maximum uptake rates, V_{max} , are (in pmol/oocyte-hr): 1921 (wild-type), 905 (S260A) and 1736 (S288A). The Hill coefficient is 1.37 for wild-type, 1.59 for S260A and 1.35 for S288A.

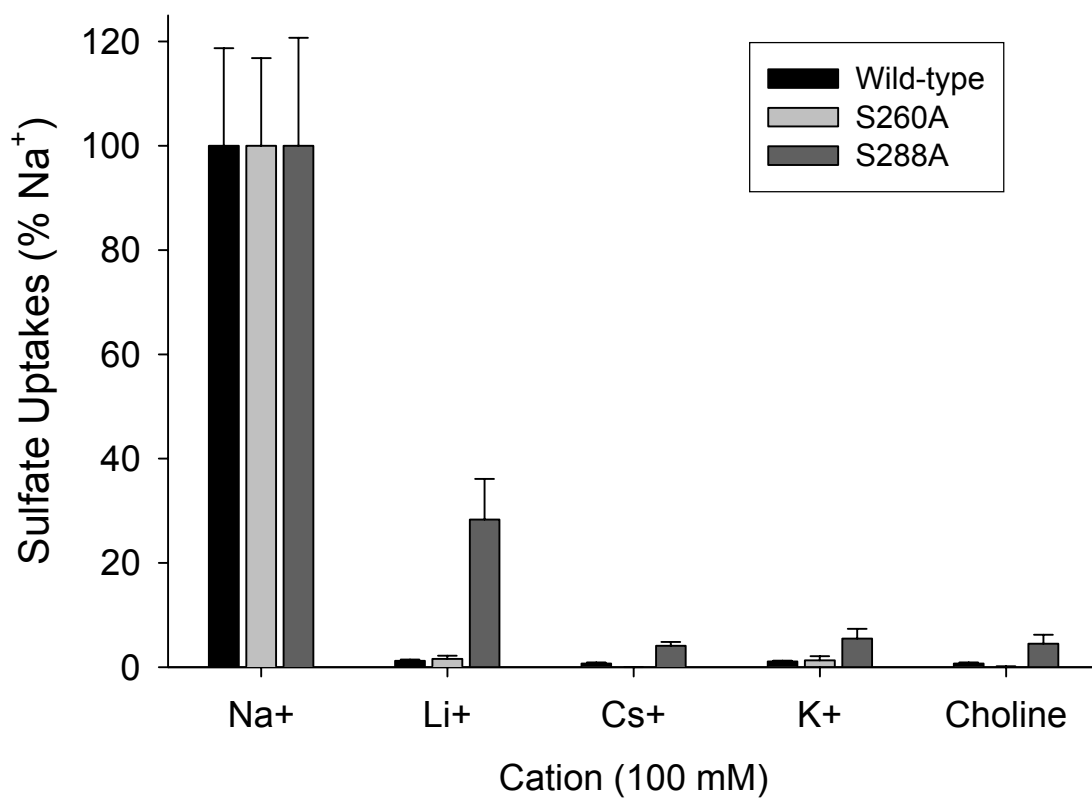


Figure 4.5 Cation selectivity of wild-type hNaSi-1 and the mutants, S260A and S288A, expressed in *Xenopus* oocytes. The figure shows one single experiment. 15-minute uptakes of 100 μ M [³⁵S]-sulfate were measured in 100 mM Na⁺, Li⁺, Cs⁺, K⁺ or choline buffer. The data are shown as a percentage of uptakes in Na⁺ buffer. The data are means \pm SEM (n = 4 or 5 oocytes).

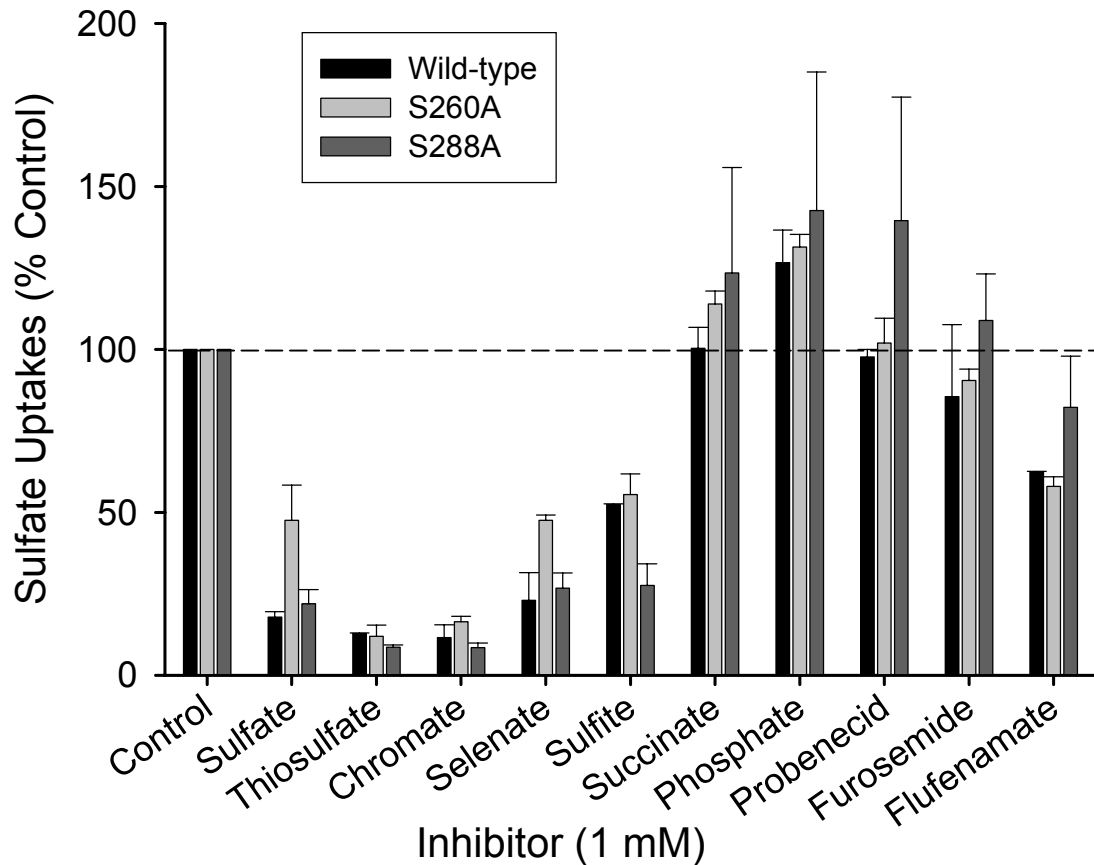


Figure 4.6 Substrate specificity of wild-type hNaSi-1 and the mutants, S260A and S288A, expressed in *Xenopus oocytes*. 15-minute uptakes of 10 μM [^{35}S]-sulfate were measured in the presence of 1 mM test inhibitors in 100 mM Na^+ buffer. The data are presented as a percentage of uptakes in the absence of test inhibitors. The data shown here are means \pm range of two separate experiments. Statistical analysis did not show any significant inhibition or stimulation by succinate, phosphate, probenecid or furosemide in wild-type and the two mutants. Statistical analysis of one experiment showed significant inhibition by flufenamate in wild-type ($P < 0.03$) and S260A ($P < 0.0002$) but another experiment did not show significant inhibition by flufenamate in either wild-type or S260A. Neither of the two experiments showed significant inhibition by flufenamate in S288A.

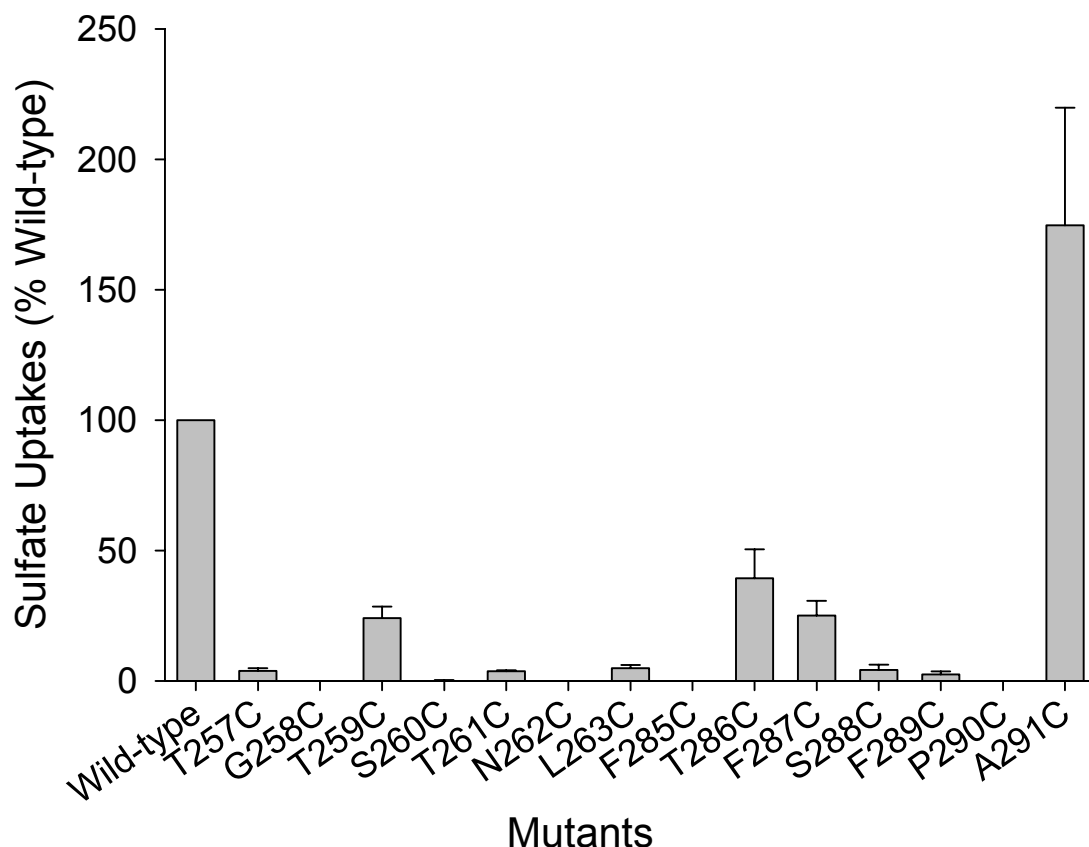


Figure 4.7 Sulfate uptakes by *Xenopus* oocytes expressing the cysteine mutants surrounding Ser-260 and Ser-288 in hNaSi-1. Uptakes of 100 μ M [35 S]-sulfate in 100 mM Na⁺ buffer were measured for 15 minutes. The uptake values for the wild-type and each mutant hNaSi-1 were corrected by subtracting uptakes of uninjected oocytes. The data are presented as a percentage of uptakes of the oocytes expressing wild-type hNaSi-1. The data shown in the figure are means \pm SEM of two or three experiments. One out of three experiments for A291C showed significantly increased uptakes ($P < 0.01$), whereas another two experiments did show significant change in uptakes of A291C.

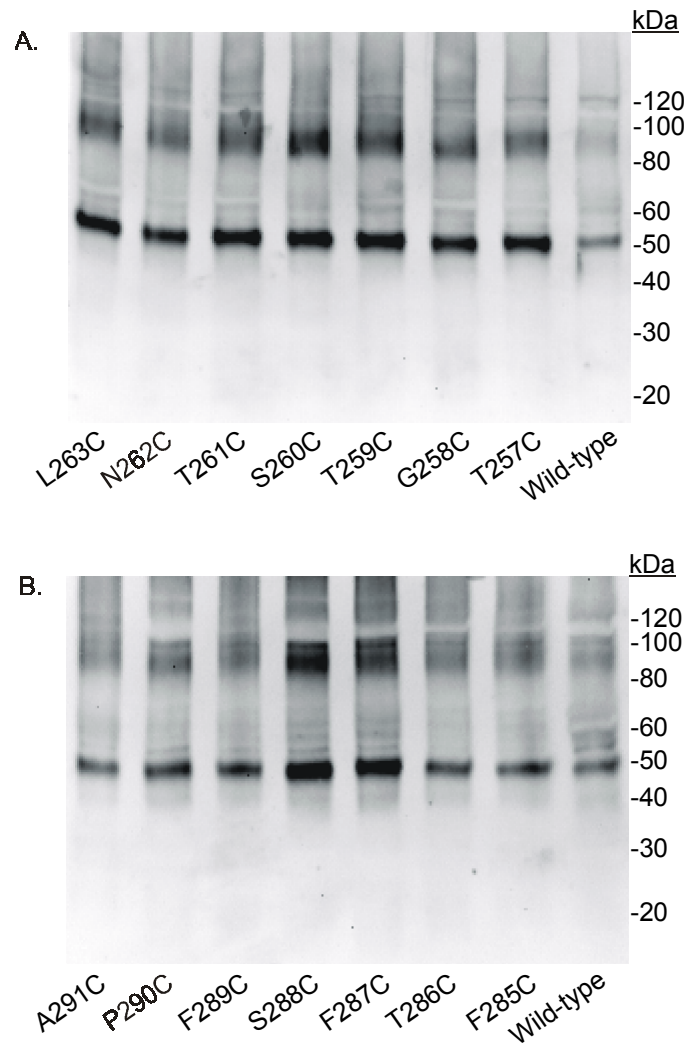


Figure 4.8 Western blots of biotinylated *Xenopus* oocytes expressing wild-type hNaSi-1 and the cysteine mutants. Oocytes were cell-surface biotinylated with Sulfo-NHS-LC biotin and the proteins were then separated on 6% tricine SDS gels, which were transferred to nitrocellulose membranes. The blots were probed with anti-hNaSi-1 antibodies as described in Methods of Chapter 3. Size standards (kDa) are shown on the right side of each panel.

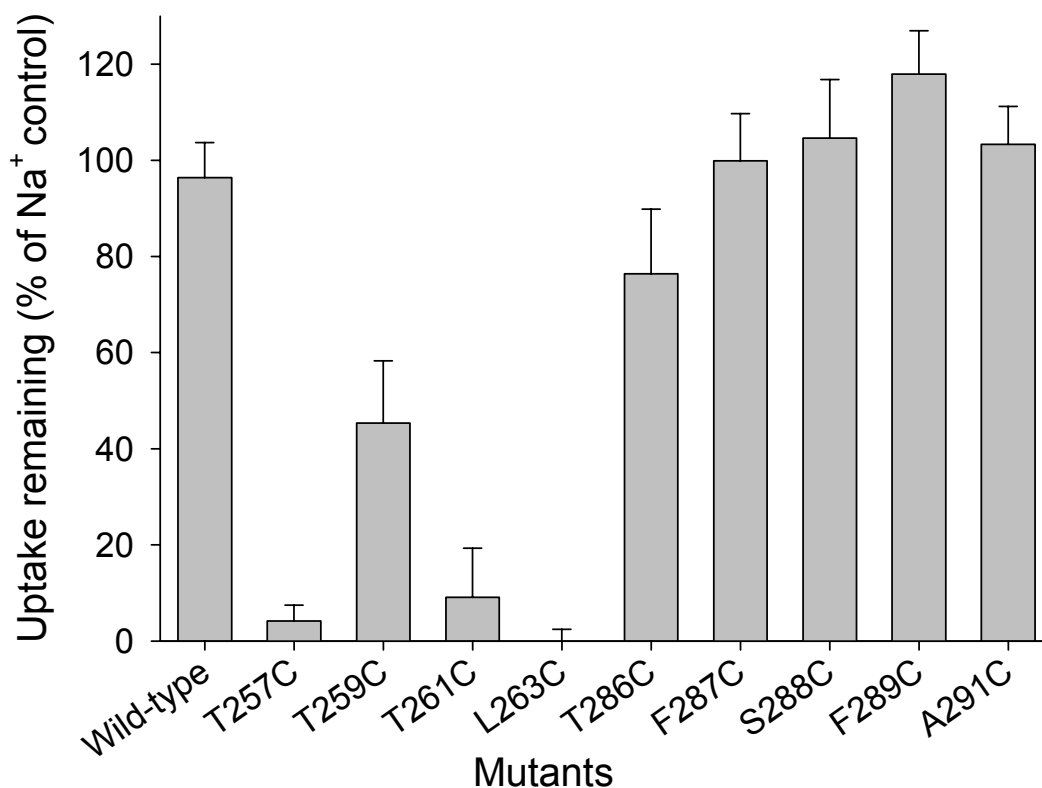


Figure 4.9 MTSET sensitivity of hNaSi-1 cysteine mutants expressed in *Xenopus* oocytes. Each group of 5 oocytes was pre-incubated for 10 minutes in 100 mM Na⁺ buffer with or without 1 mM MTSET and then washed with 100 mM choline buffer. 15-minute uptakes of 100 μ M [³⁵S]-sulfate were measured in the presence of 100 mM Na⁺. For each mutant, uptakes of oocytes preincubated in MTSET are presented as a percentage of uptakes of oocytes preincubated in Na⁺ buffer only. The data shown are means \pm range of two experiments.

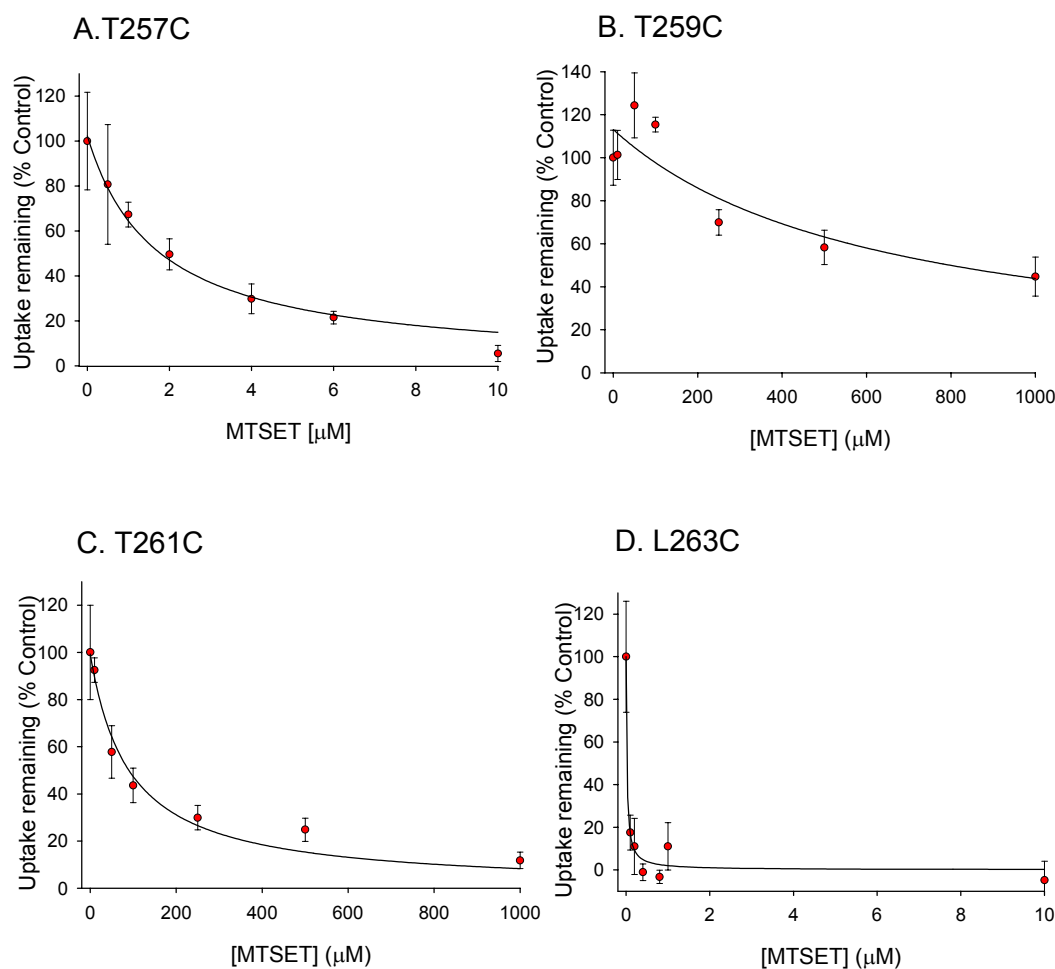


Figure 4.10 Concentration dependence of MTSET inhibition of sulfate uptakes by T257C, T259C, T261C, and L263C. Groups of 5 oocytes expressing the mutants were pre-incubated for 10 minutes in 100 mM Na⁺ buffer only (as control) or with the increasing concentrations of MTSET dissolved in the same buffer, which was then washed away with 100 mM choline buffer. Then 15-minute uptakes of 100 μM [³⁵S]-sulfate were measured in 100 mM Na⁺ buffer. Uptakes of each mutant are presented as a percentage of uptakes of control. Each data point represents the mean ± SEM of 5 oocytes. The apparent K_i for each mutant is (A) T257C: 1.7 μM, (B) T259C: 633 μM, (C) T261C: 91 μM, and (D) L263C: 0.02 μM.

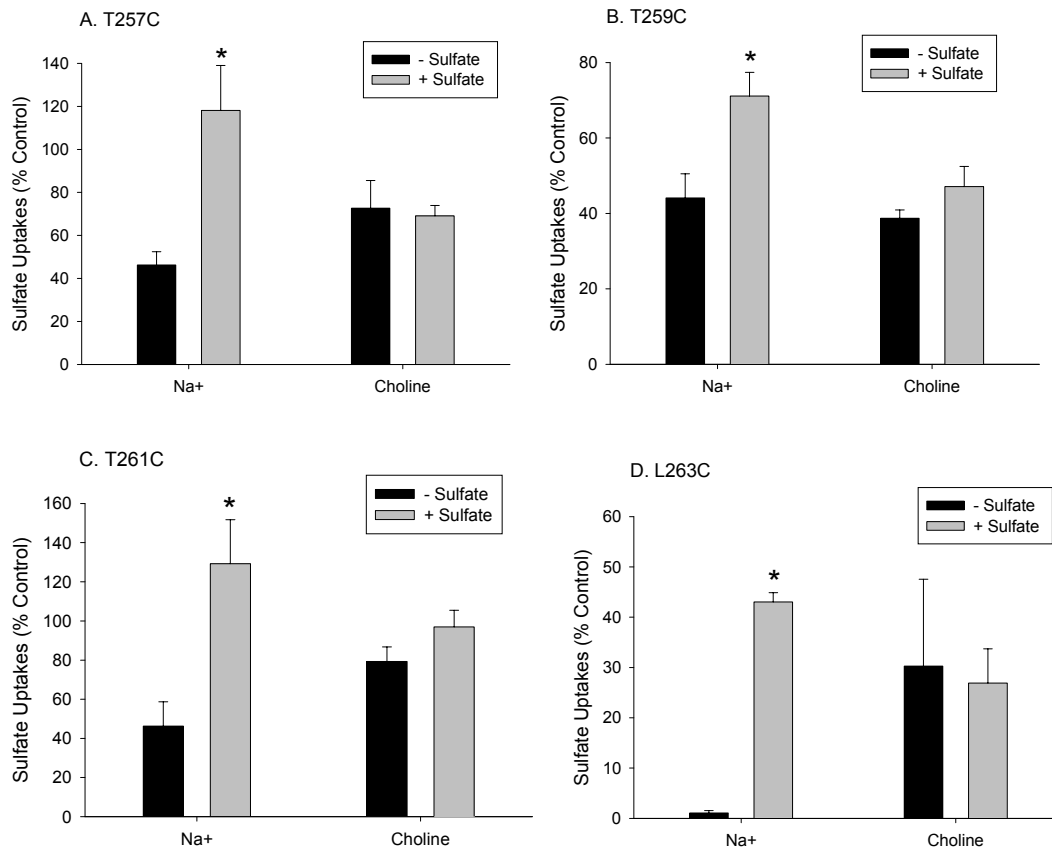


Figure 4.11 Cation and substrate dependence of MTSET inhibition of sulfate uptakes by T257C, T259C, T261C, and L263C. Based on the apparent value of K_i obtained from Figure 4.10, a concentration of MTSET was chosen to produce about 60% uptake inhibition, (A) T257C: 2.5 μ M (B) T259C: 0.5 mM (C) T261C: 0.25 mM (D) L263C: 1.0 μ M. The oocytes expressing the mutant were pre-incubated for 10 minutes in the above concentration of MTSET in 100 mM Na⁺ or choline buffer with or without 5 mM sulfate. Control groups were pre-incubated in the same buffer as the experimentals but without MTSET. After preincubation, 15-minute uptakes of 100 μ M [³⁵S]-sulfate were measured in Na⁺ buffer. The data are presented as a percentage of the control, means \pm SEM of three separate experiments. Statistical analysis showed significantly increased sulfate uptakes after preincubation with Na⁺ and sulfate together compared to Na⁺ alone (P < 0.02).

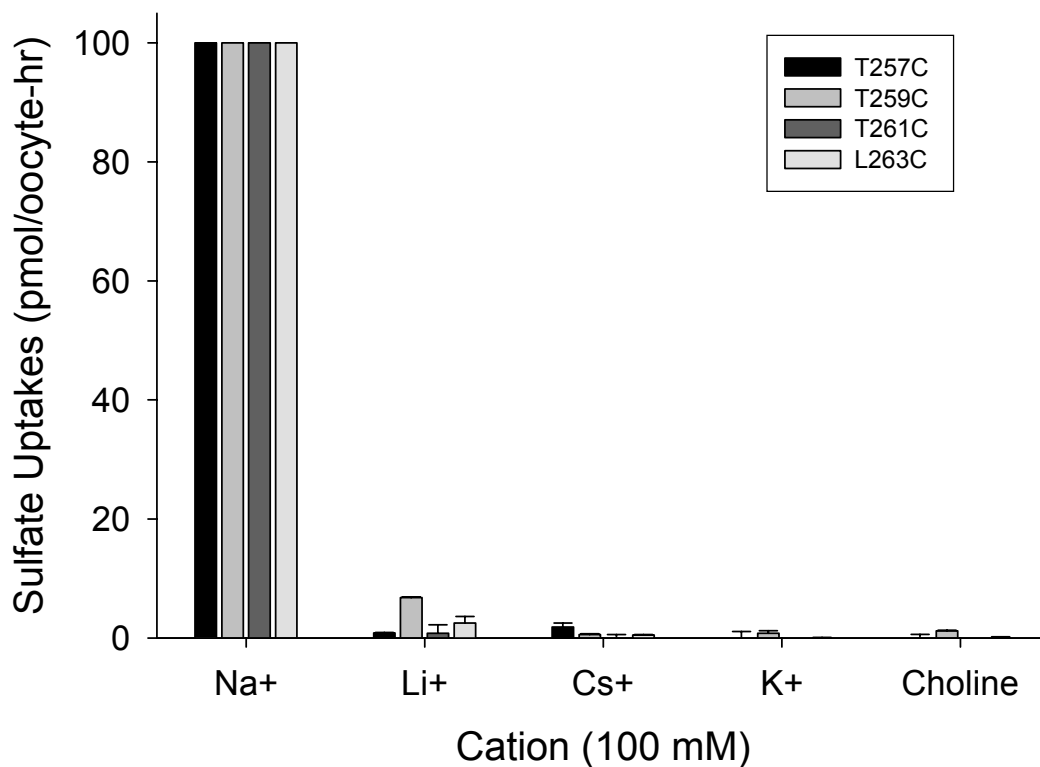


Figure 4.12 Cation selectivity of T257C, T259C, T261C, and L263C expressed in *Xenopus* oocytes. 15-minute uptakes of 100 μ M [³⁵S]-sulfate were measured in the presence of 100 mM of Na⁺, Li⁺, Cs⁺, K⁺ or choline. The data are presented as a percentage of uptakes in 100 mM Na⁺ buffer. The data shown for each mutant are the means \pm range of two separate experiments.

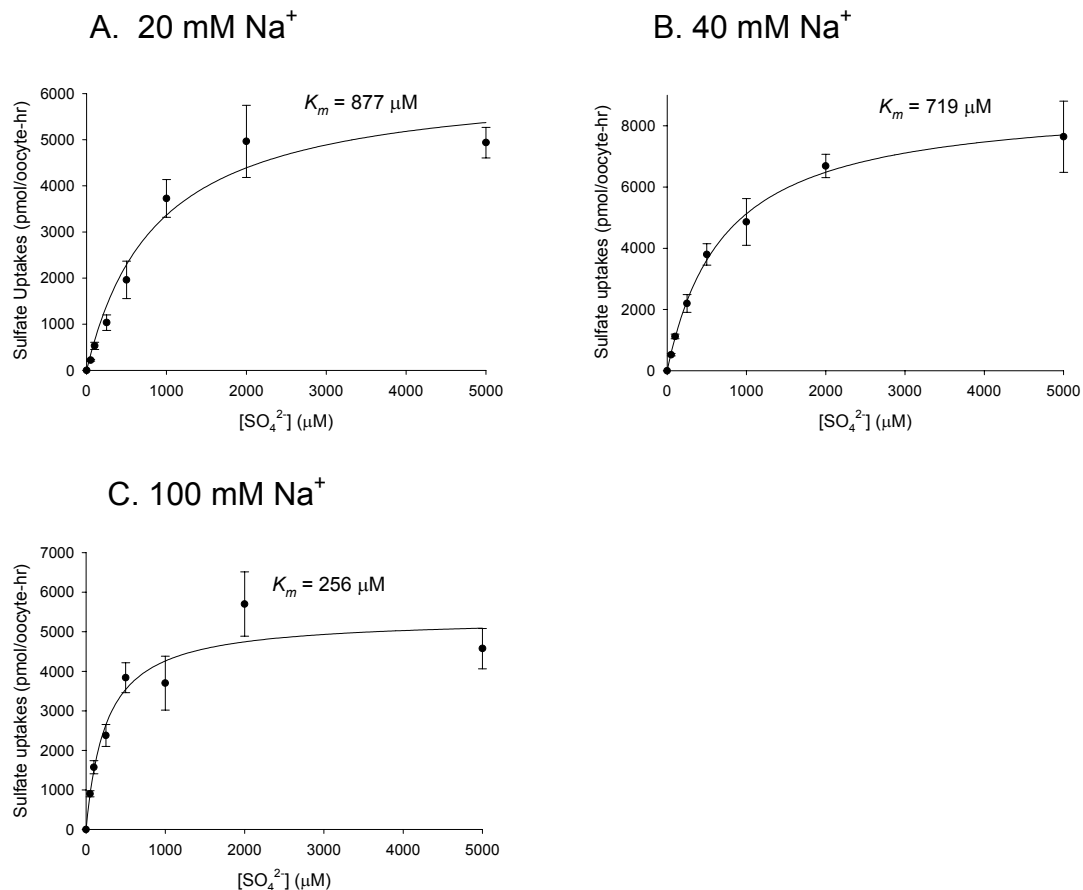
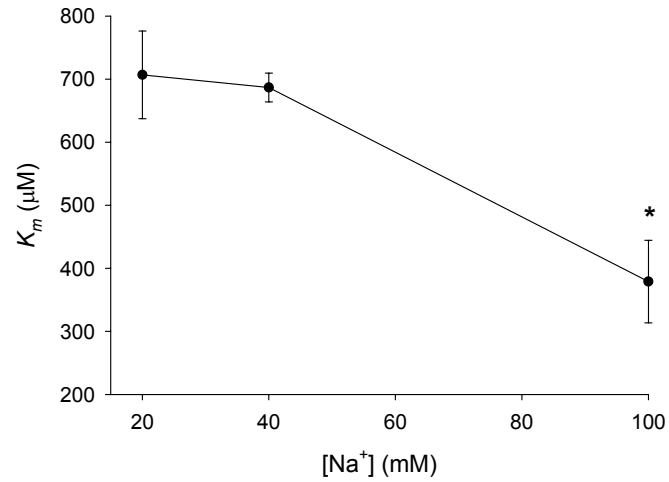


Figure 4.13 Effect of Na⁺ on substrate kinetics of hNaSi-1 expressed in *Xenopus* oocytes. 10-minute uptakes of oocytes expressing wild-type hNaSi-1 were measured with increasing concentrations of sulfate in the presence of (A) 20 mM, (B) 40 mM or (C) 100 mM Na⁺ buffer. Each data point represents the average initial uptake rate of 5 oocytes from a single frog. The K_m values (in μM), are 877 (20 mM), 719 (40 mM) and 256 (100 mM), and the V_{max} values (in pmol/oocyte-hr) are 6314 (20 mM), 8815 (40 mM) and 5352 (100 mM).

A.



B.

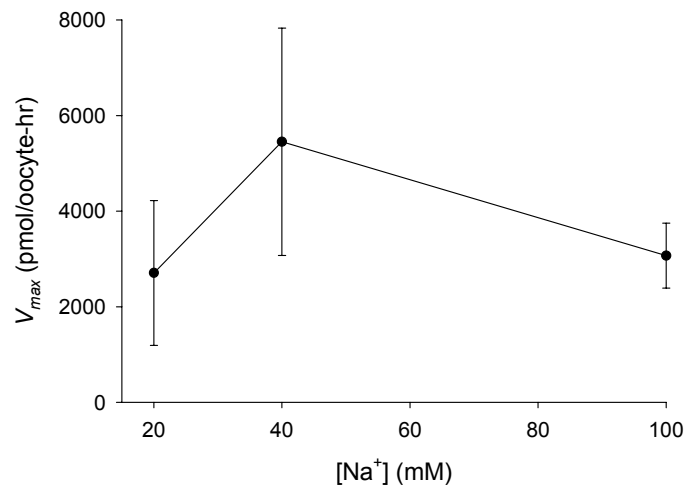


Figure 4.14 Na⁺-dependence of K_m and V_{max} of sulfate uptakes by wild-type hNaSi-1 expressed in oocytes. The Na⁺-dependence of K_m and the maximum uptake rate V_{max} is shown in (A) and (B), respectively. Statistical analysis showed that the K_m in 100 mM Na⁺ buffer is significantly lower than that in 20 mM Na⁺ buffer ($P < 0.03$). There is no significant difference in V_{max} .

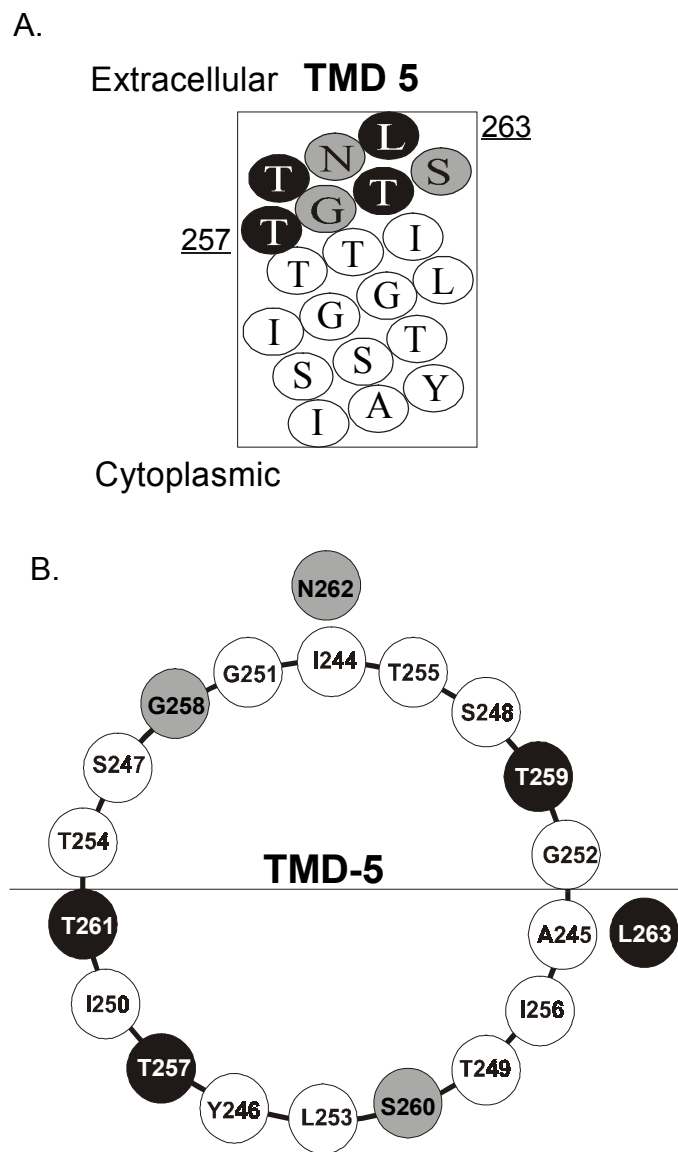
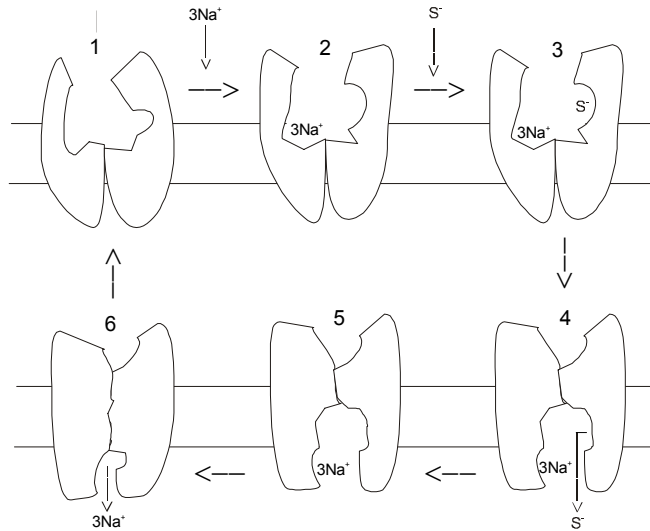


Figure 4.15 Summary of the MTSET sensitive residues surrounding Ser-260 in TMD 5 of hNaSi-1. (A) helical web figure of the 7 residues mutated to cysteine in TMD-5. (B) helical wheel projection of TMD-5 looking down from the extracellular side. Cysteine mutants at the residues highlighted in black with white text (Thr-257, Thr-259, Thr-261 and Leu-263) are sensitive to MTSET inhibition and show substrate protection in Na⁺ buffer. Cysteine replacements at the residues highlighted in gray (Gly-258, Ser-260 and Asn-262) resulted in inactive proteins.

A.



B.

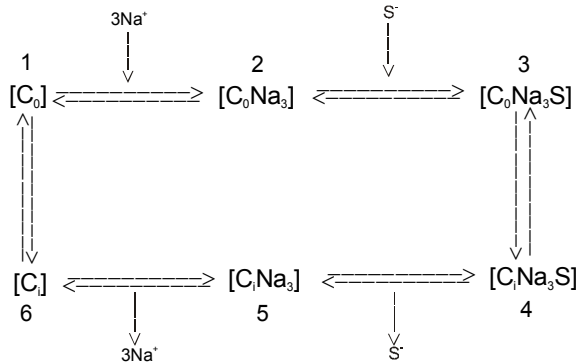


Figure 4.16 A simplified 6-state ordered binding kinetic model for the hNaSi-1 transporter. (A) Cartoon of the transport cycle for hNaSi-1 (modified from (143)). (B) The corresponding scheme of the transport cycle. In choline buffer, most of transporters exist in state 1 (C_o), in which the cation and substrate binding sites are accessible from outside of the cell. In the presence of Na⁺, binding of 3 Na⁺ ions triggers a conformational change from state 1 (C_o) to 2 (C_oNa_3), which has an increased binding affinity for sulfate. Sulfate binding to the transporter results in another conformational change, from state 2 (C_oNa_3) to 3 (C_oNa_3S). Another movement from state 3 (C_oNa_3S) to 4 (C_iNa_3S) translocates cations and substrate into inside of the cell. After releasing of cations and sulfate into the cell, the transporter reorients to outside of the cell, from state 6 (C_i) to 1 (C_o), and thus finish the whole transport cycle.

CHAPTER 5: CONCLUSIONS

The bacterial Mg^{2+} -citrate transporter, CitM

The transport of citrate in the gram-positive bacterium, *Bacillus subtilis*, was found to be dependent on Mg^{2+} about thirty years ago, (141, 86). However, since then, there had been no further reports on the Mg^{2+} -citrate transport in *B. subtilis* until 1983 when studies of citrate transport in *B. subtilis* membrane vesicles were published (11). Bergsma and Konings suggested that citrate could be transported as a complex with many other divalent metal ions and the transport is proton coupled (11). Again since then there had not been improvement on studies of the Mg^{2+} -citrate transport for another 13 years until 1996 when the cDNA coding for the protein corresponding to this transport system was cloned and termed CitM (14). Most recent studies are mainly focused on the regulation of CitM (140; 145). There had been no studies performed to outline the detailed functions and transport mechanism of CitM until 2002 when studies of Chapter 2 in this dissertation were published (67).

One of the aims in this dissertation was to characterize the function of the cloned CitM transporter in *E. coli* cells (Chapter 2), which helps to understand the transport mechanism of CitM and also makes a basis for future studies on the structure-function relationships of this transporter. Previous studies of the Mg^{2+} -citrate transport in native *B. subtilis* cells were complicated by multiple endogenous citrate transport pathway (61). This drawback is resolved by expressing the cloned CitM in *E. coli* cells, which do not have any

endogenous citrate uptake systems. The main findings of my studies on CitM are: (1) The CitM transporter has a low affinity for the complex of Mg^{2+} -citrate with an apparent K_m of ~ 0.3 mM, (2) the tridentate complex form is the preferred transported substrate, (3) citrate can also be transported as a complex with other divalent metal ions including Mn^{2+} , Ba^{2+} , Ni^{2+} , Co^{2+} , and Ca^{2+} but not with Zn^{2+} , (4) the transport is electroneutral with one proton coupled with one complex of Mg^{2+} -citrate.

Some results shown in Chapter 2 are different from previous studies of the Mg^{2+} -citrate transporter. One difference is the substrate binding affinity. In Chapter 2, the apparent K_m (~ 0.3 mM) of cloned CitM for the Mg^{2+} -citrate is close to the K_m (~ 0.55 mM) in whole cell *B. subtilis* (141). However, it is almost 5 to 8 fold higher than those reported in previous studies of *B. subtilis* membrane vesicles ($K_m = \sim 40$ μM) (11) and of the cloned CitM expressed in *E. coli* cells ($K_m = \sim 60$ μM) (14). Membrane vesicle experiments should provide more accurate results since they do not contain the cell wall. The difference between the two separate studies of cloned CitM is still unclear. One possible reason is that the buffers used in the two experiments are different, however, more experiments are required to verify this possibility. The second difference is the form of transported complex. As is discussed in the Introduction of Chapter 1, citrate can form three kinds of complexes with divalent metal ions. Previous studies suggested that the transported complex seemed to be only the bidentate form in which the two carboxylate groups of citrate are involved but the central hydroxyl group is free of binding with a metal ion (14; 51).

However, based on the substrate specificity reported here, the transported complex is more likely to be the tridentate form since the central hydroxyl group besides the two carboxylate groups seems also essential for the transported complex. Other tricarboxylic acids, isocitrate, *cis*-aconitate and tricarballic acid, and dicarboxylic acid (succinate), which lack the central hydroxyl group, could not inhibit the citrate transport in the presence of Mg^{2+} . The third difference is the metal ion selectivity. Previous studies of cloned CitM reported that CitM transported complexes of citrate with Mg^{2+} , Mn^{2+} , Ni^{2+} , Co^{2+} , and Zn^{2+} but not with Ba^{2+} and Ca^{2+} , which instead were transported as complexes with citrate by CitH (61). However, studies reported in Chapter 2 showed that Ba^{2+} and Ca^{2+} as a complex with citrate could also be transported by CitM. One possibility is that Ba^{2+} or Ca^{2+} used in my studies were contaminated by some other divalent metal ions. More experiments are needed to confirm this possibility. Another difference is the transport mechanism. Studies by Lolkema's group on cloned CitM in *E. coli* suggested a proton-coupled electrogenic transport since the K^+ ionophore, valinomycin, which can change the membrane potential, was observed to have an inhibition effect on the transport (14). However, experiments done by Lolkema's group used unpermeabilized *E. coli* cells thus it is unclear whether valinomycin reached the inner plasma membrane. Secondly, their experiments used high extracellular K^+ concentration (above 25 mM) at which valinomycin could also change the pH gradient besides the membrane potential (2) thus it is hard to tell whether the inhibition of the transport was due to the dissipation of the proton gradient or the membrane potential. My experiments in Chapter 2

overcome these two drawbacks by using permeabilized *E. coli* cells and lower extracellular K^+ concentrations (0 and 20 mM). Under these two improved conditions, valinomycin did not show effects on the transport by CitM. Therefore, I propose an electroneutral transport model for CitM with one proton coupled with one Mg^{2+} -citrate complex.

Another novel idea proposed in CitM studies reported here is that Mg^{2+} may not only be the transported substrate but also serve as an activator of the transport by CitM. This conclusion is based on the sigmoidal dependence of citrate uptake on concentrations of the Mg^{2+} -citrate complex, which is similar to the role of Mg^{2+} in the function of Mg^{2+} -ATP requiring enzymes (123). In addition, other divalent metal ions such as Ca^{2+} could also serve as an activator of the transport, therefore, additional experiments are required to confirm this conclusion.

In brief, studies reported in Chapter 2 give a functional characterization of CitM expressed in *E. coli* cells. In order to further understand the transport mechanism of CitM, there are two directions for the future studies of CitM: the structure-function relationships and crystal structure, and here I will only discuss the first direction. Based on the previous studies of cloned CitM and CitH, they belong to a distinct gene family and share 60% sequence identity but have complementary metal ion specificity (14; 61). Therefore, chimeras can be made between these two proteins to determine which part of the protein is responsible for the different metal ion-citrate binding. One of the potential

problems for chimera studies is that the chimera may be toxic to the bacteria. Site-directed mutagenesis can also be used to mutate conserved residues in the gene family, and the mutant which shows altered transport activity will indicate that the mutated residue may play a role in substrate and proton binding of CitM.

The human Na⁺-coupled sulfate transporter, hNaSi-1

The human Na⁺-coupled sulfate transporter, hNaSi-1, was cloned from human kidney cDNA library by Markovich's group two years ago (65), at the same time an unknown Genbank sequence, which has a high identity with rNaSi-1 and rbNaDC-1, was also amplified by PCR in our lab. Studies by Markovich's group were mainly focused on gene organization and chromosomal localization with some basic studies on function and tissue distribution. Some basic functional characterization and tissue distribution of rNaSi-1 and mNaSi-1 have also been performed previously (8; 78). However, the tissue distribution of NaSi-1 in human and rodents was different. Also, Markovich's group found mRNA transcripts and DNA fragment for hNaSi-1 only in kidney (65), whereas RT-PCR performed in our lab (unpublished data) found a DNA fragment for hNaSi-1 in small intestine as well as kidney. More experiments are needed to explain these differences. In addition, the *N*-glycosylation site and the functional role of *N*-glycosylation in NaSi-1 transporters are not clear yet. Therefore, one of the two aims for the studies on hNaSi-1 in this dissertation was to make antibodies against hNaSi-1 and

determine its tissue distribution and *N*-glycosylation site. Moreover, the transport mechanism or structure of substrate and cation binding sites of the NaSi-1 transporter is almost completely unknown. Sequence alignment of NaDC/NaSi transporters found that only two out of 42 serine residues in hNaSi-1 (Ser-260 and Ser-288) were conserved in all NaSi-1 but not NaDC transporters. Therefore, the second aim for the studies on hNaSi-1 is to test the functional roles of the regions surrounding these two conserved serine residues in substrate and cation binding of hNaSi-1.

Preparation of antibodies against hNaSi-1 and application of antibodies to tissue distribution and N-glycosylation

To determine the tissue distribution and *N*-glycosylation of hNaSi-1, specific antibodies against hNaSi-1 were needed. The antibodies were also a useful tool for later studies on the structure-function relationships of hNaSi-1. The fusion protein GST-Si65 was prepared by fusing a specific peptide of hNaSi-1 with GST and then used to raise polyclonal antibodies in rabbits. The immune serum was purified to remove anti-GST antibodies thus only antifusion protein antibodies were retained. The purified antibodies were tested and found to specifically recognize the hNaSi-1 peptide. Since it is difficult to get human renal BBMVs, the antibodies were tested with rat and pig renal BBMVs. Two specific protein signals at 79 kDa and 73 kDa were detected, representing the *N*-glycosylated form of native NaSi-1 transporters in rat and pig kidney, respectively. The protein signal at 79 kDa in rat kidney BBMVs agrees with those observed in previous studies (78; 69; 115). The antibodies also

recognized two protein bands at 53 kDa and 64 kDa in the plasma membrane of oocytes injected with cRNA of wild-type hNaSi-1. There are no other reports about the size of hNaSi-1 expressed on the plasma membrane of oocytes. One study of rNaSi-1 expressed in Sf9 cells reported the protein with a similar size at 55-60 kDa (34).

Strong immunofluorescence signals were observed in the nuclei of many tissues in the human tissue microarray slide used to test tissue distributions. There are at least two possibilities to explain this result. One is that the anti-GST antibodies are not completely removed from the anti-serum thus the immunofluorescence signals may represent the immunoreaction of GST antibodies with some nuclear proteins. Or some unknown nuclear proteins, which contain a peptide similar to the specific hNaSi-1 peptide used in the GST fusion protein, may cross react with the anti-fusion protein antibodies. To test the first possibility, the purified antiserum was applied to Western blots of GST and compared with unpurified antiserum. Results showed that the GST protein signals detected by purified antiserum significantly decreased compared with those detected by unpurified antiserum, indicating that most of the anti-GST antibodies have been removed from the antiserum. In the future, the second possibility will be tested by applying antiserum to purified nuclei.

There was little information on *N*-glycosylation of NaSi-1 transporters before my studies are reported in Chapter 3. Previous studies of cloned rNaSi-

1 suggested that there is one possible *N*-glycosylation site in NaSi-1 (78), but since then no more experimental evidence has been reported about *N*-glycosylation in NaSi-1. In my studies here, the conserved hNaSi-1 residue, Asn-591, which is located at the extracellular C-terminal tail of hNaSi-1, was mutated to tyrosine (N591Y) and alanine (N591A) and then the antibodies against the GST-Si65 fusion protein were applied to detect changes in mass. The wild-type hNaSi-1 expressed on plasma membrane of oocytes was deglycosylated using PNGase F. The mass of the deglycosylated wild-type protein decreased by about 4 to 15 kDa consistent with one single *N*-glycosylation site. In contrast, the enzyme-treated plasma membrane of oocytes injected with N591Y cRNA did not show change in mass compared with untreated sample, suggesting that Asn-591 is the single *N*-glycosylation site in hNaSi-1. Also, little information was known about whether *N*-glycosylation is required for the expression or transport function of hNaSi-1. Expression levels of N591Y and N591A on the plasma membrane of oocytes were tested with the antibodies using biotinylation and immunofluorescence techniques. N591Y and N591A both had more abundant expression on the plasma membrane of oocytes than the wild-type, indicating that the mutations did not prevent the protein trafficking to the cell surface. The kinetic properties of N591Y and N591A were also tested and compared with wild-type hNaSi-1. Tyrosine and alanine replacements at position 591 only significantly decreased the maximum uptake rates but did not affect the apparent K_m for substrate. Since the maximum uptake rate is dependent on the number of transporters expressed on the cell surface and the turnover number of the transporter, it is

likely that the decreased maximum uptake rate may reflect the decreased turnover number of the transporter. It seems that either the Asn-591 residue or the sugar group at Asn-591 is essential for the optimal conformational changes during the translocation process of the hNaSi-1 transporter.

Functional roles of Serines 260 and 288 in hNaSi-1

Although there have been many studies on the substrate and cation binding sites of NaDC-1 transporters in past years (89), little information had been reported about the substrate and cation binding sites of NaSi-1. Before starting studies on the structure-function relationships of hNaSi-1, functions of wild-type hNaSi-1 needed to be outlined first. My preliminary studies characterized functions of wild-type hNaSi-1 expressed in *Xenopus* oocytes. The hNaSi-1 transporter is a low affinity transporter with apparent K_m s of ~440 μ M and 26 mM for substrate and Na^+ , respectively, and with a Hill coefficient of 1.8. The hNaSi-1 has a strict cation specificity, i.e. the sulfate transport is only dependent on Na^+ but not on other tested cations including Li^+ , Cs^+ , K^+ , and choline. The transporter has a broad substrate specificity and can also transport divalent anions which have similar chemical structures to sulfate, such as thiosulfate, sulfite, chromate, and selenate. Phosphate and succinate do not inhibit sulfate uptakes. However, previous studies of cloned hNaSi-1 showed a somewhat different result that succinate could inhibit uptakes of radioactive sulfate (65), which was not observed in experiments performed in Chapter 4 of this dissertation. In addition, neither probenecid (an anion exchanger inhibitor) nor furosemide (a NaDC-1 inhibitor) produced inhibition on

sulfate uptakes by hNaSi-1 whereas another NaDC-1 inhibitor, flufenamate (96), resulted in some inhibition of transport activity.

There are a total of 42 serine residues in hNaSi-1 and the sequence alignment of members in NaDC/NaSi-1 family shows that only two serine residues, Ser-260 and Ser-288, are conserved in all of NaSi-1 and hSUT-1 transporters but not in other members of NaDC transporters. By comparison, the NaDC transporters have alanine or threonine in the same positions. Therefore, Ser-260 and 288 were originally mutated to alanine, and the S260A and S288A mutants were expressed and functionally characterized in oocytes. The functional changes of the two alanine mutants were summarized in [Table 5.1](#). Alanine replacement at Ser-260 resulted in an increased K_m for both sulfate and probably also for Na^+ . The cation selectivity and substrate specificity of S260A were similar to the wild-type. On the contrary, alanine replacement at Ser-288 did not result in changes in K_m for sulfate but produced an almost 50% decreased K_m for Na^+ . Alanine mutation at Ser-288 also resulted in a broadened cation selectivity i.e. sulfate can be transported in the presence of not only Na^+ but also Li^+ , Cs^+ , K^+ , or choline, which is not a transported ion for the wild-type. S288A also has similar substrate specificity to the wild-type. These results suggested that Ser-260 and Ser-288 are likely to be directly or indirectly involved in the structure of the substrate and cation binding sites of hNaSi-1.

In order to further test how these residues are involved in the structure of the substrate and cation binding sites of hNaSi-1, Ser-260 and Ser-288 were mutated to cysteine to test their sensitivity to inhibition by the cysteine-specific reagent, MTSET. However, cysteine replacement at Ser-260 produced an inactive protein while S288C had a very low transport activity. Therefore, residues surrounding Ser-260 and Ser-288 were also mutated to cysteine one at a time. All of the cysteine mutants were expressed well on the plasma membrane of oocytes. Most of mutants around Ser-288 were either inactive or had decreased transport activity except A291C which seemed to have somewhat increased transport activity. Three mutants around Ser-260, G258C, S260C, and N262C, were inactive and another four mutants, T257C, T259C, T261C, and L263C, had significantly decreased transport activity. Since all of these 14 mutants were expressed well on the plasma membrane, cysteine replacements did not prevent protein trafficking to membranes. Therefore, the changed transport activity should not be due to the defective expression of the protein. It is most likely that the cysteine replacements of these residues change the optimal conformation for the transport by hNaSi-1, thus producing decreased or increased transport activity. The mutants which have measurable uptakes were then tested with MTSET. All of the tested mutants around Ser-288 including S288C were not sensitive to MTSET inhibition. Only the four mutants surrounding Ser-260, T257C, T259C, T261C, and L263C, were sensitive to MTSET inhibition. The MTSET sensitivity of these four mutants suggested that these residues are probably located on the extracellular side or

in an aqueous pore of transport pathway of the protein. These results also help to verify the secondary structure model of hNaSi-1.

The MTSET accessibility of the four mutants, T257C, T259C, T261C, and L263C, was further investigated by preincubation with MTSET in different buffers. The results of the cation and substrate dependence of MTSET inhibition on sulfate uptakes by the four mutants were summarized in [Table 5.2](#). When preincubating in Na⁺ buffer, the four substituted cysteines were all sensitive to MTSET modification, thus exhibiting MTSET inhibition. However, when sulfate was added to the preincubating Na⁺ buffer, all of the four cysteines were less accessible or completely inaccessible to MTSET, thus MTSET inhibition was abolished or decreased. However, the substrate protection was not seen when the MTSET preincubation was done in choline buffer. Therefore, MTSET modification seems to be dependent on the preincubating buffer used. In order to explain this result, an ordered binding model is proposed for hNaSi-1, in which 3 Na⁺ ions bind prior to sulfate binding. This model was similar to that proposed in previous studies of the Na⁺/dicarboxylate cotransporter (144; 146). Based on this proposed binding model, the dependence of MTSET inhibition on cation and substrate used may imply that the residues substituted by cysteine are likely to be involved in the conformational changes during the transport cycle of hNaSi-1. Since these residues are located in TMD-5, this transmembrane domain is also probably involved in the conformational changes during the transport cycle of hNaSi-1.

Another interesting observation in these studies is that T259C showed MTSET inhibition in both choline and Na⁺ buffer, whereas T257C, T261C and L263C exhibited greater MTSET inhibition in Na⁺ than choline buffer. One possible explanation is that cysteine replacement at Thr-259 might decrease cation selectivity, thus choline, to some extent, could also initiate the conformational changes for sulfate uptakes by hNaSi-1. Therefore, cation selectivity of the four mutants was tested. However, there is no difference in cation selectivity compared with the wild-type protein. An alternative explanation is that the substituted cysteine residue at Thr-259 is likely to be exposed to the extracellular side or water-filled pore of hNaSi-1 thus accessible to MTSET without requiring a conformational change.

There are several directions for the future studies on the structure-function relationships of hNaSi-1. One direction is to perform cysteine-scanning mutagenesis of the rest of the residues in TMDs 5 and 6 and then test transport activity and MTSET sensitivity of each mutant. The results will be summarized in the helical wheel of TMD-5 to provide the information about how the residues of TMD-5 are involved in the transport pathway of hNaSi-1. For example, the MTSET sensitive residues will be expected to locate on the same side of the TMD-5 helical wheel to line part of the hydrophilic transport pathway, whereas the MTSET insensitive residues will be expected to be on the opposite side of the helical wheel, which should be buried in the membrane or protein interior side of hNaSi-1. Another direction is to prepare and test chimeras of hNaSi-1 and hSUT-1, which share about 50% sequence identity

but have different substrate affinity as mentioned before. The chimeras of these two transporters can be designed and the function of each chimera is tested to see which part of the protein (transmembrane domains or loops) will be likely to determine the different substrate affinity between these two transporters. If chimera studies show that a specific transmembrane domain plays a key role in determining the different substrate affinity, each amino acid residue in this transmembrane domain can be further studied in detail using site-directed mutagenesis.

Besides using *Xenopus* oocytes, there is another expression system, mammalian cell line, which can be used to study functions of hNaSi-1. Measurement of radioactive activity in a large population of cultured cells is more efficient and accurate than the assay in a group of 5 oocytes. Also, since oocytes have a different sorting process from mammalian cells, mammalian cell line is a good model to study the sorting mechanism and regulation of NaSi-1 transporters. It is important to find a cell line that has low endogenous sulfate transport activity and also can stably express the transfected hNaSi-1 transporters to get stable functions. Previous studies have tested MDCK and LLC-PK1 cells (107) as expression systems for rNaSi-1. A recent review also mentioned that OK cells (from mammalian renal proximal tubules) have been used to stably express NaSi-1 (76). I also tested several mammalian cell lines including HRPE, COS-7, HEK-293S, CHO, Balb, HUH7 and MDCK1 but they all had a high sulfate transport background. More experiments are needed to find a proper cell line that can be used to study hNaSi-1.

In conclusion, studies in this dissertation focused on two kinds of cation coupled anion transporters: bacterial proton-coupled Mg^{2+} -citrate transporter, CitM, and human Na^+ -coupled sulfate transporter, hNaSi-1. The CitM transporter has been characterized as a low affinity electroneutral transporter with a coupling stoichiometry of one proton coupled to one Mg^{2+} -citrate complex. The hNaSi-1 transporter has been studied in tissue distribution, *N*-glycosylation, and the structure of substrate and cation binding sites. There is one single *N*-glycosylation site, Asn-591, at the C-terminal tail of hNaSi-1. The residue, Asn-591, or *N*-glycosylation is not necessary for protein expression but required for the transport function of hNaSi-1. Ser-260 and Ser-288 and their surrounding residues are functionally important for the structure of substrate and cation binding sites of hNaSi-1. Finally, TMD-5 is likely to be involved in the conformational changes during the transport cycle of hNaSi-1.

Table 5.1 Comparison of functions of wild-type hNaSi-1 with the two alanine mutants, S260A and S288A.

hNaSi-1	K_m for sulfate (mM)*	V_{max} (pmol/oocyte-hr)*	K_m for Na^+ (mM)**	n_H **	Cation selectivity
Wild-type	0.44 ± 0.08	2790 ± 514	26 ± 3	1.8 ± 0.4	Na^+ only
S260A	1.12 ± 0.23	2539 ± 252	<i>n.d.</i>	<i>n.d.</i>	Na^+ only
S288A	0.43 ± 0.14	3651 ± 492	15 ± 2	1.4 ± 0.2	$\text{Na}^+ \gg \text{Li}^+ > \text{K}^+, \text{Cs}^+, \text{choline}$

*The data shown are means \pm SEM of 11, 3 or 4 experiments for the wild-type, S260A, and S288A, respectively. **The data is from one single experiment.

Table 5.2 Summary of cation/substrate dependence of MTSET inhibition of sulfate uptakes by the four cysteine mutants, T257C, T259C, T261C, and L263C*.

Mutants	MTSET concentration (μM)	Na^+	$\text{Na}^+/\text{sulfate}$	Choline	Choline/sulfate
T257C	2.5	46 ± 6	118 ± 21	73 ± 13	69 ± 5
T259C	500	44 ± 6	71 ± 6	39 ± 2	47 ± 5
T261C	250	46 ± 12	129 ± 22	79 ± 7	97 ± 8
L263C	1.0	1 ± 0.4	43 ± 2	27 ± 13	25 ± 5

*After 10-minute preincubation with or without (control) MTSET dissolved in 100 mM Na^+ or choline with or without adding 5 mM sulfate ($\text{Na}^+/\text{sulfate}$ or Choline/sulfate), sulfate uptakes were measured using radiotracer assay. The data shown are presented as a percentage of the control, means \pm SEM of 3 or 4 experiments.

APPENDIX: MUTAGENESIS OF CONSERVED TRYPTOPHAN AND ASPARTATE RESIDUES IN hNaSi-1

Introduction

As mentioned previously, there was little information on the structure of substrate and cation binding sites of hNaSi-1 before my studies are reported in Chapter 4. Previous chimera studies of rbNaDC-1 and rNaSi-1 showed that the substrate recognition site is located in the C-terminal portion of the protein, past amino acid 141 from TMD 5 to 11 (97). In this appendix, some conserved tryptophan and aspartic acid residues in hNaSi-1 were investigated. The crystal structure of the ligand-bound form of bacterial sulfate binding proteins showed that tryptophan and aspartate residues were involved in sulfate binding of the protein (103; 108). Previous crystal structure studies of other bacterial nutrient or sugar binding proteins showed that these proteins have a similar crystal structure to that of bacterial sulfate binding proteins although the amino acid sequence similarity of these proteins is small (103; 109). Therefore, it is also possible that tryptophan and aspartate residues may also be involved in sulfate binding of hNaSi-1 in spite that the amino acid sequence of hNaSi-1 is not similar to that of bacterial sulfate binding proteins. Another reason to select aspartic acid residues is due to that the carboxylic group in the side chain of aspartic acid residue could be involved in the cation binding pocket of hNaSi-1. Site-directed mutagenesis studies of acidic residues in rbNaDC-1 showed that

the carbonyl oxygen of Asp-434 (TMD-8) was important for the topological organization of the cation binding site (39).

The results from sequence alignment of the NaDC/NaSi transporter family ([Figure A.1](#)), showed that Trp-137, Trp-300, Trp-302, and Trp-572 are conserved in all of the family members, Trp-122 is conserved only in NaSi-1 transporters but not in hSUT-1 or NaDC transporters except fNaDC-3, Trp-305 is conserved in NaSi-1 and hSUT-1 transporters but not in NaDC transporters. The two aspartate residues, Asp-434 and Asp-447, are only conserved in NaSi-1 transporters but not in the hSUT-1 or NaDC transporter. All of the tryptophan residues were mutated to alanine, whereas the aspartate residues were mutated to the residues which are conserved in the corresponding positions of NaDC transporters, i.e. Asp-434 and Asp-447 are mutated to Asn and Lys, respectively. Based on the secondary structure model of hNaSi-1 as shown in [Figure A.1](#), the first two tryptophan residues (Trp-122 and Trp-137) are located in TMD-4, another three tryptophan residues (Trp-300, Trp-302, and Trp-305) reside in TMD-6, and the last one (Trp-572) is in the last transmembrane domain (TMD-11) of hNaSi-1. The two aspartate residues, Asp-434 and Asp-447, are located in the putative cytoplasmic loop between TMD-8 and TMD-9.

Radiotracer assay experiments show that neither of the mutations at the two aspartate residues resulted in significant changes on transport activity. Most of the 6 mutants of tryptophan residues were inactive except W122A,

which did not show significant change on transport activity, and W137A, which had decreased transport activity. All of the Trp to Ala mutants were expressed well on the plasma membrane of oocytes. Therefore, at least 5 of the 6 tryptophan residues, Trp-137, Trp-300, Trp-302, Trp-305 and Trp-572 are likely to be important for the transport function of hNaSi-1, whereas Trp-122 and the two aspartate residues, Asp-434 and Asp-447, appear not to be functionally required for the transporter.

Methods

The site-directed mutagenesis, transcription of cRNA, preparation and injection of oocytes, cell-surface biotinylation of oocytes, Western blots, the radiotracer assay are the same as the methods described in Chapter 3. The primers used for site-directed mutagenesis are listed in [Table A.1](#) and the mutated codons are shown in bold (see next page).

Table A.1 Oligonucleotide primers used for preparing mutants of tryptophan and aspartate residues of hNaSi-1.

Mutation	Name	Sequence of oligonucleotide primer (5' to 3')
Trp-122 to Ala	W122A	CC CAG CGT CAG CGC TGC AGG ATT TAC
Trp-137 to Ala	W137A	GTT GCT GAG CGC CAT AGA CAA AAA GGC
Trp-300 to Ala	W300A	CTG AAG CCA GAT CGC GGA TAA GAG TAG
Trp-302 to Ala	W302A	AG CCA CTG AAG CGC GAT CCA GGA TAA G
Trp-305 to Ala	W305A	AG GAA AAG CGC CTG CAG CCA GAT CCA GG
Trp-572 to Ala	W572A	CAT GGG TAC AAT CGC AGT ACA TAT GCC
Asp-434 to Asn	D434N	AAT GGC TAT ATT CCA TGG CAT GAA TGA C
Asp-447 to Lys	D447K	CTC ACA ACC CTT GGC CAG GGC AAA CCC

Results

Transport activity of the mutants expressed in *Xenopus* oocytes

Sulfate uptakes of the mutants were measured by radiotracer assay. As shown in [Figure A.2](#), the two aspartic acid mutants, D434N and D447K, had similar sulfate transport activity as the wild-type. Four out of the six Trp to Ala mutants, W300A, W302A, W305A, and W572A, were inactive. For W122A, two out of the four separate experiments showed significantly decreased transport activity whereas another two experiments did not show significant change compared with the wild-type. Therefore, no significant change is considered to occur for the mutant W122A. Finally, in all four separate experiments, W137A showed significantly decreased but still measurable transport activity compared with the wild-type.

Expression of the mutants

The intact plasma membrane of *Xenopus* oocytes injected with the cRNA of the Trp to Ala mutants was labeled with Sulfo-NHS-LC biotin and then prepared for Western blotting. The antifusion protein antibodies prepared in Chapter 3 were used to detect the expression of these mutants. As shown in [Figure A.3](#), all of these mutants were expressed well in oocytes, showing a protein signal at ~55kDa. The larger band at ~110 kDa is likely to represent the dimeric form of the protein, similar to previous results shown in Chapter 3 and 4. W122A and W137A seem to have similar expression as the wild-type, whereas the other four mutants, W300A, W302A, W305A and W572A, seem to

have more abundant expression than the wild-type. The Western blots of D434N and D447K were not done yet, but these mutants had no change in transport activity.

Discussion and future direction

It seems that neither of the two mutated aspartate residues are functionally required for hNaSi-1. However, 5 of the 6 mutated tryptophan residues, Trp-137, Trp-300, Trp-302, Trp-305, and Trp-572, are essential for the transport of hNaSi-1. Trp-122 also seems not be important for transport activity.

Most of the Trp to Ala mutants except Trp-122 either are inactive or have decreased transport activity. However, all of these mutants are expressed on the plasma membrane as well as the wild-type. Therefore, it seemed that alanine replacements at these tryptophan residues did not reduce the protein trafficking to the cell surface but only changed the optimal conformation for the transport. Alanine replacement at Trp-122 (TMD 4), which is conserved only in NaSi-1 transporters but not in hSUT-1 and NaDC transporters, seems not to produce significant change in transport activity. However, alanine mutations at the four residues, Trp-137 (TMD 4), Trp-300 (TMD 6), Trp-302 (TMD 6), and Trp-572 (TMD 11), which are conserved in all family members, either produced decreased transport activity or inactive transporters. Alanine replacement at Trp-305 (TMD 6), which is conserved in all Na⁺-coupled sulfate transporters

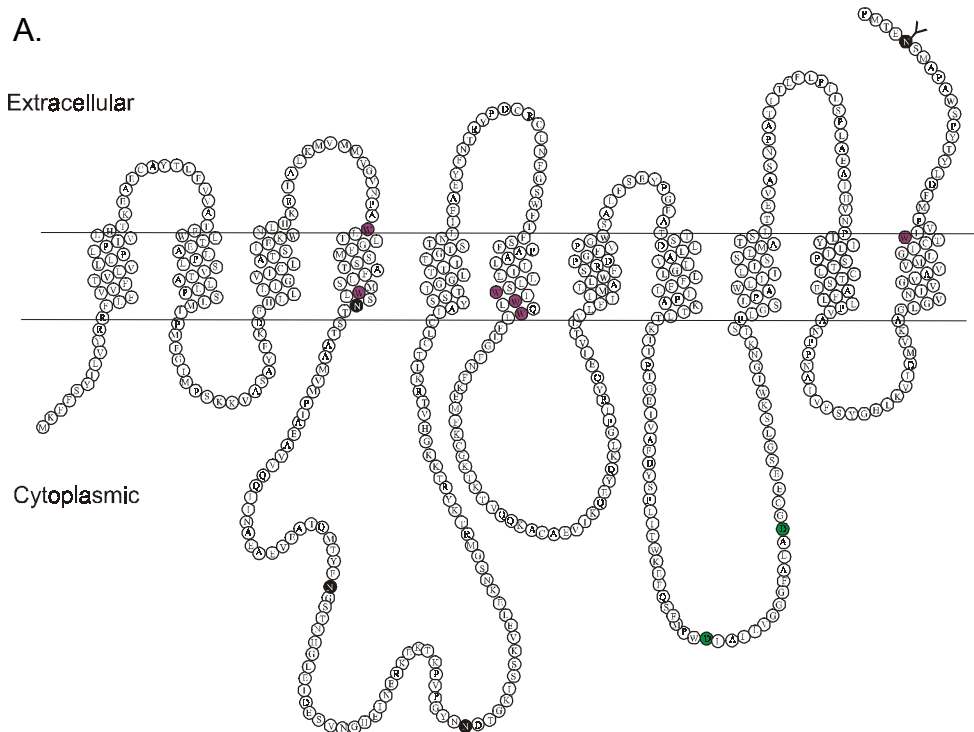
including hSUT-1, also resulted in an inactive transporter. These results seem consistent with previous chimera studies that the substrate binding site was likely to be located in C-terminal portion, past amino acid 141 from TMD 5 to 11 (97) , although Trp-137 in TMD 4 is also probably involved in the transport function.

Since W137A showed decreased but still measurable transport activity, future studies can be focused on this mutant. Firstly, functions of the W137A mutant, including the substrate kinetic curve, Na^+ -activation curve, cation specificity, and substrate specificity, will be measured to see if the mutations change the substrate and/or cation binding affinity. Furthermore, cysteine mutagenesis of Trp-137 or residues surrounding it can be performed and the functions can be tested with MTS reagents to see if these residues are involved in the conformational changes during the transport cycle of hNaSi-1. For the inactive mutants W300, W302A, W305A, and W572A, there are two alternative strategies for mutating these four tryptophan residues. One is to mutate Trp-305, which is conserved only in Na^+ -coupled sulfate transporter but not in NaDC transporters, to the corresponding residue conserved in NaDC-1 such as valine or isoleucine. The other strategy is to mutate Trp-300, Trp-302 and Trp-572, which are conserved in all family members, to phenylalanine which has a similar large aromatic side chain as tryptophan. If Trp to Phe mutation can retain the transport activity, the aromatic side chain of tryptophan may play a role in the transport function of hNaSi-1.

Previous studies of NaDC-1 found that two negatively charged residues, Asp-373 and Glu-475, are likely to be involved in the substrate and cation binding affinity (39). However, studies shown here found that mutations of the two negatively charged aspartate residues, Asp-434 and Asp-447, located in the cytoplasmic loop between TMDs 8 and 9 in hNaSi-1, did not significantly change the transport activity of hNaSi-1. More interestingly, even though the negatively charged Asp-447 was mutated to a positively charged residue (Lys), the function still did not show any significant difference from the wild-type.

In conclusion, it appears that the two aspartate residues, Asp-434 and Asp-447, located in the cytoplasmic loop between TMDs 8 and 9 in hNaSi-1, are not important for the transport of hNaSi-1. However, five of the six conserved tryptophan residues, Trp-137, Trp-300, Trp-302, Trp-305, and Trp-572, which are located in TMDs 4, 6 and 11, are functionally required for the hNaSi-1 transporter. Trp-122 appears not to be required for the transport by hNaSi-1.

Figure A.1 The aspartate and tryptophan residues mutated in hNaSi-1. (A) Secondary structure model of hNaSi-1. The mutated aspartate residues are highlighted in green (Asp-434 and Asp-477) and the mutated tryptophan residues are highlighted in magenta (Trp-122, Trp-137, Trp-300, Trp-302, Trp-305, and Trp-572). (B) Partial multiple sequence alignment of members in NaDC/NaSi family. The sequence alignment was performed using Pileup program of Genetics Computer Group (GCG). Most of the tryptophan residues are highly conserved in all family members except Trp-122 and Trp-305, which are conserved in most of Na⁺-dependent sulfate transporters but not in NaDC transporters. The two aspartate residues, Asp-434 and Asp-447, are conserved in NaSi-1 transporters but not in hSUT-1 or NaDC transporters. (The four asparagine residues highlighted in black represent the N-glycosylation consensus sequences in hNaSi-1.)



B.

	117			296	
hNaSi-1	GVNPA ¹¹⁷ LT ¹¹⁸ LG FMSSTAFLSM WLSNTSTAAM...			LLLS ²⁹⁶ NIWLQ ²⁹⁷ LFLGFNFKEM	
rNaSi-1	GVNPA ¹¹⁷ LT ¹¹⁸ LG FMSSTAFLSM WLSNTSTAAM...			LLLS ²⁹⁶ NIWLQ ²⁹⁷ LFLGFNFKEM	
mNaSi-1	GVNPA ¹¹⁷ LT ¹¹⁸ LG FMSSTAFLSM WLSNTSTAAM...			LLLS ²⁹⁶ NIWLQ ²⁹⁷ LYLGDFDK.M	
hSUT-1	GAKPGMLLLC FMCCTLLSM WLSNTSTTAM...			LVVSWFWMH ²⁹⁶ LFLGCNFKET	
rbNaDC-1	GVRPALLILG FMVVTAF ¹¹⁷ LSM WISNTASTAM...			LLLS ²⁹⁶ NLWLQ ²⁹⁷ LFLGINFRKN	
hNaDC-1	GVRPAPLILG FMLVTAFLSM WISNTATSAM...			LLL ²⁹⁶ ANLWLQ ²⁹⁷ LFLGFNFRKN	
rNaDC-1	GVRPALLLLG FMLVTAFLSM WISNTATTAM...			LLL ²⁹⁶ ANLWLQ ²⁹⁷ LFLGVNFRKN	
mNaDC-1	GVRPALLLLG FMLVTAFLSM WISNTATTAM...			LLL ²⁹⁶ ANLWLQ ²⁹⁷ LFLGVNFRKN	
xNaDC-2	GVKPALLLLG FMVVTAF ¹¹⁷ LSM WISNTATTAM...			LALS ²⁹⁶ NLWLQ ²⁹⁷ IYLGVNFKKN	
hNaDC-3	GVQPARLILG MMVTTSFLSM WLSNTASTAM...			LLAG ²⁹⁶ NLWISF LYGGLSFR.G	
rNaDC-3	GVQPARLILG MMVTTSFLSM WLSNTASTAM...			LLVG ²⁹⁶ NLWISF LYGGMSWR.G	
mNaDC-3	GVQPARLILG MMVTTSFLSM WLSNTASTAM...			LLVG ²⁹⁶ NLWISF LYGGMSWR.S	
fNaDC-3	GVKPAWLIFG MMTSAFLSM WLSNTATTAM...			LFVG ²⁹⁶ NLWIAY LYGGLNTR.L	

	425			555	
hNaSi-1	KEFQSFMPW ⁴²⁵ D IAILVGGGFA LADGCEESGL...			LGVNIVGVAV VMLGICT ⁵⁵⁵ IV	
rNaSi-1	KEFQSFMPW ⁴²⁵ D IAILVGGGFA LADGCVSGL...			LGVNIVGVAV VMLGMFT ⁵⁵⁵ IE	
mNaSi-1	KEFQSFMPW ⁴²⁵ D IAILVGGGFA LADGCVSGL...			LGVNIVGVAV VMLGMFT ⁵⁵⁵ IE	
hSUT-1	KDFQKTMPWE IVILVGGGYA LASGSKSSGL...			LGVNIVGLVI VMVAINT ⁵⁵⁵ GV	
rbNaDC-1	KLVNKKMPWN IVLLLGGGYA LAKGSEESGL...			IMLNIIIGVLV IMLAINS ⁵⁵⁵ GV	
hNaDC-1	KTVNQKMPWN IVLLLGGGYA LAKGSERSGL...			FLLNIIIGVLI IALAINS ⁵⁵⁵ GI	
rNaDC-1	KTVNDKMPWN IVILLGGGFA LAKGSEQSGL...			FLLNIIIGVLA ITLSINS ⁵⁵⁵ SI	
mNaDC-1	KTVNDKMPWN IILLGGGFA LAKGSEESGL...			FLLNIIIGVLT ITLSINS ⁵⁵⁵ SI	
xNaDC-2	KTVNEKMPWN IVILLGGGFA LAKGSEESGL...			LLLNIIGVLT ITLAINS ⁵⁵⁵ GF	
hNaDC-3	KKAQETVPWN IILLGGGFA MAKGCEESGL...			LLMNLMGVLL LSLAMNT ⁵⁵⁵ AAQ	
rNaDC-3	KKAQETVPWN IILLGGGFA MAKGCEESGL...			LLMNLMGVLL LSLAMNT ⁵⁵⁵ AAQ	
mNaDC-3	KKAQETVPWN IILLGGGFA MAKGCEESGL...			LLMNLMGVLL LSLAMNT ⁵⁵⁵ AAQ	
fNaDC-3	QKAQDSIPWN IILLGGGFA MAKACEESGL...			FVMNIIIGILC VSLAMNT ⁵⁵⁵ GV	

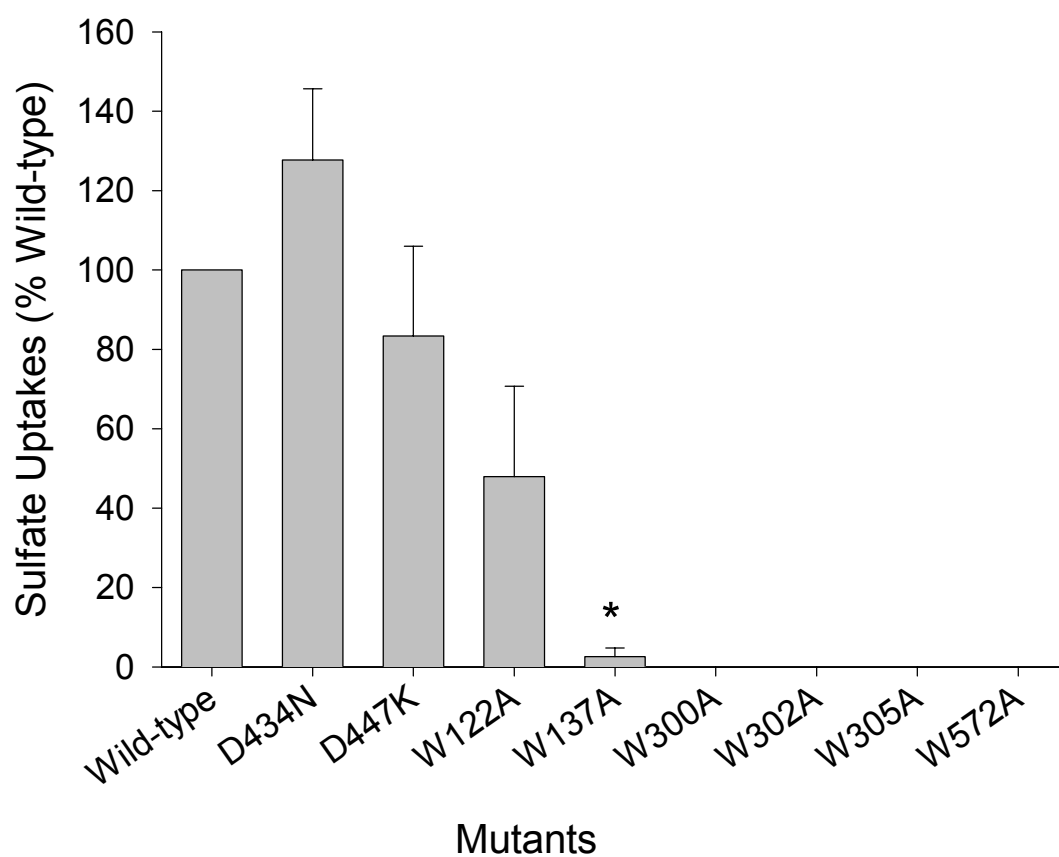


Figure A.2 Sulfate uptakes of *Xenopus* oocytes expressing mutants of tryptophan and aspartate residues in hNaSi-1. 15-minute uptakes of 100 μ M sulfate were measured in the presence of 100 mM Na^+ . Uptakes in the mutants are presented as a percentage of uptakes in wild-type hNaSi-1. The data represent means \pm SEM (n = 2 or 4 separate experiments).

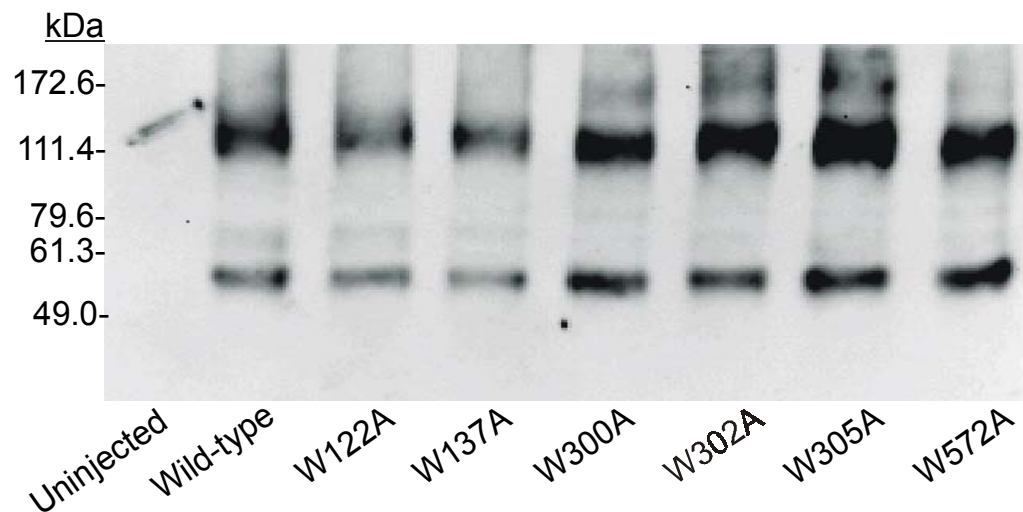


Figure A.3 Western blot of biotinylated *Xenopus* oocytes expressing wild-type and tryptophan to alanine mutants of hNaSi-1. The plasma membranes were biotinylated with Sulfo-NHS-LC biotin. The blots were probed with anti-hNaSi-1 antibodies. Uninjected oocytes did not show immunoreactive signals. Size standards are shown in kDa on the left side of the image.

REFERENCES

1. Ahearn, G. A. and H. Murer. Functional roles of Na^+ and H^+ in SO_4^{2-} transport by rabbit ileal brush border membrane vesicles. *J.Membr.Biol.* 78: 177-186, 1984.
2. Ahmed, S. and I. R. Booth. The use of valinomycin, nigericin and trichlorocarbanilide in control of the proton motive force in *Escherichia coli* cells. *Biochem J.* 212: 105-112, 1983.
3. Akabas, M. H., D. A. Stauffer, M. Xu, and A. Karlin. Acetylcholine receptor channel structure probed in cysteine-substitution mutants. *Science* 258: 307-310, 1992.
4. Alcamo, I. E. Bacterial structure and growth. Fundamentals of Microbiology. Sudbury, MA, Jones and Bartlett Publishers, Inc. 2001, 91-125.
5. Asano, T., H. Katagiri, K. Takata, J. L. Lin, H. Ishihara, K. Inukai, K. Tsukuda, M. Kikuchi, H. Hirano, and Y. Yazaki. The role of *N*-glycosylation of GLUT1 for glucose transport activity. *J.Biol.Chem.* 266: 24632-24636, 1991.
6. Bai, L. and A. M. Pajor. Expression cloning of NaDC-2, an intestinal Na^+ - or Li^+ -dependent dicarboxylate transporter. *Am.J.Physiol.* 273: G267-G274, 1997.
7. Bastlein, C. and G. Burckhardt. Sensitivity of rat renal luminal and contraluminal sulfate transport systems to DIDS. *Am.J.Physiol* 250: F226-F234, 1986.
8. Beck, L. and D. Markovich. The mouse Na^+ -sulfate cotransporter gene *Nas1*. Cloning, tissue distribution, gene structure, chromosomal assignment, and transcriptional regulation by vitamin D. *J.Biol.Chem.* 275: 11880-11890, 2000.

9. Beck, L. and C. Silve. Molecular aspects of renal tubular handling and regulation of inorganic sulfate. *Kidney Int.* 59: 835-845, 2001.
10. Beers, K. W. and T. P. Dousa. Thyroid hormone stimulates the Na^+ - PO_4 symporter but not the Na^+ - SO_4 symporter in renal brush border. *Am.J.Physiol* 265: F323-F326, 1993.
11. Bergsma, J. and W. N. Konings. The properties of citrate transport in membrane vesicles from *Bacillus subtilis*. *Eur.J.Biochem.* 134: 151-156, 1983.
12. Bers, D. and C. N. R. Patton. A practical guide to the preparation of Ca buffers. *Methods cell Biol.* 40: 3-29, 1994.
13. Blostein, R., A. Wilczynska, S. J. Karlish, J. M. Arguello, and J. B. Lingrel. Evidence that Ser775 in the alpha subunit of the Na,K-ATPase is a residue in the cation binding pocket. *J.Biol.Chem.* 272: 24987-24993, 1997.
14. Boorsma, A., M. E. van der Rest, J. S. Lolkema, and W. N. Konings. Secondary transporters for citrate and the Mg^{2+} -citrate complex in *Bacillus subtilis* are homologous proteins. *J.Bacteriol.* 178: 6216-6222, 1996.
15. Bracht, A., A. K. Bracht, A. J. Schwab, and R. Scholz. Transport of inorganic anions in perfused rat liver. *Eur.J.Biochem.* 114: 471-479, 1981.
16. Briuce, T. W. and G. L. Kenyon. Novel alkyl alkanethiolsulfonate sulfhydryl reagents. Modification of derivatives of L-Cysteine. *Journal of Protein Chemistry* 1: 47-58, 1982.
17. Brynhildsen, L. and T. Rosswall. Effect of cadmium, copper, magnesium, and zinc on the decomposition of citrate by a *Klebsilla* sp. *Appl.envir.Microbiol.* 55: 1375-1379, 1989.
18. Buchel, D. E., B. Gronenborn, and B. Muller-Hill. Sequence of the lactose permease gene. *Nature* 283: 541-545, 1980.

19. Busch, A. E., S. Waldegger, T. Herzer, J. Biber, D. Markovich, H. Murer, and F. Lang. Electrogenic cotransport of Na^+ and sulfate in *Xenopus* oocytes expressing the cloned $\text{Na}^+/\text{SO}_4^{2-}$ transport protein NaSi-1. *J.Biol.Chem.* 269: 12407-12409, 1994.
20. Chen, X., H. Tsukaguchi, X. Z. Chen, U. V. Berger, and M. A. Hediger. Molecular and functional analysis of SDCT2, a novel rat sodium-dependent dicarboxylate transporter. *J.Clin.Invest.* 103: 1159-1168, 1999.
21. Chen, X. Z., C. Shayakul, U. V. Berger, W. Tian, and M. A. Hediger. Characterization of rat Na^+ -dicarboxylate cotransporter. *J.Biol.Chem.* 273: 20972-20981, 1998.
22. Clarke, H. B., D. C. Cusworth, and S. P. Datta. Thermodynamic quantities for the dissociation equilibria of biologically important compounds. *Biochem J.* 58: 146-154, 1954.
23. Custer, M., H. Murer, and J. Biber. Nephron localization of $\text{Na}/\text{SO}_4^{2-}$ -cotransport-related mRNA and protein. *Pflugers Arch.* 429: 165-168, 1994.
24. Danek Burgess, K. S. and J. B. Justice, Jr. Effects of serine mutations in transmembrane domain 7 of the human norepinephrine transporter on substrate binding and transport. *J.Neurochem.* 73: 656-664, 1999.
25. Danielson, M. A., R. B. Bass, and J. J. Falke. Cysteine and disulfide scanning reveals a regulatory alpha-helix in the cytoplasmic domain of the aspartate receptor. *J.Biol.Chem.* 272: 32878-32888, 1997.
26. Dawson, P. A. and M. I. Filipe. Uptake of [^{35}S]sulphate in human colonic mucosa associated with carcinoma: an autoradiographic analysis at the ultrastructural level. *Histochem.J.* 15: 3-13, 1983.
27. Doege, H., A. Schurmann, H. Ohnimus, V. Monser, G. D. Holman, and H. G. Joost. Serine-294 and threonine-295 in the exofacial loop domain between helices 7 and 8 of glucose transporters (GLUT) are involved in

the conformational alterations during the transport process. *Biochem.J.* 329 (Pt 2): 289-293, 1998.

28. Eki, T., M. Abe, M. Naitou, S. I. Sasanuma, J. Nohata, K. Kawashima, I. Ahmad, F. Hanaoka, and Y. Murakami. Cloning and characterization of novel gene, DCRR1, expressed from Down's syndrome critical region of human chromosome 21q22.2. *DNA Seq.* 7: 153-164, 1997.
29. Fernandes, I., G. Hampson, X. Cahours, P. Morin, C. Coureau, S. Couette, D. Prie, J. Biber, H. Murer, G. Friedlander, and C. Silve. Abnormal sulfate metabolism in vitamin D-deficient rats. *J.Clin.Invest* 100: 2196-2203, 1997.
30. Filipe, M. I. Mucins in the human gastrointestinal epithelium: a review. *Invest Cell Pathol.* 2: 195-216, 1979.
31. Fleming, K. G. Riding the wave: structural and energetic principles of helical membrane proteins. *Curr.Opin.Biotechnol.* 11: 67-71, 2000.
32. Francis, A. J., C. J. Dodge, and J. B. Gillow. Biodegradation of metal citrate complexes and implications for toxic-metal mobility. *Nature* 356: 140-142, 1992.
33. Frillingos, S., M. Sahin-Toth, J. Wu, and H. R. Kaback. Cys-scanning mutagenesis: a novel approach to structure function relationships in polytopic membrane proteins. *FASEB J.* 12: 1281-1299, 1998.
34. Fucentese, M., K. H. Winterhalter, H. Murer, and J. Biber. Functional expression and purification of histidine-tagged rat renal Na/Phosphate (NaPi-2) and Na/Sulfate (NaSi-1) cotransporters. *J.Membr.Biol.* 160: 111-117, 1997.
35. Geering, K., I. Theulaz, F. Verrey, M. T. Hauptle, and B. C. Rossier. A role for the beta-subunit in the expression of functional Na⁺-K⁺-ATPase in *Xenopus* oocytes. *Am.J.Physiol* 257: C851-C858, 1989.

36. Girard, J. P., E. S. Baekkevold, J. Feliu, P. Brandtzaeg, and F. Amalric. Molecular cloning and functional analysis of SUT-1, a sulfate transporter from human high endothelial venules. *Proc.Natl.Acad.Sci., USA* 96: 12772-12777, 1999.
37. Glusker, J. P. Citrate conformation and chelation: enzymatic implications. *Acc.Chem.Res.* 13: 345-352, 1980.
38. Good, N. E., G. D. Winget, W. Winter, T. N. Connolly, S. Izawa, and R. M. M. Singh. Hydrogen ion buffers for biological research. *Biochemistry* 5: 467-477, 1966.
39. Griffith, D. A. and A. M. Pajor. Acidic residues involved in cation and substrate interactions in the Na⁺/dicarboxylate cotransporter, NaDC-1. *Biochemistry* 38: 7524-7531, 1999.
40. Grinstein, S., R. J. Turner, M. Silverman, and A. Rothstein. Inorganic anion transport in kidney and intestinal brush border and basolateral membranes. *Am.J.Physiol* 238: F452-F460, 1980.
41. Hayes, G., A. Busch, M. Lotscher, S. Waldegger, F. Lang, F. Verrey, J. Biber, and H. Murer. Role of N-linked glycosylation in rat renal Na/P_i-cotransport. *J.Biol.Chem.* 269: 24143-24149, 1994.
42. Hediger, M. A., J. Mendlein, H. S. Lee, and E. M. Wright. Biosynthesis of the cloned intestinal Na⁺/glucose cotransporter. *Biochim.Biophys.Acta* 1064: 360-364, 1991.
43. Hierholzer, K., R. Cade, R. Gurd, R. Kessler, and R. Pitts. Stop flow analysis of renal reabsorption and excretion of sulfate in the dog. *Am.J.Physiol* 198: 833-837, 1960.
44. Hille, A., A. Waheed, and K. von Figura. The ligand-binding conformation of Mr 46,000 mannose 6-phosphate-specific receptor. Acquisition of binding activity during *in vitro* synthesis. *J.Biol.Chem.* 264: 13460-13467, 1989.

45. Hirayama, B. A. and E. M. Wright. Glycosylation of the rabbit intestinal brush border Na⁺/glucose cotransporter. *Biochim.Biophys.Acta* 1103: 37-44, 1992.
46. Holmgren, M., Y. Liu, Y. Xu, and G. Yellen. On the use of thiol-modifying agents to determine channel topology. *Neuropharmacology* 35: 797-804, 1996.
47. Ingram, J. Effect of temperature, pH, water activity, and pressure on growth. In Neidhardt, F. C., ed. *Escherichia coli* and *Salmonella typhimurium*. American Society for Microbiology. 1987, 1543-1554.
48. Inoue, K., Y. J. Fei, W. Huang, L. Zhuang, Z. Chen, and V. Ganapathy. Functional identity of *Drosophila melanogaster* Indy as a cation-independent, electroneutral transporter for tricarboxylic acid-cycle intermediates. *Biochem.J.* 367: 313-319, 2002.
49. Inoue, K., L. Zhuang, D. M. Maddox, S. B. Smith, and V. Ganapathy. Structure, function, and expression pattern of a novel sodium-coupled citrate transporter (NaCT) cloned from mammalian brain. *J.Biol.Chem.* 277: 39469-39476, 2002.
50. Jameson, B. A. and H. Wolf. The antigenic index: a novel algorithm for predicting antigenic determinants. *Comput.Appl.Biosci.* 4: 181-186, 1988.
51. Joshi-Tope, G. and A. J. Francis. Mechanisms of biodegradation of metal-citrate complexes by *Pseudomonas fluorescens*. *J.Bacteriol.* 177: 1989-1993, 1995.
52. Kaback, H. R. The *lac* carrier protein in *Escherichia coli*. *J.Membr.Biol.* 76: 95-112, 1983.
53. Kaback, H. R. *Lac* permease of *Escherichia coli*: on the path of the proton. *Phil.Trans.R.Soc.Lond. B* 326: 425-436, 1990.

54. Kahn, E. S. and A. M. Pajor. Determinants of substrate and cation affinities in the Na⁺/dicarboxylate cotransporter. *Biochemistry* 38: 6151-6156, 1999.
55. Karlin, A. and M. H. Akabas. Substituted-cysteine accessibility method. *Methods Enzymol.* 293: 123-145, 1998.
56. Kekuda, R., H. Wang, W. Huang, A. M. Pajor, F. H. Leibach, L. D. Devoe, P. D. Prasad, and V. Ganapathy. Primary structure and functional characteristics of a mammalian sodium-coupled high affinity dicarboxylate transporter. *J.Biol.Chem.* 274: 3422-3429, 1999.
57. Khatri, S. A., G. G. Forstner, and J. F. Forstner. Suggestive evidence for two different mucin genes in rat intestine. *Biochem.J.* 294: 391-399, 1993.
58. Knauf, F., B. Rogina, Z. Jiang, P. S. Aronson, and S. L. Helfand. Functional characterization and immunolocalization of the transporter encoded by the life-extending gene *Indy*. *Proc.Natl.Acad.Sci.U.S.A* 99: 14315-14319, 2002.
59. Koser, S. A. Correlation of citrate utilization by members of the colon-aerogenes group with other differential characteristic and with habitat. *J.Bacteriol.* 9: 59-77, 1924.
60. Krom, B. P., H. Huttinga, J. B. Warner, and J. S. Lolkema. Impact of the Mg²⁺-citrate transporter CitM on heavy metal toxicity in *Bacillus subtilis*. *Arch.Microbiol.* 178: 370-375, 2002.
61. Krom, B. P., J. B. Warner, W. N. Konings, and J. S. Lolkema. Complementary metal ion specificity of the metal-citrate transporters CitM and CitH of *Bacillus subtilis*. *J.Bacteriol.* 182: 6374-6381, 2000.
62. Kunkel, T. A. Rapid and efficient site-specific mutagenesis without phenotypic selection. *Proc.Natl.Acad.Sci.USA* 82: 488-492, 1985.

63. Kyte, J. and R. F. Doolittle. A simple method for displaying the hydropathic character of a protein. *J.Mol.Biol.* 157: 105-132, 1982.
64. Lara, E. J. S. and J. L. Stokes. Oxidation of citrate by *Escherichia coli*. *J.Bacteriol.* 63: 415-420, 1952.
65. Lee, A., L. Beck, and D. Markovich. The human renal sodium sulfate cotransporter (SLC13A1; hNaSi-1) cDNA and gene: organization, chromosomal localization, and functional characterization. *Genomics* 70: 354-363, 2000.
66. Leive, L. Studies on the permeability change produced in coliform bacteria by ethylenediaminetetraacetate. *J.Biol.Chem.* 243: 2373-2380, 1968.
67. Li, H. and A. M. Pajor. Functional characterization of CitM, the Mg^{2+} -Citrate transporter. *J.Membr.Biol.* 185: 9-16, 2002.
68. Liu, Y., U. Eckstein-Ludwig, J. Fei, and W. Schwarz. Effect of mutation of glycosylation sites on the Na^+ dependence of steady-state and transient currents generated by the neuronal GABA transporter. *Biochim.Biophys.Acta* 1415: 246-254, 1998.
69. Lotscher, M., M. Custer, E. S. Quabius, B. Kaissling, H. Murer, and J. Biber. Immunolocalization of Na/SO_4 -cotransport (NaSi-1) in rat kidney. *Pflugers Arch.* 432: 373-378, 1996.
70. Low, I., T. Friedrich, and G. Burckhardt. Properties of an anion exchanger in rat renal basolateral membrane vesicles. *Am.J.Physiol* 246: F334-F342, 1984.
71. Lucke, H., G. Stange, and H. Murer. Sulphate-ion/sodium-ion co-transport by brush-border membrane vesicles isolated from rat kidney cortex. *Biochem.J.* 182: 223-229, 1979.

72. Lucke, H., G. Stange, and H. Murer. Sulfate-sodium cotransport by brush-border membrane vesicles isolated from rat ileum. *Gastroenterology* 80: 22-30, 1981.
73. Madsen, E. L. and M. Alexander. Effect of chemical speciation on the mineralization of organic compounds by microorganisms. *Appl.envir.Microbiol.* 50: 342-349, 1985.
74. Magni, C., P. Lopez, and D. de Mendoza. The properties of citrate transport catalyzed by CitP of *Lactococcus lactis* ssp. *lactis* biovar *diacetylactis*. *FEMS Microbiol.Lett.* 142: 265-269, 1996.
75. Maley, F., R. B. Trimble, A. L. Tarentino, and Jr. T. H. Plummer. Characterization of glycoproteins and their associated oligosaccharides through the use of endoglycosidases. *Anal.Biochem.* 180: 195-204, 1989.
76. Markovich, D. Physiological roles and regulation of mammalian sulfate transporters. *Physiol Rev.* 81: 1499-1533, 2001.
77. Markovich, D., M. Bissig, V. Sorribas, B. Hagenbuch, P. J. Meier, and H. Murer. Expression of rat renal sulfate transport systems in *Xenopus laevis* oocytes. Functional characterization and molecular identification. *J.Biol.Chem.* 269: 3022-3026, 1994.
78. Markovich, D., J. Forgo, G. Stange, J. Biber, and H. Murer. Expression cloning of rat renal $\text{Na}^+/\text{SO}_4^{2-}$ cotransport. *Proc.Natl.Acad.Sci.USA* 90: 8073-8077, 1993.
79. Markovich, D., H. Murer, J. Biber, K. Sakhaee, C. Pak, and M. Levi. Dietary sulfate regulates the expression of the renal brush border Na/Si cotransporter NaSi-1. *J.Am.Soc.Nephrol.* 9: 1568-1573, 1998.
80. Marty-Teyssset, C., J. S. Lolkema, P. Schmitt, C. Divies, and W. N. Konings. Membrane potential-generating transport of citrate and malate catalyzed by CitP of *Leuconostoc mesenteroides*. *J.Biol.Chem.* 270: 25370-25376, 1995.

81. McKern, N. M. Comparison of sulfate metabolism in costal cartilage of normal and 'little' mice. *Aust.J.Biol.Sci.* 36: 263-270, 1983.
82. Morris, M. E. and H. Murer. Molecular mechanisms in renal and intestinal sulfate (re)absorption. *J.Membr.Biol.* 181: 1-9, 2001.
83. Morris, M. E. and K. Sagawa. Molecular mechanisms of renal sulfate regulation. *Crit Rev.Clin.Lab Sci.* 37: 345-388, 2000.
84. Murer, H., M. Manganel, and F. Roch-Ramel. Tubular transport of monocarboxylates, Krebs cycle intermediates, and inorganic sulfate. In Windhager, E. E., ed. *Handbook of Physiology-Renal Physiology*. New York, Am. Physiol. Soc. 1992, 2165-2188.
85. Norbis, F., C. Perego, D. Markovich, G. Stange, T. Verri, and H. Murer. cDNA cloning of a rat small intestinal $\text{Na}^+/\text{SO}_4^{2-}$ cotransporter. *Pflugers Arch.* 428: 217-223, 1994.
86. Oehr, P. and K. Willecke. Citrate- Mg^{2+} transport in *Bacillus subtilis*. Studies with 2-fluoro-L-erythro-citrate as a substrate. *J.Biol.Chem.* 249: 2037-2042, 1974.
87. Pajor, A. M. Sequence and functional characterization of a renal sodium/dicarboxylate cotransporter. *J.Biol.Chem.* 270: 5779-5785, 1995.
88. Pajor, A. M. Molecular cloning and functional expression of a sodium-dicarboxylate cotransporter from human kidney. *Am.J.Physiol.* 270: F642-F648, 1996.
89. Pajor, A. M. Molecular properties of sodium/dicarboxylate cotransporters. *J.Membr.Biol.* 175: 1-8, 2000.
90. Pajor, A. M. Conformationally-sensitivity residues in transmembrane domain 9 of the $\text{Na}^+/\text{dicarboxylate}$ cotransporter. *J.Biol.Chem.* 276: 29961-29968, 2001.

91. Pajor, A. M., R. Gangula, and X. Yao. Cloning and functional characterization of a high-affinity Na⁺/dicarboxylate cotransporter from mouse brain. *Am.J.Physiol Cell Physiol* 280: C1215-C1223, 2001.
92. Pajor, A. M., B. A. Hirayama, and E. M. Wright. Molecular evidence for two renal Na⁺/glucose cotransporters. *Biochim.Biophys.Acta* 1106: 216-220, 1992.
93. Pajor, A. M., E. S. Kahn, and R. Gangula. Role of cationic amino acids in the sodium/dicarboxylate co-transporter NaDC-1. *Biochem.J.* 350: 677-683, 2000.
94. Pajor, A. M., S. J. Krajewski, N. Sun, and R. Gangula. Cysteine residues in the Na⁺/dicarboxylate cotransporter, NaDC-1. *Biochem.J.* 344: 205-209, 1999.
95. Pajor, A. M. and N. Sun. Characterization of the rabbit renal Na⁺/dicarboxylate cotransporter using anti-fusion protein antibodies. *Am.J.Physiol.* 271: C1808-C1816, 1996.
96. Pajor, A. M. and N. Sun. Functional differences between rabbit and human Na⁺-dicarboxylate cotransporters, NaDC-1 and hNaDC-1. *Am.J.Physiol.* 271: F1093-F1099, 1996.
97. Pajor, A. M., N. Sun, L. Bai, D. Markovich, and P. Sule. The substrate recognition domain in the Na⁺/dicarboxylate and Na⁺/sulfate cotransporters is located in the carboxy-terminal portion of the protein. *Biochim.Biophys.Acta* 1370: 98-106, 1998.
98. Pajor, A. M., N. Sun, and H. G. Valmonte. Mutational analysis of histidines in the Na⁺/dicarboxylate cotransporter, NaDC-1. *Biochem.J.* 331: 257-264, 1998.
99. Pajor, A. M. and N. N. Sun. Molecular cloning, chromosomal organization, and functional characterization of a sodium-dicarboxylate cotransporter from mouse kidney. *Am.J.Physiol Renal Physiol* 279: F482-F490, 2000.

100. Parent, L., S. Supplisson, D. D. F. Loo, and E. M. Wright. Electrogenic properties of the cloned Na⁺/glucose cotransporter: II. A transport model under nonrapid equilibrium conditions. *J.Membrane Bio.* 125: 63-79, 1992.
101. Paulson, J. C. Glycoproteins: what are the sugar chains for? *Trends Biochem.Sci.* 14: 272-276, 1989.
102. Perczel, A., E. Kollat, M. Hollosi, and G. D. Fasman. Synthesis and conformational analysis of *N*-glycopeptides. II. CD, molecular dynamics, and NMR spectroscopic studies on linear *N*-glycopeptides. *Biopolymers* 33: 665-685, 1993.
103. Pflugrath, J. W. and F. A. Quiocho. The 2 Å resolution structure of the sulfate-binding protein involved in active transport in *Salmonella typhimurium*. *J.Mol.Biol.* 200: 163-180, 1988.
104. Pressman, B. C. Biological applications of ionophores. *Ann.Rev.Biochem.* 45: 501-530, 1976.
105. Pritchard, J. B. and J. L. Renfro. Renal sulfate transport at the basolateral membrane is mediated by anion exchange. *Proc.Natl.Acad.Sci.U.S.A* 80: 2603-2607, 1983.
106. Puttaparthi, K., D. Markovich, N. Halaihel, P. Wilson, H. K. Zajicek, H. Wang, J. Biber, H. Murer, T. Rogers, and M. Levi. Metabolic acidosis regulates rat renal Na-Si cotransport activity. *Am.J.Physiol* 276: C1398-C1404, 1999.
107. Quabius, E. S., H. Murer, and J. Biber. Expression of proximal tubular Na-Pi and Na-SO₄ cotransporters in MDCK and LLC-PK1 cells by transfection. *Am.J.Physiol* 270: F220-F228, 1996.
108. Quiocho, F. A. Atomic basis of the exquisite specificity of the phosphate and sulfate transport receptors. *Kidney International* 49: 943-946, 1996.

109. Quijcho, F. A., J. S. Sack, and N. K. Vyas. Stabilization of charges on isolated ionic groups sequestered in proteins by polarized peptide units. *Nature* 329: 561-564, 1987.
110. Rachidi, M., C. Lopes, S. Gassanova, P. M. Sinet, M. Vekemans, T. Attie, A. L. Delezoide, and J. M. Delabar. Regional and cellular specificity of the expression of TPRD, the tetratricopeptide Down syndrome gene, during human embryonic development. *Mechanisms of Development* 93: 189-193, 2000.
111. Rao, J. K. M. and P. Argos. A conformational preference parameter to predict helices in integral membrane proteins. *Biochim.Biophys.Acta* 869: 197-214, 1986.
112. Renfro, J. L., N. B. Clark, R. E. Metts, and M. A. Lynch. Glucocorticoid inhibition of Na-SO₄ transport by chick renal brush-border membranes. *Am.J.Physiol* 256: R1176-R1183, 1989.
113. Roepe, P. D., T. G. Consler, M. E. Menezes, and H. R. Kaback. The *Lac* permease of *Escherichia coli*: site-directed mutagenesis studies on the mechanism of β -galactoside/H⁺ symport. *Res.Microbiol.* 141: 290-308, 1990.
114. Sagawa, K., I. M. Darling, H. Murer, and M. E. Morris. Glucocorticoid-induced alterations of renal sulfate transport. *J.Pharmacol.Exp.Ther.* 294: 658-663, 2000.
115. Sagawa, K., D. C. DuBois, B. Han, R. R. Almon, J. Biber, H. Murer, and M. E. Morris. Detection and quantitation of a sodium-dependent sulfate cotransporter (NaSi-1) by sandwich-type enzyme-linked immunosorbent assay. *Pflugers Arch.* 437: 123-129, 1998.
116. Sagawa, K., B. Han, D. C. DuBois, H. Murer, R. R. Almon, and M. E. Morris. Age- and growth hormone-induced alterations in renal sulfate transport. *J.Pharmacol.Exp.Ther.* 290: 1182-1187, 1999.

117. Sagawa, K., H. Murer, and M. E. Morris. Effect of experimentally induced hypothyroidism on sulfate renal transport in rats. *Am.J.Physiol Renal Physiol* 276: F164-F171, 1999.
118. Saier, M. H. Genome archeology leading to the characterization and classification of transport proteins. *Curr.Opin.Microbiol.* 2: 555-561, 1999.
119. Saier, M. H., Jr. A functional-phylogenetic classification system for transmembrane solute transporters. *Microbiology and Molecular Biology Reviews* 64: 354-411, 2000.
120. Sambrook, J., E. F. Fritsch, and T. Maniatis. Molecular cloning: a laboratory manual. Cold Spring Harbor Laboratory Press. 1989.
121. Sarkar, H. K., B. Thorens, H. F. Lodish, and H. R. Kaback. Expression of the human erythrocyte glucose transporter in *Escherichia coli*. *Proc.Natl.Acad.Sci.* 85: 5463-5467, 1988.
122. Schneider, E. G., J. C. Durham, and B. Sacktor. Sodium-dependent transport of inorganic sulfate by rabbit renal brush-border membrane vesicles. Effects of other ions. *J.Biol.Chem.* 259: 14591-14599, 1984.
123. Segel, I. H. Enzyme Activation. Enzyme Kinetics. New York, John Wiley & Sons. 1975, 227-272.
124. Segel, I. H. Enzyme kinetics. NY, John Wiley and Sons. 1975.
125. Sekine, T., S. H. Cha, M. Hosoyamada, Y. Kanai, N. Watanabe, Y. Furuta, K. Fukuda, T. Igarishi, and H. Endou. Cloning, functional characterization and localization of a rat renal Na⁺-dicarboxylate cotransporter. *Am.J.Physiol.(Renal Fluid Electrolyte Physiol.)* 275: F298-F305, 1998.
126. Smith, C. D., B. A. Hirayama, and E. M. Wright. Baculovirus-mediated expression of the Na⁺/glucose cotransporter in Sf9 cells. *Biochim.Biophys.Acta* 1104: 151-159, 1992.

127. Stauffer, D. A. and A. Karlin. Electrostatic potential of the acetylcholine binding sites in the nicotinic receptor probed by reaction of binding-site cysteines with charged methanethiosulfonates. *Biochemistry* 33: 6840-6849, 1994.
128. Steffgen, J., B. C. Burckhardt, C. Langenberg, L. Kuhne, G. A. Muller, G. Burckhardt, and N. A. Wolff. Expression cloning and characterization of a novel sodium-dicarboxylate cotransporter from winter flounder kidney. *J.Biol.Chem.* 274: 20190-20196, 1999.
129. Strouse, J., S. W. Layten, and C. E. Strouse. Structural studies of transition metal complexes of triionized and tetraionized citrate. Models for the coordination of the citrate ion to transition metal ions in solution and at the active site of aconitase. *J.Am.chem.Soc.* 99: 562-572, 1977.
130. Sur, C., H. Betz, and P. Schloss. A single serine residue controls the cation dependence of substrate transport by the rat serotonin transporter. *Proc.Natl.Acad.Sci.U.S.A* 94: 7639-7644, 1997.
131. Tenenhouse, H. S., J. Lee, and N. Harvey. Renal brush-border membrane Na^+ -sulfate cotransport: stimulation by thyroid hormone. *Am.J.Physiol* 261: F420-F426, 1991.
132. Tenenhouse, H. S. and J. Martel. Na^+ -dependent sulfate transport in opossum kidney cells is DIDS sensitive. *Am.J.Physiol* 265: C54-C61, 1993.
133. Turner, R. J. Sodium-dependent sulfate transport in renal outer cortical brush border membrane vesicles. *Am.J.Physiol* 247: F793-F798, 1984.
134. van der Rest, M. E., T. Abee, D. Molenaar, and W. N. Konings. Mechanism and energetics of a citrate-transport system of *Klebsiella pneumoniae*. *Eur.J.Biochem.* 195: 71-77, 1991.
135. van der Rest, M. E., R. M. Siewe, T. Abee, E. Schwarz, D. Oesterhelt, and W. N. Konings. Nucleotide sequence and functional properties of a

sodium-dependent citrate transport system from *Klebsiella pneumoniae*. *J.Biol.Chem.* 267: 8971-8976, 1992.

136. van Winkle, L. J., O. Bussolati, G. Gazzola, J. McGiven, B. Mackenzie, M. H. J. Saier, P. M. Taylor, M. J. Rennie, and S. Y. Low. A proposed system for the classification of transmembrane transport proteins in living organisms. *Biomembrane transport*. San Diego, CA, Academic Press. 1999, 265-276.
137. von Dippe, P. and D. Levy. Analysis of the transport system for inorganic anions in normal and transformed hepatocytes. *J.Biol.Chem.* 257: 4381-4385, 1982.
138. Wang, H., Y. J. Fei, R. Kekuda, T. L. Yang-Feng, L. D. Devoe, F. H. Leibach, P. D. Prasad, and V. Ganapathy. Structure, function, and genomic organization of human Na⁺-dependent high-affinity dicarboxylate transporter. *Am.J.Physiol Cell Physiol* 278: C1019-C1030, 2000.
139. Wang, J. and K. M. Giacomini. Serine 318 is essential for the pyrimidine selectivity of the N2 Na⁺-nucleoside transporter. *J.Biol.Chem.* 274: 2298-2302, 1999.
140. Warner, J. B., B. P. Krom, C. Magni, W. N. Konings, and J. S. Lolkema. Catabolite repression and induction of the Mg²⁺-citrate transporter CitM of *Bacillus subtilis*. *J.Bacteriol.* 182: 6099-6105, 2000.
141. Willecke, K., E.-M. Gries, and P. Oehr. Coupled transport of citrate and magnesium in *Bacillus subtilis*. *J.Biol.Chem.* 248: 807-814, 1973.
142. Willecke, K. and A. B. Pardee. Inducible transport of citrate in a Gram-positive bacterium, *Bacillus subtilis*. *J.Biol.Chem.* 246: 1032-1040, 1971.
143. Wright, E. M., D. D. Loo, M. Panayotova-Heiermann, B. A. Hirayama, E. Turk, S. Eskandari, and J. T. Lam. Structure and function of the Na⁺/glucose cotransporter. *Acta Physiol Scand.Suppl* 643: 257-264, 1998.

144. Wright, S. H., B. Hirayama, J. D. Kaunitz, I. Kippen, and E. M. Wright. Kinetics of sodium succinate cotransport across renal brush-border membranes. *J.Biol.Chem.* 258: 5456-5462, 1983.
145. Yamamoto, H., M. Murata, and J. Sekiguchi. The CitST two-component system regulates the expression of the Mg-citrate transporter in *Bacillus subtilis*. *Mol.Microbiol.* 37: 898-912, 2000.
146. Yao, X. and A. M. Pajor. The transport properties of the human renal Na/dicarboxylate cotransporter under voltage clamp conditions. *Am.J.Physiol.* 279: F54-F64, 2000.
147. Yao, X. and A. M. Pajor. Arginine-349 and aspartate-373 of the Na⁺/dicarboxylate cotransporter are conformationally sensitive residues. *Biochemistry* 41: 1083-1090, 2002.
148. Zhang, F. F. and A. M. Pajor. Topology of the Na⁺/dicarboxylate cotransporter: the N-terminus and hydrophilic loop 4 are located intracellularly. *Biochim.Biophys.Acta* 1511: 80-89, 2001.
149. Zhang, Y. and B. I. Kanner. Two serine residues of the glutamate transporter GLT-1 are crucial for coupling the fluxes of sodium and the neurotransmitter. *Proc.Natl.Acad.Sci.U.S.A* 96: 1710-1715, 1999.

VITA

Hongyan Li, daughter of Fengcai Li and Wenbin Zhang, was born in Beijing, People's Republic of China on December 23, 1970. After graduating from Capital University of Medical Sciences at Beijing, People's Republic of China in 1994 with a Bachelor degree in Biomedical Engineering, Hongyan attended Tsinghua University at Beijing, People's Republic of China, where she received a Master degree in Biophysics in 1998. In the same year, Hongyan entered the Cellular Physiology and Molecular Biophysics graduate program at the University of Texas Medical Branch at Galveston.

EDUCATION

B.S., July 1994, Capital University of Medical Sciences, Beijing, P.R.China.
M.S., May 1998, Tsinghua University, Beijing, P.R.China.

Permanent address:

3-203 Qing Nian Hu Xi Li
Dongcheng District
Beijing, P.R. China 100011

This dissertation was typed by Hongyan Li

PUBLICATIONS

Li, H and A. M. Pajor, Functional characterization of CitM, the Mg^{2+} -citrate transporter. *J. Mem. Biol.* 185: 9-16, January, 2002.

Li, H, X. Zhang and F. Zhuang, The effect of Interleukin-1 on human endothelial cell surface Intercellular Adhesion Molecule-1. *Medical Journal of Chinese People's Liberation Army*, 24 (3): 179, June, 1998.

ABSTRACTS

Li, H and A. M. Pajor, Conformational sensitive residues around Ser-260 in the human Na⁺/sulfate cotransporter (hNaSi-1). *FASEB J.*, 17(4): A472 (330.2), 2003.

Li, H and A. M. Pajor, Tryptophan and serine residues may be involved in the function of the human Na⁺/sulfate cotransporter, hNaSi-1. *FASEB J.*, 16(5): A807 (626.6), 2002.

Li, H and A. M. Pajor, Transport activity of CitM, the Mg²⁺-Citrate complex transporter, expressed in *E.coli*. *FASEB J.*, 15(4): A434 (395.1), 2001.